

**UCLA**

**UCLA Electronic Theses and Dissertations**

**Title**

Synthesis of New and Improved Stimuli-Responsive Polymer Materials

**Permalink**

<https://escholarship.org/uc/item/9754w2db>

**Author**

Askounis, Erin

**Publication Date**

2020

Peer reviewed|Thesis/dissertation

UNIVERSITY OF CALIFORNIA

Los Angeles

Synthesis of New and Improved Stimuli- Responsive Polymer Materials

A dissertation submitted in partial satisfaction of the requirements for the degree Doctor of Philosophy  
in Materials Science and Engineering

by

Erin Askounis

2020

© Copyright by

Erin Askounis

2020

## ABSTRACT OF THE DISSERTATION

Synthesis of New and Improved Stimuli- Responsive Polymer Materials

by

Erin Askounis

Doctor of Philosophy in Materials Science and Engineering

University of California, Los Angeles, 2020

Professor Qibing Pei, Chair

Stimuli-responsive polymers are materials that undergo physical or chemical properties changes triggered by light, temperature, mechanical force, insertion of small molecules, electric fields, magnetic fields, or pH. Stimuli-responsive materials can be designed for a desired physical response, such as compression, shape change, or variable stiffness and have been used in coatings, sensors, drug delivery, self-healing, and mechanical actuators. Some stimuli-responsive materials utilize several trigger mechanisms to amplify and increase the resulting change in physical properties. For example, cellulose polymer nanocomposites exhibit stiffness changes triggered by both water and temperature to increase the modulus differential of the material. The modulus ranges from GPa range to the low MPa range with the assistance of the dual-stimuli technique. Although this modulus differential is large, for applications in biomaterials, the low-end modulus of the material must be in the kPa range to limit mechanical mismatch of an implant for practical use. Another category of stimuli-responsive materials is dielectric

elastomer materials, electric-field responsive materials that expand and contract with an applied voltage. Rather than change stiffness, these materials change shape. When sandwiched between two compliant electrodes and an electric field is applied, the material is compressed by the attraction of the opposite charges formed on the electrodes. With electro-response, these materials are useful in soft robotics applications, however, commercially available dielectric elastomer materials require prestretching for high actuation performance and are incapable of molecular modification. Additionally, dielectric elastomers are difficult to process due to the crosslinked nature, a controlled synthetic approach to more precisely design molecular architectures is desired. Overall, these materials can be precisely tuned to respond to triggers based on the application requirements. Synthesizing and optimizing new stimuli-responsive materials that are precisely tuned opens the door for expanded applications in fields such as biomedicine or soft robotics.

The research outlined in this dissertation focuses on the synthesis and fabrication of novel stimuli-responsive polymer materials to address challenges previously outlined. The main body of this dissertation describes new cellulose polymer composite materials with ultra-wide stiffness range, new dielectric elastomers with high actuation performance without prestretch, and new BAB triblock copolymers with variable stiffness. The first chapter surveys current stimuli-responsive polymer materials technology with a focus on thermo-responsive, photo-responsive, electro-responsive, and dual responsive materials. The second chapter outlines research aimed to increase the modulus differential in cellulose composite materials using a thermo-responsive variable stiffness polymer and cellulose microfibers. The resulting composite utilizes two stimuli, the first is temperature to soften the stiff polymer matrix by melting the crystalline segments to form a soft crosslinked polymer. The second stimulus is the addition of water, to nullify the reinforcing network formed by percolating cellulose fibers and further soften the material. The material exhibits an ultra wide modulus differential from 1

GPa down to 40 kPa stimulated by water and temperature. An ultra wide modulus range allows for further applications development with potential for biomedical devices. The third chapter outlines a new dielectric elastomer (DE) material that exhibits performance similar to commercially available materials in an aim to address the limitations of prestretching and to introduce DEs capable of modification. A bimodal interpenetrating crosslinked network was established by combining a short chain di-functional acrylate monomer with a long-chain high molecular weight di-functional acrylate monomer to form a material with mechanical properties similar to commercially available DEs. Additional mono-functional diluents were added to further tune the electro-mechanical properties and improve performance. The new DE exhibited maximum actuation strains near 200% and rapid response over 100% strain at 2 Hz. The new DE material exhibits performance higher than other synthetic dielectric elastomer and opens the door to optimization of DE materials for a new generation of polymer actuator materials. The fourth and last chapter of the main text presents a comparison study of three different length BAB triblock copolymers in an aim to synthesize a triblock copolymer for use as a bistable electroactive polymer (BSEP). BSEP materials are stiff at room temperature and softened at elevated temperature to actuate as dielectric elastomers. BSEP is typically processed by bulk polymerization making it difficult to modify post-fabrication. In the BAB polymer described, a two-sided RAFT chain transfer agent was synthesized, for symmetrical synthetic processing, using poly (ethylene glycol) for high stiffness at room temperature and increased flexibility at elevated temperature. The poly (stearyl acrylate) B-blocks were then incorporated to add further stiffness at room temperature and control the material microstructure. Of the three BAB copolymers synthesized, two exhibited variable stiffness from 1 GPa to 10 kPa with spherulite microstructural formations confirmed by optical and scanning electron microscopy. By introducing a controlled synthetic pathway using RAFT living polymerization, these materials can be finely tuned for specific properties before and after fabrication.

The dissertation of Erin Askounis is approved.

Ximin He

Yu Huang

Andrea Kasko

Qibing Pei, Committee Chair

University of California, Los Angeles

2020

## TABLE OF CONTENTS

ABSTRACT OF THE DISSERTATION .....	ii
LIST OF FIGURES .....	ix
LIST OF TABLES .....	xii
LIST OF EQUATIONS .....	xii
LIST OF SCHEMES .....	xii
ACKNOWLEDGEMENTS .....	xiii
VITA .....	xv
PUBLICATIONS .....	xv
Chapter 1. INTRODUCTION AND DISSERTATION OBJECTIVES .....	1
1.1. An overview of stimuli responsive polymers .....	1
1.2. Thermo-responsive materials .....	2
1.2.1 <i>Thermo-responsive dynamic bonds</i> .....	2
1.2.2 <i>Shape memory polymers</i> .....	4
1.3. Photo-responsive materials .....	5
1.4. Electro-responsive materials .....	6
1.4.1 <i>Dielectric elastomers</i> .....	7
1.5. Dual responsive materials systems .....	8
1.6. Motivation of this dissertation .....	9
1.7. Scope and layout of the dissertation .....	11
1.8. References .....	12
Chapter 2. DUAL STIMULI-RESPONSIVE POLYMER COMPOSITE WITH ULTRA-WIDE TUNABLE STIFFNESS RANGE TRIGGERED BY WATER AND TEMPERATURE .....	21
2.1. Background of this study .....	21
2.1.1 <i>Synthetic variable stiffness materials</i> .....	21
2.1.2 <i>Bistable electroactive polymer</i> .....	22
2.1.3 <i>Bacterial cellulose</i> .....	23
2.1.4 <i>Bacterial cellulose reinforced BSEP composite</i> .....	24
2.2. Experimental section .....	25
2.2.1 <i>Raw materials</i> .....	25



2.2.2	<i>Preparation of BSEP prepolymer solution and thin film fabrication</i>	25
2.2.3	<i>Preparation of bacterial cellulose aerogel</i>	25
2.2.4	<i>Fabrication of BC-BSEP composite</i>	26
2.2.5	<i>Biocompatibility test for BC-BSEP composite</i>	26
2.3.	Results and discussion	27
2.3.1	<i>Composite fabrication design</i>	27
2.3.2	<i>Matrix modification of BSEP</i>	29
2.3.3	<i>BC-BSEP composite</i>	34
2.3.4	<i>Biocompatibility of BC-BSEP composite</i>	38
2.4.	Conclusion	40
2.5.	References	41
Chapter 3.	A DIELECTRIC ELASTOMER WITH HIGH STRAIN AND RAPID RESPONSE	44
3.1.	Background of this study	44
3.1.1	<i>Dielectric elastomer principles</i>	44
3.1.2	<i>Current DE technology and downfalls</i>	46
3.1.3	<i>New DE material with high performance</i>	46
3.2.	Experimental section	47
3.2.1	<i>Raw materials</i>	47
3.2.2	<i>Preparation of DE prepolymer solution and thin film fabrication</i>	47
3.2.3	<i>Dynamic mechanical analysis</i>	48
3.2.4	<i>Permittivity measurement</i>	48
3.2.5	<i>DE actuation measurement</i>	48
3.3.	Results and discussion	49
3.3.1	<i>Design principles of new DE materials</i>	49
3.3.2	<i>Permittivity determination of new DEs</i>	51
3.3.2	<i>Mechanical properties of new DEs</i>	52
3.3.3	<i>Static actuation performance of DEs</i>	53
3.3.4	<i>Cyclic actuation performance of DEs</i>	55
3.3.5	<i>Comparison of DEs to VHB<sup>TM</sup></i>	57
3.4.	Conclusion	58
3.5.	References	59

Chapter 4. SYNTHESIS AND COMPARISON OF THREE BAB TRIBLOCK COPOLYMERS FEATURING POLY (ETHYLENE GLYCOL) AND POLY (STEARYL ACRYLATE) USING RAFT POLYMERIZATION .....	62
4.1. Background of this study .....	62
4.1.1 Triblock copolymers .....	62
4.1.2 RAFT polymerization .....	63
4.1.3 Synthesized BAB triblock copolymers .....	64
4.2. Experimental section .....	64
4.2.1 Raw materials .....	64
4.2.2 Proton nuclear magnetic resonance ( $^1\text{H NMR}$ ) .....	64
4.2.3 Gel permeation chromatography (GPC) .....	65
4.2.4 Fourier transform infrared spectroscopy (FTIR) .....	65
4.2.5 Differential scanning calorimetry (DSC) .....	65
4.2.6 Dynamic mechanical analysis (DMA) .....	65
4.2.7 Scanning electron microscopy (SEM) .....	66
4.2.8 Synthesis of RAFT PEG chain transfer agent .....	66
4.2.9 Synthesis of PSA-PEG-PSA copolymer .....	67
4.3. Results and discussion .....	68
4.3.1 Proton nuclear magnetic resonance ( $^1\text{H NMR}$ ) .....	68
4.3.2 Gel permeation chromatography (GPC) .....	70
4.3.3 Fourier transform infrared spectroscopy (FTIR) .....	71
4.3.4 Differential scanning calorimetry (DSC) .....	74
4.3.5 Dynamic mechanical analysis (DMA) .....	75
4.3.3 Scanning electron microscopy (SEM) .....	78
4.4. Conclusion .....	79
4.5. References .....	80
Chapter 5. CONCLUSIONS AND FUTURE DIRECTIONS .....	82
5.1. Summary of the dissertation .....	82
5.2. Future directions .....	83

## LIST OF FIGURES

<b>Figure 1-1.</b> Stimuli-responsive systems found in nature. a) chameleons and b) muscles. Adopted from Ref 8.....	<b>2</b>
<b>Figure 1-2.</b> Variable stiffness polyacrylate with Diels-Alder bonds. a) Polyacrylate crosslinked by a thermo-reversible Diels-Alder reaction. b) Cyclic thermal treatment for modulus reversibility. Adopted from Ref 37.....	<b>3</b>
<b>Figure 1-3.</b> Shape memory polymer principles.....	<b>5</b>
<b>Figure 1-4.</b> a) Anthracene dimerization reaction. b) Coumarin dimerization reaction c) Thymine dimerization reaction. Adopted from Ref 40. d) Images of polymer film bending in different directions in response to irradiation from different angles of 366 nm light, then flattening with visible light longer than 540 nm with chemical structures of liquid crystalline monomers (mono-functional) and crosslinker (di-functional) used for light controllable photo-switching. Adopted from Ref 47 .....	<b>6</b>
<b>Figure 1-5.</b> Operating actuation principles of planar DEAs. Adopted from Ref 53.....	<b>7</b>
<b>Figure 1-6.</b> a) BSEP triggered by elevated temperature and electric field. Adopted from Ref 54. b) Cellulose polymer nanocomposites triggered by temperature and solvent. Adopted from Ref 57.....	<b>9</b>
<b>Figure 2-1.</b> Chemical structure and production of bacterial cellulose. Adopted from Ref 79.....	<b>24</b>
<b>Figure 2-2.</b> Fabrication process of the BC-BSEP composite material. ....	<b>29</b>
<b>Figure 2-3.</b> Storage modulus versus temperature of the BSEPs with transition temperature below, at, and above body temperature.....	<b>32</b>
<b>Figure 2-4.</b> Tensile stress-strain behavior of BSEPs in the soft state with different amount of CEA at 40 °C. ....	<b>33</b>

**Figure 2-5.** a) SEM images of the cross section from a BC-BSEP composite. b) A closer view of the cross section showing BC nanofibers deeply embedded in the BSEP matrix. ....34

**Figure 2-6.** Tensile stress-strain behavior of BC-BSEPs in the soft state with different filler content in water at 50 °C. ....35

**Figure 2-7.** Storage modulus comparison of BS-BSEP composites in the rigid (dry and low temperature) and soft (wet and high temperature) state. ....36

**Figure 2-8.** The storage modulus measurement of BC-BSEP-3 in room temperature-dry state, room temperature-wet state, high temperature-dry state, and high temperature-wet state. ....38

**Figure 2-9.** Representative fluorescent staining images of live (green) and dead (red) assay of NIH3T3 cells 3 days after cell seeding on BSEP matrix a) and BC-BSEP composite b). Scale bar = 100 μm. ....40

**Figure 3-1.** Dielectric elastomer actuator working principle. Adopted from Ref 53.....45

**Figure 3-2.** Mechanical properties of new DEs a) tensile stress-strain properties of four different formulations with four different diluents b) modulus as a function of temperature for AA(2.5) and P(10)-BA(13) c) tan delta as a function of temperature for AA(2.5) and P(10)-BA(13). ....52

**Figure 3-3.** a) Static actuation performance of four formulations with different diluent materials b) Images of dome shape formed when AA(2.5) is actuated at 4.5 kV. ....55

**Figure 3-4.** Frequency response of AA(2.5) and P(10)-BA(13) at 2 Hz .....56

**Figure 3-5.** a) Static actuation of AA(2.5) and P(10)-BA(13) compared to 300% biaxially prestretched VHB 4905. b) Comparison of the Maxwell pressure of AA(2.5) and P(10)-BA(13) to VHB 4905 300% biaxially prestretched. Information for VHB 4905 adopted from Ref 96.....58

<b>Figure 4-1.</b> Morphology of symmetrical amphiphilic BAB triblock copolymers in A-selecting solvent. Adopted from Ref 113 .....	<b>63</b>
<b>Figure 4-2.</b> DDMAT-PEG100K <sup>1</sup> H NMR in chloroform-d <sub>1</sub> .....	<b>68</b>
<b>Figure 4-3.</b> PSA50-PEG-PSA50 (red), PSA100-PEG-PSA100 (green), PSA200-PEG-PSA200 (blue) <sup>1</sup> HNMR in chloroform-d <sub>1</sub> .....	<b>69</b>
<b>Figure 4-4.</b> FTIR overlay of each synthesized triblock copolymer compared to PEG Mn=100,000 g/mol .....	<b>72</b>
<b>Figure 4-5.</b> a) Zoom in of FTIR for long chain alkyl peak from 3000-2600 cm <sup>-1</sup> b) Zoom in of FTIR carbonyl peak from 1770-1650 cm <sup>-1</sup> .....	<b>73</b>
<b>Figure 4-6.</b> Differential scanning calorimetry of synthesized triblock copolymers and PEG100K. ....	<b>75</b>
<b>Figure 4-7.</b> Modulus as a function of temperature for PSA100-PEG-PSA100 and PSA50-PEG-PSA50 with optical microscope images under polarized light at 10x magnification. ....	<b>77</b>
<b>Figure 4-8.</b> SEM images of a) PEG100K b) PSA50-PEG-PSA50 bulk material (left) and individual spherulites (right) c) PSA100-PEG-PSA100 bulk material (left) and individual spherulites (right) .....	<b>79</b>

## LIST OF TABLES

<b>Table 2-1.</b> Filler content of BC-BSEP composite and density of resulting aerogel from BC aqueous solution with different concentrations... ..	<b>28</b>
<b>Table 2-2.</b> Formulations of different BSEPs.....	<b>31</b>
<b>Table 3-1.</b> Chemical structures of formulation components and materials selection of new DE polymer materials.....	<b>51</b>
<b>Table 4-1.</b> Gel permeation chromatography results for PSA <sub>x</sub> -PEG-PSA <sub>x</sub> .....	<b>51</b>
<b>Table 4-2.</b> Average DMA results for PSA <sub>x</sub> -PEG-PSA <sub>x</sub> .....	<b>51</b>

## LIST OF EQUATIONS

<b>Equation 3-1.</b> Maxwell stress of a dielectric elastomer .....	<b>44</b>
<b>Equation 3-2.</b> Energy density of a dielectric elastomer .....	<b>45</b>
<b>Equation 3-3.</b> Relative permittivity derived from capacitance equation .....	<b>48</b>
<b>Equation 3-4.</b> Surface area of a dome used for calculating area strain .....	<b>49</b>
<b>Equation 4-1.</b> RAFT polymerization prediction model .....	<b>71</b>
<b>Equation 4-2.</b> Example of theoretical prediction for PSA100-PEG-PSA100 .....	<b>71</b>

## LIST OF SCHEMES

<b>Scheme 4-1.</b> Synthetic process for PEG-based macro-RAFT chain transfer agent, DDMAT-PEG .....	<b>67</b>
<b>Scheme 4-2.</b> Synthetic process for BAB Triblock PSA <sub>x</sub> -PEG-PSA <sub>x</sub> .....	<b>67</b>

## ACKNOWLEDGEMENTS

I would like to give thanks to my adviser, Professor Qibing Pei, for his advice and financial support during my Ph.D. studies. Professor Pei has provided inspiration and guidance for research projects, as well as taught me how to think and work in a scientific way.

Also, I would like to thank Professor Ximin He, Professor Yu Huang, and Professor Andrea Kasko for serving as my committee members and their comments.

I would like to acknowledge the Department of Defense for supporting my research through the National Defense Science and Engineering Graduate Fellowship for 3 years. Additional support came from DARPA SHRIMP Initiative and NSF National Robotics Initiative.

I would like to acknowledge the co-authors, Yu Qiu, Fangyi Guan, Zihang Peng, Weikin Xiao, and Qibing Pei, of Chapter 2, which is adapted with permission from “Dual-Stimuli-Responsive Polymer Composite with Ultrawide Tunable Stiffness Range Triggered by Water and Temperature”. *ACS Applied Polymer Materials*, 2020, 2 (5), 2008–2015. <https://doi.org/10.1021/acspm.0c00181>. Copyright 2020 American Chemical Society.

I would like to especially thank Dr. Ye Shi, Dr. Jake Hajagos, Dr. David Kishpaugh, Dr. Yuan Meng, and Dr. Wei Hu for their guidance in research and helping me gain fundamental skills in a laboratory setting. Without their training, my research could not have progressed in the way it did. I would also like to give my thanks to Mr. Roshan Plamthottam and Mr. Kareem Youssef who were always there to bounce ideas off and have in-depth discussions. Thank you all for being supportive. Additionally, I would like to thank my group members Mr. Jason (Zhixin) Xie, Dr. Roger (Hongxiang) Zhao, Dr. Yu Xie, Dr. Ziyang Zhang, Mr. Hexing Yin, Ms. Zihang Peng, Ms. Jianghan Wu, Mr. Jiacheng Fan, Mr. Hao Yu, Dr. Meng Gao, Ms. Fangyi Guan. I would thank Ms. Mikayla Klein and Ms. Daniela Marques for working with me as

undergraduates in my first few years of graduate school. Your company and positive energy was a driving force. I would also like to thank Mr. Nick Sebastiani and Mr. Alex Cheng for working together with me in Chapter 4. All your support in my research has made it better and more enjoyable.

A big thanks to my husband, Mr. Brian Zutter, for always being there and supporting me throughout my undergraduate and graduate career. I want to thank my family, Mr. Paul Askounis, Ms. Marilyn Francesco, and Mr. Devin Askounis for their support and encouragement. Special thanks to my amazing dog, Buggy, for his undying affection and love during my studies.



## VITA

2015

B. S.

Chemistry with Minor in Mathematics,

Northeastern University

### Publications

Qiu, Y\*.; **Askounis, E.\***; Guan, F.; Peng, Z.; Xiao, W.; Pei, Q. (2020) Dual-Stimuli-Responsive Polymer Composite with Ultrawide Tunable Stiffness Range Triggered by Water and Temperature. *ACS Applied Polymer Materials*, 2 (5), 2008–2015. \* These authors contribute equally to this work.

Wang, L., Yang, Y., Chen, Y., Majidi, C., Iida, F., **Askounis, E.**, and Pei, Q. (2018). Controllable and Reversible Tuning of Material Rigidity for Robot Applications. *Materials Today* 21: 563–576.

Ghabbour, E. A.; Davies, G.; Misiewicz, T.; Alami, R. A.; **Askounis, E. M.**; Cuozzo, N. P.; Filice, A. J.; Haskell, J. M.; Moy, A. K.; Roach, A. C.; Shade, J. (Elsevier, 2017) National Comparison of the Total and Sequestered Organic Matter Contents of Conventional and Organic Farm Soils. *Advances in Agronomy* Vol. 146, pp 1–35.

Hu, W., Ren, Z., Li, J., **Askounis, E.**, Xie, Z. and Pei, Q. (2015). New Dielectric Elastomers with Variable Moduli. *Advanced Functional Materials* 25: 4827–4836.

# Chapter 1. Introduction and Dissertation Objectives

## 1.1. An overview of stimuli- responsive polymers

Quintessential polymer materials, such as polyethylene or polyurethane, are synthesized and designed for fixed mechanical, thermal, and photo properties, for utilization defined by specific applications. Polyethylene is ubiquitous, found in biomedical implants, sealants, packaging, and many other applications<sup>1-3</sup>. Polyurethanes are used as insulation, adhesives, and fibers.<sup>4,5</sup> These materials have set purposes and are designated for use in static, stationary applications that require motionless, set parameters and properties. In some applications, however, properties controlled or activated by external triggers are desired for materials used in varying working conditions such as soft robotics, biomedicine, or wearable electronics.<sup>6-9</sup>

Stimuli- responsive materials change properties when an internal or external trigger is applied, such as light, heat, or electric fields. Several stimuli-responsive systems are seen in nature from the chameleon responding to its surroundings to human muscle (Fig. 1-1). These materials represent an enormous field of research with applications spanning across all platforms. Synthetic stimuli-responsive materials can utilize dynamic bonding or phase-change as tools to control crosslink density or polymer architectures for a resulting change in physical properties.<sup>10</sup> The overall chemical structure is dependent on the stimulus chosen or the application. Stimuli-responsive materials are often used for biomedical applications in targeted drug delivery systems,<sup>11-14</sup> and engineered tissues scaffolds,<sup>15-17</sup> triggered by light,<sup>18-21</sup> heat,<sup>22-24</sup> electric/magnetic fields,<sup>25,26</sup> and many more.<sup>27-30</sup> They can also be used in robotics for actuation,<sup>8,31</sup> locomotion<sup>32-34</sup> or even autonomous deployment.<sup>35</sup>

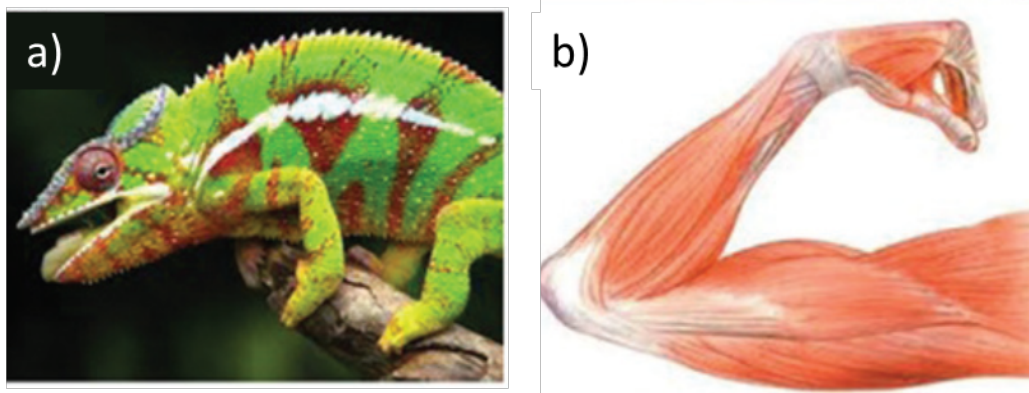


Figure 1-1. Stimuli-responsive systems found in nature, a) chameleons and b) muscles. Adopted from Ref 8.

## 1.2. Thermo-responsive materials

Thermo-responsive materials are one of the largest categories of stimuli responsive materials due to the rapid response, ease of fabrication and ease of design. Many dynamic bonds are triggered by thermal response, such as Diels-Alder bonding or hydrogen bonding, but additionally, polymer materials can be designed to undergo phase changes with elevated temperatures, such as shape memory polymers. Rather than using dynamic covalent or secondary bonding, targeted polymer crystalline domains melt to change the physical and mechanical properties of the material.

### 1.2.1. Thermo-responsive dynamic bonds

Stimuli-responsive materials triggered by temperature can be designed by using thermo-responsive dynamic bonding for controlling crosslink density or polymer architecture. Several examples of this exist, but Diels-Alder (DA) bonding between furan/maleimide moieties have been extensively studied for their self-healing properties and tunable stiffness.<sup>36, 37</sup> DA bonds undergo a [4+2] cycloaddition involving a diene and dienophile, furan and maleimide are typically used in thermally reversible applications due to the mild reaction temperature. The Wudl group exploited this attribute to improve capabilities and

mechanical properties of self-healing materials by synthesizing a tetra-functional furan monomer and tri-functional maleimide monomer for a macromolecular network formed entirely of thermally reversible bonds.<sup>38</sup> The reversibility of Diels-Alder reactions can also be used to control stiffness of materials. Hu et al established a material with thermally reversible modulus controlled by the concentration of Diels-Alder moieties for a polyacrylate-based reversibly crosslinked polymer with variable stiffness (Fig. 1-2a). The DA adduct is repeatedly formed and broken for controlled crosslink density and variable elastic modulus. Initially, the DA adduct is fully formed, as synthesized. The material is heated at 130 °C to break the DA bonds and soften the polymer. The polymer is heated once again at 80 °C to reform the adduct and stiffen the material for a variable stiffness range from 0.17 MPa (DA adducts broken) to 0.52 MPa (DA adduct present) (Fig. 1-2b).

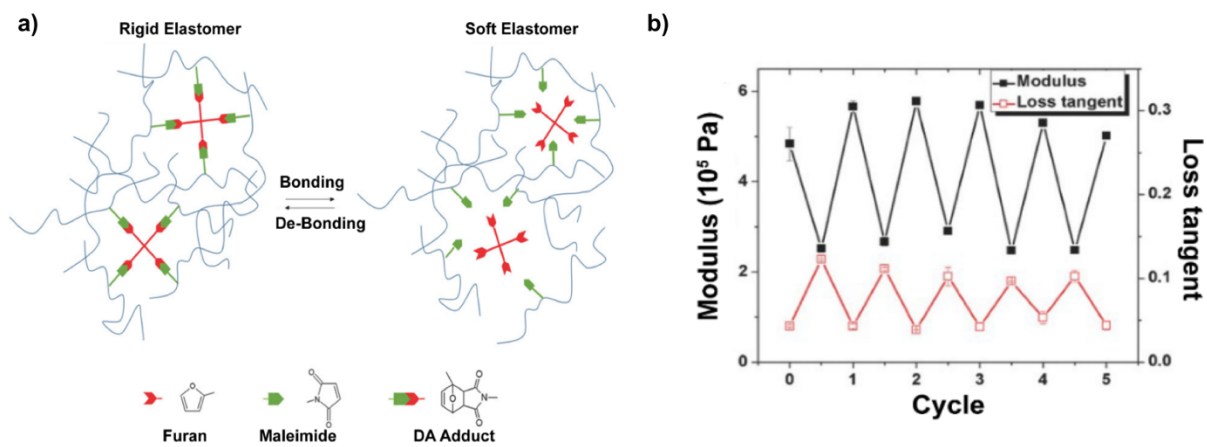


Figure 1-2. Variable stiffness polyacrylate with Diels-Alder bonds. a) Polyacrylate crosslinked by a thermo-reversible Diels-Alder reaction. b) Cyclic thermal treatment for modulus reversibility. Adopted from Ref 37.

### 1.2.2. *Shape memory polymers*

Shape memory polymers (SMPs), a large class of stimuli-responsive materials, are polymers that can deform into temporarily fixed, strained, non-equilibrium shapes. The fixed shape comes about when strong-intermolecular interactions between polymer chains overcomes restoring forces allowing for shape fixture. Energy is stored within the material until triggered, usually by heating, to revert to the permanent equilibrium state. The general principal is outline in Figure 1-3 showing the stiff material at room temperature, heated above a transition temperature ( $T_{\text{trans}}$ ), formed or shaped, cooled below the transition temperature, to freeze the molded form, then heated again to revert to the original, programmed shape. Typically, these materials are block-copolymers or elastomers controlled by dynamic bonding or cooling into a crystalline or glassy state to ensure shape fixture. Block co-polymer SMPs must have covalently bonded copolymers with a soft block, low transition temperature ( $T_{\text{trans}}$ ) and a hard block, with high  $T_{\text{trans}}$ . When heated, the soft block melts while the hard block remains stiff, preventing a full melt, but allowing for flexibility to form a shape. For this reason, semi-crystalline elastomer materials are typically used, for elastic properties above  $T_{\text{trans}}$ , and stiff below the transition temperature. One example of this, presented by Meng and company, describes a body temperature triggered shape memory polymer that changes stiffness when heated. The transition temperature is adjusted by changing the size of the crosslinker in the poly (caprolactone) (PCL) network. The storage modulus of the PCL network when heated at body temperature changed from 650 MPa at room temperature to around 40 MPa at body temperature.<sup>39</sup>

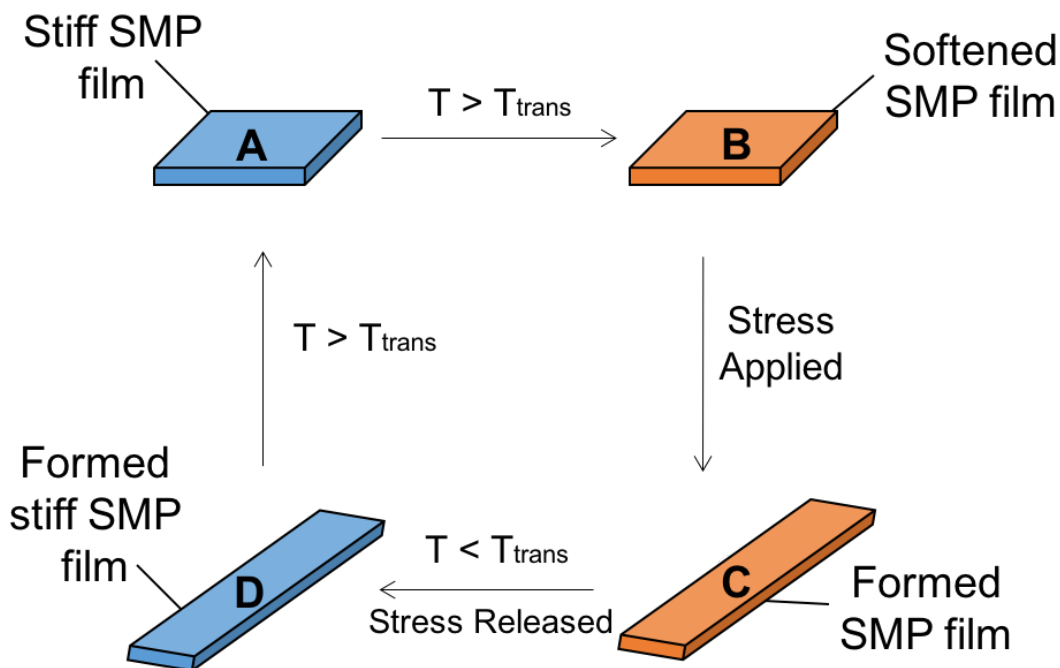


Figure 1-3. Shape memory polymer principles

### 1.3. Photo-responsive materials

Photo-response is an attractive sub-class of stimuli-responsive materials due to the non-destructive nature of light and the allowance for remote, localized activation. Additionally, reactions can be conducted at room temperature and often in the solid-state.<sup>40</sup> These materials can be designed to induce shape change<sup>17, 41</sup> or drug delivery<sup>20</sup> and in some cases these changes are reversible<sup>42, 43</sup>. Mechanisms for reversible photo-response typically utilize dynamic bonds, such as azo-benzenes or moieties that undergo dimerization, such as anthracene, which undergoes a  $[4\pi+4\pi]$  cycloaddition,<sup>42</sup> thymine<sup>44, 45</sup>, or coumarin<sup>43, 46</sup> which undergo  $[2\pi+2\pi]$  cycloadditions (Fig. 1-4a-c). One such example uses azobenzene, which upon radiation, reversibly undergoes *cis-trans* isomerization. This small change in form and ordering results in a volume contraction thereby converting light energy into mechanical energy. Combining a mono-functional azo-benzene monomer with an azo-benzene-containing crosslinker (Fig. 1-4d) results in a highly crosslinked film that will change shape upon exposure to different wavelengths of light. As

fabricated, the azo-benzene moieties within the film are in the *trans* conformation, but when exposed to long wave UV (356 nm), the azo bond isomerizes to the *cis* conformation. This causes a molecular disordering to occur, resulting in a macroscopic volume contraction of the film. The *cis-trans* isomerization is reversed by exposure to visible light (over 540 nm), resulting in the macroscopic flattening of the film (Fig. 1-3d).<sup>47</sup>

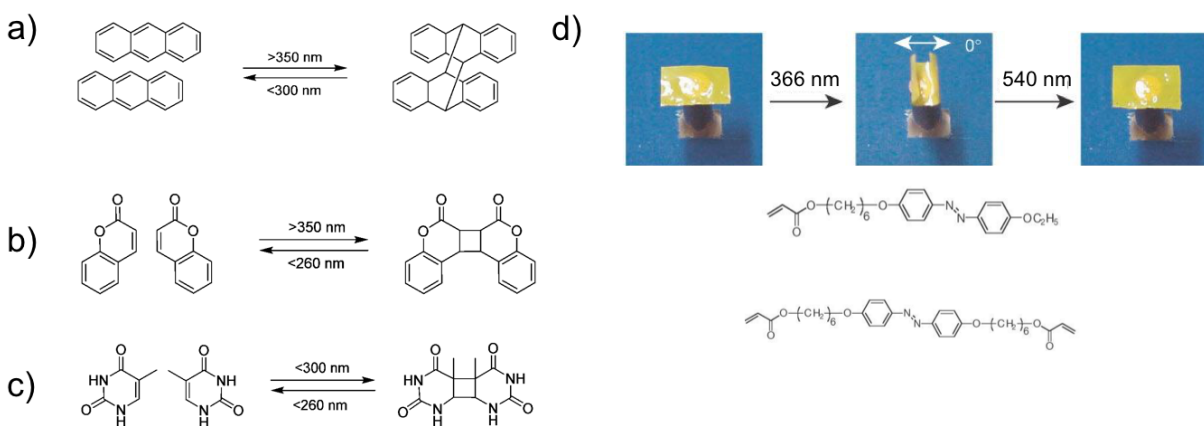


Figure 1-4. a) Anthracene dimerization reaction. b) Coumarin dimerization reaction. c) Thymine dimerization reaction. Adopted from Ref 40. d) Images of polymer film bending in different directions in response to irradiation from different angles of 366 nm light, then flattening with visible light longer than 540 nm with chemical structures of liquid crystalline monomers (mono-functional) and crosslinker (di-functional) used for light controllable photo-switching. Adopted from Ref 47.

#### 1.4. Electro-responsive materials

Electro-responsive materials change their physical properties upon application of an electrical stimulus or electric field. Electro-responsive materials are of particular interest due to the convenience of applying an electric field, tunability afforded by electric fields, and their particular use in sensing and actuation.

Electro-responsive materials include ionic types such as conducting polymers,<sup>48, 49</sup> ionic polymers,<sup>25, 50</sup> and electronic type such as dielectric elastomers.<sup>26, 51</sup>

#### 1.4.1. Dielectric elastomers

Dielectric elastomers (DEs) are low modulus crosslinked polymers that act as flexible capacitors when sandwiched between two compliant electrodes. When a voltage is applied, the opposite charges on the electrodes attract towards each other, compressing the polymer. Due to the incompressible nature of the material, when a voltage is applied and an electric field is generated, the material expands outward (Fig. 1-5). By this mechanism, DEs can expand and contract in response to an applied electric field.<sup>52</sup> DE actuators (DEA) can exhibit large strains, large stresses, fast response speeds, good reliability, and high energy density. The Clarke and Wood groups were able to achieve controlled flight of a microrobot powered by silicone based dielectric elastomers. They achieved lift-off of 23 cm by actuating a bi-layer silicone elastomer at 300 Hz with applied voltage of 1.3 kV.<sup>34</sup>

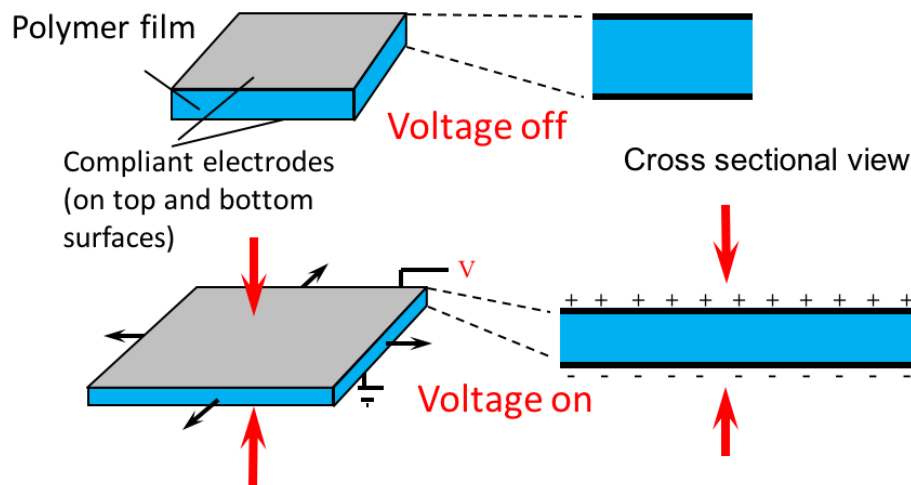


Figure 1-5. Operating actuation principles of planar DEAs. Adopted from Ref 53.



## 1.5 Dual responsive materials systems

Dual or multi-responsive polymers have been considered advanced smart materials because of their applications in the fields of biomedicine and sensors. Using multiple stimuli can widen the applications of stimuli-responsive materials and amplify physical or chemical changes. One such example is the bistable electroactive polymer (BSEP) which combines shape memory polymer thermo-response with that of dielectric elastomer electro-response.<sup>54</sup> The BSEP is stiff at room temperature, can be heated past a transition temperature to become a soft polymer. This rigid to soft transition exhibits a stiffness change of about 3,000x, making BSEP a very useful variable stiffness material.<sup>54,55</sup> Once softened, it can be actuated as a dielectric elastomer, then cooled back below the transition temperature to “freeze” the actuated state. Heated once more, it will revert to the original form (Fig. 1-6a). These materials exhibit rigid-to-rigid actuation with a narrow temperature transition band for rapid heating.<sup>54</sup> One of the most notable applications is in tactile displays.<sup>55</sup>

Another material that utilizes dual-response is cellulose polymer nanocomposites. These materials exhibit variable stiffness by the reversible reinforcement effect of cellulose percolating networks. Cellulose fibers are strongly bonded together by hydrogen bonds. When used as a filler material, they offer strong mechanical reinforcement. These bonds can be reversibly controlled by the addition of water or other polar solvent, at which point the filler-to-filler interaction is broken in favor of filler-solvent interaction. By utilizing cellulose nanofibers as a filler material within a phase-changing, thermally responsive polymer matrix, such as poly (vinyl acetate) (PVAc),<sup>56</sup> the composite changes stiffness with both temperature and water. The PVAc composites exhibit modulus change from 5.3 GPa at room temperature to 12.7 MPa at elevated temperature, in water. Both dual-stimuli responsive materials exhibit unique properties that can be useful in biomedicine or actuators.

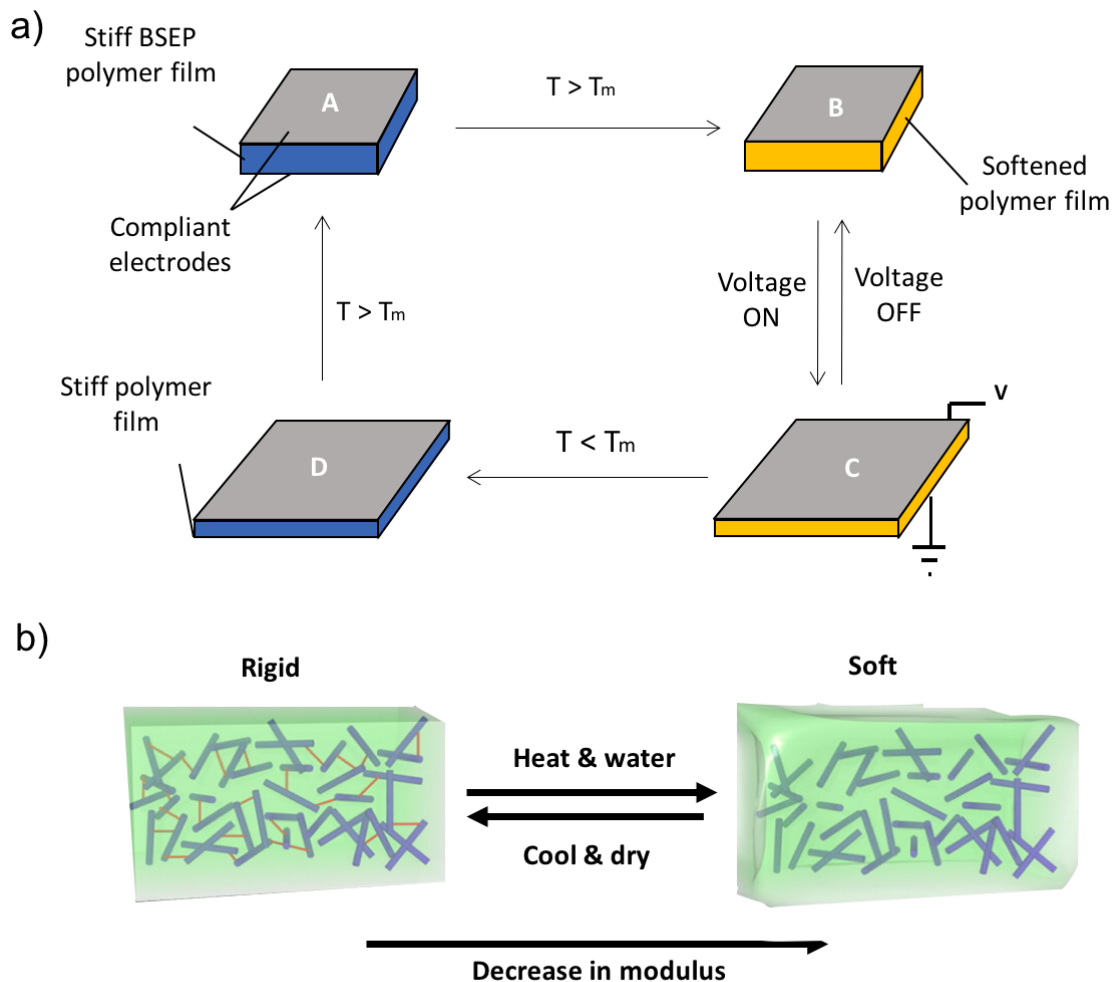


Figure 1-6. a) BSEP triggered by elevated temperature and electric field. Adopted from Ref 54. b) Cellulose polymer nanocomposites triggered by temperature and solvent. Adopted from Ref 57.

## 1.6 Motivation of this dissertation

Stimuli responsive materials exist over an extremely wide range of applications with varying trigger mechanisms. One important area of focus is variable stiffness polymers (VSPs). Synthetic variable stiffness materials exhibit stiffness changes using dynamic bonds, external addition of soft media, or phase transitions. Exploiting previously studied mechanisms to fabricate new materials for improved response

speed and improved stiffness change is beneficial to widen the application range of VSPs. A material that can change stiffness from GPa range, ensuring structural support and load bearing, down to kPa range, modulus range of many biomaterials and tissues, could be used in biomedical implant applications. Typically, materials with stiffness in the kPa range are hydrogels with low mechanical strength. Thus, there is a need to develop new VSPs or improve current VSPs for wider tunable stiffness range from rigid to soft regions, while maintaining high mechanical strength. Thus, a VSP materials with an ultra-wide temperature range must be developed.

Current high-performance dielectric elastomer (DE) materials are based on commercial films, e.g. VHB™ acrylate adhesive films, or resins, e.g., silicone elastomers, that are manufactured for unrelated applications.<sup>58-61</sup> The VHB™ films require high-strain pretretching to achieve the high actuation performance, are viscoelastic, and lack the processing flexibility essential for many applications that require high actuation force and work output.<sup>62,63</sup> Silicone elastomers, have low viscoelasticity but exhibit lower maximum strains and energy density due to their low maximum stable operable field.<sup>64</sup> Despite efforts to improve these materials, the field remains reliant upon prestretching to exhibit high strain in acrylic elastomers, and rapid response in silicone elastomers. Thus, a new DE that does not require prestretching with that exhibits high performance actuation with rapid response, is needed for further development of dielectric elastomer actuators.

Lastly, suitable synthesis and fabrication methods are required to best utilize the variable stiffness properties of VSPs. Previously mentioned bistable electroactive polymers (BSEP), require a random, bulk polymerization mechanism that leaves much up to chance, with difficulty controlling molecular architectures and limiting materials processability, due to the crosslinked nature. BSEP materials show a

wide stiffness range that can be beneficial in many applications, such as actuators or sensors. By developing a controlled synthetic approach to the fabrication of these materials, BSEP can be finely tuned for wide stiffness change, transition temperature, and actuation performance with the processability afforded to linear polymers.

## **1.7 Scope and layout of the dissertation**

This dissertation consists of five chapters.

Chapter 1 gives an introduction into stimuli responsive polymer materials outlining the importance and broad range of applications of these materials. This is followed by an explanation of several different types of trigger mechanisms divided into thermo-responsive, photo-responsive, electro-responsive, and dual-responsive materials. These sections will correspond to other chapters.

Chapter 2 presents the development of a variable stiffness composite material using a modified BSEP matrix and bacterial cellulose microfibrils. The composite combines temperature-responsive phase changing BSEP with reversible water-responsive reinforcement of cellulose filler. The material exhibits an ultra-wide modulus differential from 1 GPa down to 40 kPa stimulated by water and temperature. An ultra-wide modulus range allows for further applications development with potential for biomedical implant devices.

Chapter 3 presents a new dielectric elastomer material that exhibits performance similar to commercially available materials without prestretching. The new DE exhibited maximum actuation strains near 200% with energy density of  $3.5 \text{ J/cm}^3$  and rapid response over 100% strain at 2 Hz. The new DE material

exhibits performance higher than other synthetic dielectric elastomer and opens the door for the next generation of polymer actuator materials.

Chapter 4 outlines a multiblock copolymer thermoplastic elastomer as a bistable electroactive polymer. Three BAB triblock copolymers of different lengths were synthesized for use as a bistable electroactive polymer with reversible variable stiffness and a controlled synthetic pathway using RAFT polymerization. This material is then characterized by <sup>1</sup>H NMR, GPC, FTIR, DSC, DMA, and SEM.

Chapter 5 summarizes each chapter and discusses the potential directions of each project.

## 1.8 References

- (1) Kurtz, S. M. The Clinical Performance of Historical and Conventional UHMWPE in Hip Replacements. In *UHMWPE Biomaterials Handbook*; Elsevier, 2016; pp 45–56. <https://doi.org/10.1016/B978-0-323-35401-1.00005-3>.
- (2) Jeremic, D. Polyethylene. In *Ullmann's Encyclopedia of Industrial Chemistry*; Wiley-VCH Verlag GmbH & Co. KGaA, Ed.; Wiley-VCH Verlag GmbH & Co. KGaA: Weinheim, Germany, 2014; pp 1–42. [https://doi.org/10.1002/14356007.a21\\_487.pub3](https://doi.org/10.1002/14356007.a21_487.pub3).
- (3) Ji, L. N. Study on Preparation Process and Properties of Polyethylene Terephthalate (PET). *Appl. Mech. Mater.* **2013**, *312*, 406–410. <https://doi.org/10.4028/www.scientific.net/AMM.312.406>.
- (4) Seymour, R. B.; Kauffman, G. B. Polyurethanes: A Class of Modern Versatile Materials. *J. Chem. Educ.* **1992**, *69* (11), 909. <https://doi.org/10.1021/ed069p909>.

- (5) Delebecq, E.; Pascault, J.-P.; Boutevin, B.; Ganachaud, F. On the Versatility of Urethane/Urea Bonds: Reversibility, Blocked Isocyanate, and Non-Isocyanate Polyurethane. *Chem. Rev.* **2013**, *113* (1), 80–118. <https://doi.org/10.1021/cr300195n>.
- (6) Stuart, M. A. C.; Huck, W. T. S.; Genzer, J.; Müller, M.; Ober, C.; Stamm, M.; Sukhorukov, G. B.; Szleifer, I.; Tsukruk, V. V.; Urban, M.; Winnik, F.; Zauscher, S.; Luzinov, I.; Minko, S. Emerging Applications of Stimuli-Responsive Polymer Materials. *Nat. Mater.* **2010**, *9* (2), 101–113. <https://doi.org/10.1038/nmat2614>.
- (7) Gao, Y.; Wei, M.; Li, X.; Xu, W.; Ahiabu, A.; Perdiz, J.; Liu, Z.; Serpe, M. J. Stimuli-Responsive Polymers: Fundamental Considerations and Applications. *Macromol. Res.* **2017**, *25* (6), 513–527. <https://doi.org/10.1007/s13233-017-5088-7>.
- (8) Hu, L.; Zhang, Q.; Li, X.; Serpe, M. J. Stimuli-Responsive Polymers for Sensing and Actuation. *Mater. Horiz.* **2019**, *6* (9), 1774–1793. <https://doi.org/10.1039/C9MH00490D>.
- (9) Wei, M.; Gao, Y.; Li, X.; Serpe, M. J. Stimuli-Responsive Polymers and Their Applications. *Polym. Chem.* **2017**, *8* (1), 127–143. <https://doi.org/10.1039/C6PY01585A>.
- (10) Wojtecki, R. J.; Meador, M. A.; Rowan, S. J. Using the Dynamic Bond to Access Macroscopically Responsive Structurally Dynamic Polymers. *Nat. Mater.* **2011**, *10* (1), 14–27. <https://doi.org/10.1038/nmat2891>.
- (11) Mura, S.; Nicolas, J.; Couvreur, P. Stimuli-Responsive Nanocarriers for Drug Delivery. *Nat. Mater.* **2013**, *12* (11), 991–1003. <https://doi.org/10.1038/nmat3776>.
- (12) Tagami, T.; Foltz, W. D.; Ernsting, M. J.; Lee, C. M.; Tannock, I. F.; May, J. P.; Li, S.-D. MRI Monitoring of Intratumoral Drug Delivery and Prediction of the Therapeutic Effect with a Multifunctional Thermosensitive Liposome. *Biomaterials* **2011**, *32* (27), 6570–6578. <https://doi.org/10.1016/j.biomaterials.2011.05.029>.

- (13) Al-Ahmady, Z. S.; Al-Jamal, W. T.; Bossche, J. V.; Bui, T. T.; Drake, A. F.; Mason, A. J.; Kostarelos, K. Lipid–Peptide Vesicle Nanoscale Hybrids for Triggered Drug Release by Mild Hyperthermia *in Vitro* and *in Vivo*. *ACS Nano* **2012**, *6* (10), 9335–9346.  
<https://doi.org/10.1021/nn302148p>.
- (14) Donnelly, R. F.; Singh, T. R. R.; Garland, M. J.; Migalska, K.; Majithiya, R.; McCrudden, C. M.; Kole, P. L.; Mahmood, T. M. T.; McCarthy, H. O.; Woolfson, A. D. Hydrogel-Forming Microneedle Arrays for Enhanced Transdermal Drug Delivery. *Adv. Funct. Mater.* **2012**, *22* (23), 4879–4890. <https://doi.org/10.1002/adfm.201200864>.
- (15) Lutolf, M. P.; Hubbell, J. A. Synthetic Biomaterials as Instructive Extracellular Microenvironments for Morphogenesis in Tissue Engineering. *Nat. Biotechnol.* **2005**, *23* (1), 47–55. <https://doi.org/10.1038/nbt1055>.
- (16) Han, L.-H.; Lai, J. H.; Yu, S.; Yang, F. Dynamic Tissue Engineering Scaffolds with Stimuli-Responsive Macroporosity Formation. *Biomaterials* **2013**, *34* (17), 4251–4258.  
<https://doi.org/10.1016/j.biomaterials.2013.02.051>.
- (17) Käpylä, E.; Delgado, S. M.; Kasko, A. M. Shape-Changing Photodegradable Hydrogels for Dynamic 3D Cell Culture. *ACS Appl. Mater. Interfaces* **2016**, *8* (28), 17885–17893.  
<https://doi.org/10.1021/acsami.6b05527>.
- (18) Hardy, J. G.; Larrañeta, E.; Donnelly, R. F.; McGoldrick, N.; Migalska, K.; McCrudden, M. T. C.; Irwin, N. J.; Donnelly, L.; McCoy, C. P. Hydrogel-Forming Microneedle Arrays Made from Light-Responsive Materials for On-Demand Transdermal Drug Delivery. *Mol. Pharm.* **2016**, *13* (3), 907–914. <https://doi.org/10.1021/acs.molpharmaceut.5b00807>.

- (19) Chen, M.-C.; Lin, Z.-W.; Ling, M.-H. Near-Infrared Light-Activatable Microneedle System for Treating Superficial Tumors by Combination of Chemotherapy and Photothermal Therapy. *ACS Nano* **2016**, *10* (1), 93–101. <https://doi.org/10.1021/acsnano.5b05043>.
- (20) Griffin, D. R.; Schlosser, J. L.; Lam, S. F.; Nguyen, T. H.; Maynard, H. D.; Kasko, A. M. Synthesis of Photodegradable Macromers for Conjugation and Release of Bioactive Molecules. *Biomacromolecules* **2013**, *14* (4), 1199–1207. <https://doi.org/10.1021/bm400169d>.
- (21) Griffin, D. R.; Kasko, A. M. Photoselective Delivery of Model Therapeutics from Hydrogels. *ACS Macro Lett.* **2012**, *1* (11), 1330–1334. <https://doi.org/10.1021/mz300366s>.
- (22) Chilkoti, A.; Dreher, M. R.; Meyer, D. E.; Raucher, D. Targeted Drug Delivery by Thermally Responsive Polymers. *Adv. Drug Deliv. Rev.* **2002**, *54* (5), 613–630. [https://doi.org/10.1016/S0169-409X\(02\)00041-8](https://doi.org/10.1016/S0169-409X(02)00041-8).
- (23) Klouda, L.; Mikos, A. G. Thermoresponsive Hydrogels in Biomedical Applications. *Eur. J. Pharm. Biopharm.* **2008**, *68* (1), 34–45. <https://doi.org/10.1016/j.ejpb.2007.02.025>.
- (24) Tang, L.; Liu, W.; Liu, G. High-Strength Hydrogels with Integrated Functions of H-Bonding and Thermoresponsive Surface-Mediated Reverse Transfection and Cell Detachment. *Adv. Mater.* **2010**, *22* (24), 2652–2656. <https://doi.org/10.1002/adma.200904016>.
- (25) Keplinger, C.; Sun, J.-Y.; Foo, C. C.; Rothmund, P.; Whitesides, G. M.; Suo, Z. Stretchable, Transparent, Ionic Conductors. *Science* **2013**, *341* (6149), 984–987. <https://doi.org/10.1126/science.1240228>.
- (26) Shankar, R.; Ghosh, T. K.; Spontak, R. J. Dielectric Elastomers as Next-Generation Polymeric Actuators. *Soft Matter* **2007**, *3* (9), 1116. <https://doi.org/10.1039/b705737g>.



- (27) Mitsumata, T.; Okazaki, T. Magnetization-Induced Reduction in Dynamic Modulus of Polyurethane Elastomers Loaded with Ferrite. *Jpn. J. Appl. Phys.* **2007**, *46* (7A), 4220–4224. <https://doi.org/10.1143/JJAP.46.4220>.
- (28) Davis, D. A.; Hamilton, A.; Yang, J.; Cremar, L. D.; Van Gough, D.; Potisek, S. L.; Ong, M. T.; Braun, P. V.; Martínez, T. J.; White, S. R.; Moore, J. S.; Sottos, N. R. Force-Induced Activation of Covalent Bonds in Mechanoresponsive Polymeric Materials. *Nature* **2009**, *459* (7243), 68–72. <https://doi.org/10.1038/nature07970>.
- (29) Du, J.-Z.; Du, X.-J.; Mao, C.-Q.; Wang, J. Tailor-Made Dual PH-Sensitive Polymer–Doxorubicin Nanoparticles for Efficient Anticancer Drug Delivery. *J. Am. Chem. Soc.* **2011**, *133* (44), 17560–17563. <https://doi.org/10.1021/ja207150n>.
- (30) Han, X.-J.; Dong, Z.-Q.; Fan, M.-M.; Liu, Y.; li, J.-H.; Wang, Y.-F.; Yuan, Q.-J.; Li, B.-J.; Zhang, S. PH-Induced Shape-Memory Polymers. *Macromol. Rapid Commun.* **2012**, *33* (12), 1055–1060. <https://doi.org/10.1002/marc.201200153>.
- (31) Zhang, Q. M.; Serpe, M. J. Stimuli-Responsive Polymers for Actuation. *ChemPhysChem* **2017**, *18* (11), 1451–1465. <https://doi.org/10.1002/cphc.201601187>.
- (32) Jin, B.; Song, H.; Jiang, R.; Song, J.; Zhao, Q.; Xie, T. Programming a Crystalline Shape Memory Polymer Network with Thermo- and Photo-Reversible Bonds toward a Single-Component Soft Robot. *Sci. Adv.* **2018**, *4* (1), eaao3865. <https://doi.org/10.1126/sciadv.aao3865>.
- (33) Firouzeh, A.; Salerno, M.; Paik, J. Stiffness Control With Shape Memory Polymer in Underactuated Robotic Origamis. *IEEE Trans. Robot.* **2017**, *33* (4), 765–777. <https://doi.org/10.1109/TRO.2017.2692266>.

- (34) Chen, Y.; Zhao, H.; Mao, J.; Chirarattananon, P.; Helbling, E. F.; Hyun, N. P.; Clarke, D. R.; Wood, R. J. Controlled Flight of a Microrobot Powered by Soft Artificial Muscles. *Nature* **2019**, *575* (7782), 324–329. <https://doi.org/10.1038/s41586-019-1737-7>.
- (35) Wehner, M.; Truby, R. L.; Fitzgerald, D. J.; Mosadegh, B.; Whitesides, G. M.; Lewis, J. A.; Wood, R. J. An Integrated Design and Fabrication Strategy for Entirely Soft, Autonomous Robots. *Nature* **2016**, *536* (7617), 451–455. <https://doi.org/10.1038/nature19100>.
- (36) Liu, Y.-L.; Chuo, T.-W. Self-Healing Polymers Based on Thermally Reversible Diels–Alder Chemistry. *Polym. Chem.* **2013**, *4* (7), 2194. <https://doi.org/10.1039/c2py20957h>.
- (37) Hu, W.; Ren, Z.; Li, J.; Askounis, E.; Xie, Z.; Pei, Q. New Dielectric Elastomers with Variable Moduli. *Adv. Funct. Mater.* **2015**, *25* (30), 4827–4836. <https://doi.org/10.1002/adfm.201501530>.
- (38) Chen, X.; Dam, M.; Ono, K.; Mal, A.; Shen, H.; Nutt, S. R.; Sheran, K.; Wudl, F. A Thermally Re-Mendable Cross-Linked Polymeric Material. *Science* **2002**, *295* (5560), 1698–1702. <https://doi.org/10.1126/science.1065879>.
- (39) Meng, Y.; Jiang, J.; Anthamatten, M. Body Temperature Triggered Shape-Memory Polymers with High Elastic Energy Storage Capacity. *J. Polym. Sci. Part B Polym. Phys.* **2016**, *54* (14), 1397–1404. <https://doi.org/10.1002/polb.23990>.
- (40) Kaur, G.; Johnston, P.; Saito, K. Photo-Reversible Dimerisation Reactions and Their Applications in Polymeric Systems. *Polym Chem* **2014**, *5* (7), 2171–2186. <https://doi.org/10.1039/C3PY01234D>.
- (41) Kloxin, A. M.; Kasko, A. M.; Salinas, C. N.; Anseth, K. S. Photodegradable Hydrogels for Dynamic Tuning of Physical and Chemical Properties. *Science* **2009**, *324* (5923), 59–63. <https://doi.org/10.1126/science.1169494>.

- (42) Froimowicz, P.; Frey, H.; Landfester, K. Towards the Generation of Self-Healing Materials by Means of a Reversible Photo-Induced Approach. *Macromol. Rapid Commun.* **2011**, *32* (5), 468–473. <https://doi.org/10.1002/marc.201000643>.
- (43) Nagata, M.; Yamamoto, Y. Photoreversible Poly (Ethylene Glycol) s with Pendent Coumarin Group and Their Hydrogels. *React. Funct. Polym.* **2008**, *68* (5), 915–921.
- (44) Moghaddam, M. J.; Hozumi, S.; Inaki, Y.; Takemoto, K. Functional Monomers and Polymers 159 Synthesis and Photochemical Reactions of Polymers Containing Thymine Photodimer Units in the Main Chain. *J. Polym. Sci. Part Polym. Chem.* **1988**, *26* (12), 3297–3308. <https://doi.org/10.1002/pola.1988.080261215>.
- (45) Ohtani, Y.; Inaki, Y.; Miyata, M. Photo-Cross-Linking of Polyvinyl Alcohol Containing Uracil in Concentrated Solution. *J. Photopolym. Sci. Technol.* **2001**, *14* (2), 295–296. <https://doi.org/10.2494/photopolymer.14.295>.
- (46) Ling, J.; Rong, M. Z.; Zhang, M. Q. Coumarin Imparts Repeated Photochemical Remendability to Polyurethane. *J. Mater. Chem.* **2011**, *21* (45), 18373. <https://doi.org/10.1039/c1jm13467a>.
- (47) Yu, Y.; Nakano, M.; Ikeda, T. Directed Bending of a Polymer Film by Light. *Nature* **2003**, *425* (6954), 145–145. <https://doi.org/10.1038/425145a>.
- (48) Bredas, J. L.; Street, G. B. Polarons, Bipolarons, and Solitons in Conducting Polymers. *Acc. Chem. Res.* **1985**, *18* (10), 309–315.
- (49) Zhao, Y.; Cao, L.; Li, L.; Cheng, W.; Xu, L.; Ping, X.; Pan, L.; Shi, Y. Conducting Polymers and Their Applications in Diabetes Management. *Sensors* **2016**, *16* (11), 1787. <https://doi.org/10.3390/s16111787>.
- (50) Katchalsky, A. Rapid Swelling and Deswelling of Reversible Gels of Polymeric Acids by Ionization. *Experientia* **1949**, *5* (8), 319–320. <https://doi.org/10.1007/BF02172636>.

- (51) Matysek, M.; Lotz, P.; Winterstein, T.; Schlaak, H. F. Dielectric Elastomer Actuators for Tactile Displays. *Proc. - 3rd Jt. EuroHaptics Conf. Symp. Haptic Interfaces Virtual Environ. Teleoperator Syst. World Haptics 2009* **2009**, 290–295.  
<https://doi.org/10.1109/WHC.2009.4810822>.
- (52) Pelrine, R.; Kornbluh, R. D.; Pei, Q.; Joseph, J. High-Speed Electrically Actuated Elastomers with Strain Greater Than 100%. *Science* **2000**, 287 (5454), 836–839.  
<https://doi.org/10.1126/science.287.5454.836>.
- (53) Qiu, Y.; Zhang, E.; Plamthottam, R.; Pei, Q. Dielectric Elastomer Artificial Muscle: Materials Innovations and Device Explorations. *Acc. Chem. Res.* **2019**, 52 (2), 316–325.  
<https://doi.org/10.1021/acs.accounts.8b00516>.
- (54) Ren, Z.; Hu, W.; Liu, C.; Li, S.; Niu, X.; Pei, Q. Phase-Changing Bistable Electroactive Polymer Exhibiting Sharp Rigid-to-Rubbery Transition. *Macromolecules* **2016**, 49 (1), 134–140.  
<https://doi.org/10.1021/acs.macromol.5b02382>.
- (55) Qiu, Y.; Lu, Z.; Pei, Q. Refreshable Tactile Display Based on a Bistable Electroactive Polymer and a Stretchable Serpentine Joule Heating Electrode. *ACS Appl. Mater. Interfaces* **2018**, 10 (29), 24807–24815. <https://doi.org/10.1021/acsami.8b07020>.
- (56) Capadona, J. R.; Shanmuganathan, K.; tyler, D. J.; Rowan, S. J.; Weder, C. Stimuli-Responsive Polymer Nanocomposites Inspired by the Sea Cucumber Dermis. *Science* **2008**, 319 (5868), 1370–1374. <https://doi.org/10.1126/science.1153625>.
- (57) Jorfi, M.; Roberts, M. N.; Foster, E. J.; Weder, C. Physiologically Responsive, Mechanically Adaptive Bio-Nanocomposites for Biomedical Applications. *ACS Appl. Mater. Interfaces* **2013**, 5 (4), 1517–1526. <https://doi.org/10.1021/am303160j>.

- (58) 3M™ VHB™ Tape - Specialty Tape 4910 - Technical Data Sheet  
<https://3m.citration.com/pif/000344?locale=en-US> (accessed Apr 14, 2020).
- (59) Shit, S. C.; Shah, P. A Review on Silicone Rubber. *Natl. Acad. Sci. Lett.* **2013**, *36* (4), 355–365.  
<https://doi.org/10.1007/s40009-013-0150-2>.
- (60) O'Halloran, A.; O'Malley, F.; McHugh, P. A Review on Dielectric Elastomer Actuators, Technology, Applications, and Challenges. *J. Appl. Phys.* **2008**, *104* (7), 071101.  
<https://doi.org/10.1063/1.2981642>.
- (61) Brochu, P.; Pei, Q. Advances in Dielectric Elastomers for Actuators and Artificial Muscles. *Macromol. Rapid Commun.* **2010**, *31* (1), 10–36. <https://doi.org/10.1002/marc.200900425>.
- (62) Kovacs, G.; Düring, L.; Michel, S.; Terrasi, G. Stacked Dielectric Elastomer Actuator for Tensile Force Transmission. *Sens. Actuators Phys.* **2009**, *155* (2), 299–307.  
<https://doi.org/10.1016/j.sna.2009.08.027>.
- (63) Kovacs, G.; Düring, L. Contractive Tension Force Stack Actuator Based on Soft Dielectric EAP; Bar-Cohen, Y., Wallmersperger, T., Eds.; San Diego, California, USA, 2009; p 72870A.  
<https://doi.org/10.1117/12.815195>.
- (64) Carpi, F.; De Rossi, D. Improvement of Electromechanical Actuating Performances of a Silicone Dielectric Elastomer by Dispersion of Titanium Dioxide Powder. *IEEE Trans. Dielectr. Electr. Insul.* **2005**, *12* (4), 835–843. <https://doi.org/10.1109/TDEI.2005.1511110>.

## **Chapter 2. Dual stimuli-responsive polymer composite with ultra-wide tunable stiffness range triggered by water and temperature**

### **2.1. Background of this study**

Variable stiffness materials are materials that change stiffness with different loads or output variations and represent an important class of polymer materials. Most commercially used materials have a fixed modulus, unchanging over time or under operating conditions. For examples, contact lenses require relatively low stiffness, around 1 MPa,<sup>65</sup> ideal to hold the contoured shape to fit the human eye, and building materials, such as steel alloys, must be stiff, around 200 GPa<sup>66</sup> for practical use. However, tunable materials that vary stiffness are desirable for application in soft robotics, reconfigurable devices, and artificial muscle.<sup>67–69</sup> Variable stiffness polymers (VSPs) are defined as polymer materials that change stiffness in response to external stimuli (i.e. temperature, humidity, electric field, etc.) and are useful for increasing adaptability and robustness of materials in different environments. Explorations of VSP materials have been widely targeted to utilize the polymer networks for shape transitions and elastic energy storage. However, limited explorations have been done to improve the stiffness variation, essential to broader application of VSPs.<sup>27, 39, 70–72</sup>

#### *2.1.1 Synthetic variable stiffness materials*

VSP materials can be found in nature or are synthesized to fit the desired application. In nature, there are several examples of VSPs, such as human muscle and tendon tissues, which change stiffness in response to the load applied. Additionally, the *Cucumaria frondosa* (sea cucumber) dermis stiffens in response to predatory triggers from 5 to 50 MPa.<sup>73</sup> Strategies reported to achieve tunable stiffness in synthetic materials can be divided into several categories. The first utilizes reversible dynamic bonds, such as Diels-Alder<sup>37</sup> or hydrogen bonding,<sup>74</sup> to vary the chain segment lengths, and crosslink density to adjust the

polymer stiffness. The second requires the insertion and/or subtraction of external media, i.e. solvent or gas. An example of this can be seen in polypyrrole, used as an electroactive polymer artificial muscle, triggered during electrochemical oxidation, during which the stiffness, as well as other properties, vary as a result of charge balance and ion swelling.<sup>75</sup> Another example draws inspiration from the sea cucumber dermis, which stiffens as a result of reversible interactions between adjacent collagen fibrils. The Weder group utilized cellulose nanowhiskers (isolated from tunicates) within a rubber matrix to create a polymer nanocomposite that can change from a few GPa to 10 MPa.<sup>56, 76</sup> The material exhibits thermally induced transition of the rubber polymer matrix in conjunction with the cellulose softening in water and isopropanol to change modulus at 42 °C. However, the material developed by the Weder group has a transition temperature that is too high for use in the human body and is not biocompatible due to the possible diffusion of cellulose nanowhiskers out of the polymer matrix to puncture human cells. The final category of VSP materials exhibits stiffness change through phase transitions of semi-crystalline, glass transition polymers, and magneto-rheological elastomers. For example, many shape memory polymers (SMPs) are glass transition polymers. The stiffness variation property of an SMP is achieved by changing from glassy state to rubbery state with temperature stimulus. These materials have slow stiffness variation, limiting applications where quick transitions are desired.

### 2.1.2 *Bistable electroactive polymer*

A bistable electroactive polymer (BSEP) is a unique VSP that combines the properties of semi-crystalline VSPs with glass transition polymer for a material with temperature activated stiffness variation properties.<sup>54, 77</sup> BSEP realizes its stiffness change by phase changing from semicrystalline to amorphous, exhibiting steep modulus change, tunable transition temperature, and narrow transition temperature range. The phase-changing BSEP exhibits a drastically narrowed temperature transition band of 10 °C range and a low inflection point below 50 °C, ideal for applications involving human-contact. The phase changing

BSEP is mainly comprised of stearyl acrylate (SA) and long chain urethane diacrylate (UDA) to form a crosslinked polymer network. The narrow transition range results from the rapid crystallization and melting of SA moieties in the polymer network. By varying the ratio between SA and UDA, the modulus and the temperature inflection point can be adjusted to fit various applications. Adding a small amount of acrylic acid could increase the stiffness variation to 3000-fold.<sup>55</sup>

### *2.1.3 Bacterial cellulose*

Bacterial cellulose (BC) has been widely studied due to the beneficial properties of high aspect ratio, high porosity, biocompatibility, biodegradability, and high hydrophilicity, assisting in high water holding ability. BC has shown promise in the fields of biomedicine, electronics, and the food industry.<sup>78</sup> The molecular structure of BC comprises terminal hydroxyl groups susceptible to inter- and intra-molecular hydrogen bonding. The BC fibers form a percolated network derived from strong hydrogen-bond interactions. Fiber-fiber interaction is then broken in water, or other polar solvents, due to the competitive hydrogen bonding between the solvent and fiber.<sup>76</sup> By this mechanism, BC nanofibers create a percolating, stiff, network when “switched on” in the dry state and are “switched off” in water or other polar solvents. When embedded into a polymer matrix, the switching of the nanofiber can create a material with variable stiffness. BC is desirable for switching due to the unique three-dimensional porous network, consisting of continuous nanofibers. Each nanofiber is a bundle of cellulose microfibrils, the key to the porous nature of this material (Fig. 2-1). Due to the low stress-bearing threshold of BC, it is ideal for use in a composite material, with the porosity allowing infiltration of another material to form a homogeneous matrix interaction. In forming composite materials, BC maintains its original functionality, while providing additional properties to the composite.



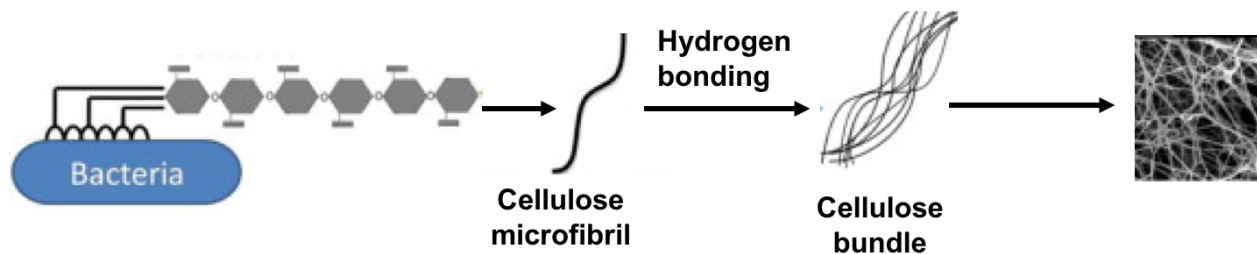


Figure 2-1. Chemical structure and production of bacterial cellulose. Adopted from Ref 79.

#### 2.1.4 Bacterial cellulose reinforced BSEP composite

We report a novel biocompatible polymer composite combining the phase-changing BSEP and tunable stiffness mechanism of bacterial cellulose (BC) for an ultrawide modulus differential. The BSEP polymer matrix contributes a sharp transition temperature tuned to around human body temperature. The BC nanofiber percolating network increases the storage modulus in ambient conditions to as high as 1 GPa. Upon heating, and exposure to water, the BC reinforcement effect nullifies to form water channels allowing for water uptake into the composite. With the plasticization effect from the water molecules, and the softening of the BSEP matrix, the material softens to 40 kPa. The BC-BSEP composite exhibits a large stiffness change of 24 000 times with a dual stimulus of temperature and water. The composites also show good biocompatibility. Although cellulose composites with variable stiffness have been developed, a modulus variation of this magnitude has not been observed before.

## 2.2. Experimental design

### 2.2.1 Raw materials

Urethane diacrylate (UDA, catalog name: CN9021), SR9035, and SR415 were obtained from SARTOMER and used as received. Stearyl acrylate (SA), trimethylolpropane triacrylate (TMPTA), acrylic acid (AA), 2-carboxyethyl acrylate (CEA), 2,2-Dimethoxy-2-phenylacetophenone (DMPA), benzophenone (BP), and isopropyl alcohol (IPA) were purchased from Sigma-Aldrich and used as received. Hexadecyl acrylate (HA) was purchased from Tokyo Chemical Industry Co., LTD. and used as received. Bacterial cellulose was obtained from Hannan Yeguo Foods Co., Ltd.

### 2.2.2 Preparation of BSEP prepolymer solution and thin film fabrication

The BSEP prepolymer solution was made by mixing the components listed in the Table 2-2 at 50 °C. To make a BSEP thin film, the prepolymer solution was then injected between a pair of glass slides on a hot plate with two strips of tape as spacers. The thickness of the liquid layer was defined by the thickness of the spacers. Spacers of 90 µm were used to fabricate the BSEP film. Next, the prepolymer was cured through a UV conveyor equipped with a Fusion 300S type “H” UV curing bulb for about 3 minutes. Then the film was gently peeled off the glass slide after cooling to room temperature.

### 2.2.3 Preparation of bacterial cellulose aerogel

The bacterial cellulose was first dissolved in boiling deionized water with different BC content. The solutions were sonicated for 30 minutes to degas and form uniform aqueous solutions. The solutions were then carefully poured into plastic petri dishes and sealed using Petri Seal™. Next, the petri dishes were placed in Nalgene® Mr. Frost® Cryo 1 °C (Thermo Scientific™) freezing containers filled with isopropyl alcohol (IPA) and placed in a -80 °C freezer. The system was designed to achieve a rate of cooling close to -1 °C/minute for uniform freezing process. Finally, the frozen cellulose solution was freeze-dried

overnight to sublime the water molecules. The resulting cellulose aerogel formed a 3D percolative network with porous structure. The pore size is determined by the concentration of the BC aqueous solution. Thicker solution results in denser aerogel.

#### *2.2.4 Fabrication of BC-BSEP composite*

The freeze-dried BC aerogel was first immersed in a BSEP prepolymer solution at 50 °C. The porous structure enables the BSEP prepolymer solution to absorb into the BC foam, filling the pores inside the aerogel. The system was then transferred into a vacuum oven with the temperature and the pressure set at 50 °C and 30 torr, respectively. The vacuum oven was used to initiate the infiltration of the BSEP prepolymer solution into the BC network. Next, the fully soaked BC foam was compressed between two glass substrates with applied pressure of 1.7 kPa for 10 min. The BC-BSEP prepolymer “sponge” was then cured by UV conveyor equipped with a Fusion 300S type “H” UV curing bulb in ambient temperature for 3 minutes. Finally, the composite film is gently peeled off after the BSEP matrix cooled down to room temperature.

#### *2.2.5 Biocompatibility test for BC-BSEP composite*

All cell culture materials were purchased from ThermoFisher Scientific. To ensure normal cellular growth and low cytotoxicity of the materials, cell viability test was carried out according to ISO 10993-5.<sup>80</sup> In a certified A2 biosafety cabinet, BSEP matrix and BC-BSEP composite were placed at bottoms of a standard 12-well cell culture plate. A total of 100,000 NIH3T3 mouse fibroblast cells were seeded in each well and cultured in Dulbecco’s modified eagle medium with 10% fetal bovine serum plus 1% penicillin. The cell cultures were placed in 37 °C and 5% CO<sub>2</sub> cell incubator for 72 hrs. At the end of 72 hrs., LIVE/DEADTM assay working solution (Catalog number L3224) was prepared in phosphate buffered saline and warmed to 37 °C in heated water bath. Cell culture medium was replaced with the prepared working solution and

incubated in 37 °C and 5% CO<sub>2</sub> for another 30 mins. Last, all samples were imaged with Zeiss Axio-Observer microscope (Carl Zeiss). All fluorescent/phase contrast images within the same comparison groups were imaged with same parameters, and all samples within each comparison group were prepared and processed together.

## **2.3. Results and discussion**

### *2.3.1 Composite fabrication design*

The BC-BSEP composite material includes the hydrophobic BSEP matrix and hydrophilic bacterial cellulose filler, combining the tunable stiffness mechanism of the temperature induced phase changing and water induced competitive hydrogen bond switching. However, preparation of the BC-BSEP homogenous composite could not be conducted by a simple solution casting method with difficulty combining a hydrophilic cellulose filler with a hydrophobic polymer matrix. Here, a new fabrication method is introduced that combines the matrix and filler materials with different hydrophilicity into a uniform thin film composite using dry BC foam with vacuum assistance. Previously fabricated BC composite use a wet template method with water or solvent swollen BC.<sup>76, 81-83</sup> This procedure includes three main steps: (1) freeze-dry, (2) immerse-vacuum, (3) compress-cure (Fig. 2-2). The process begins by freeze-drying frozen BC aqueous solution to create a 3D percolative network of bacterial cellulose as the foundational structure for the composite. The BC aerogel is then immersed in the BSEP prepolymer solution, under vacuum to ensure the full penetration of the BSEP solution into the BC network. The low pressure of the vacuum oven forces the diffusion of the hydrophobic BSEP prepolymer solution by “pumping” the solution into the hydrophilic BC network. The resulting BC-BSEP soaked “sponge” was compressed into a thin film with thickness reduced from 2 mm (original BC aerogel) to a range of 0.1 – 0.3 mm (BC-BSEP composite) dependent on the BC loading. The BC-BSEP compressed “sponge” was cured under UV light. The difference in the thickness of the final BC-BSEP composite is a result of the

different densities of the BC aerogel. BC aerogel with higher density is more difficult to compress, thus, BC-BSEP film with higher BC loading are thicker. The three-step procedure offers a simple and effective way to fabricate a uniform cellulose composite with the different hydrophilicity of matrix and filler materials, while maintaining functionality for both BC and BSEP.

BC-BSEP composite with different filler contents can be achieved by controlling the density of the BC aerogel. The density of the aerogel is determined by the concentration of BC in the aqueous solution. As seen in Table 2-1, increasing the concentration of BC aqueous solution causes the density of the resulting aerogel and the filler content of the composite to increase. Thus, BC-BSEP composite with different filler content can be obtained.

Table 2-1. Filler content of BC-BSEP composite and density of resulting aerogel from BC aqueous solution with different concentrations.

	BC concentration in aqueous solution (wt%)	BC aerogel density (mg/ml)	Filler content (wt%)
BC-BSEP-1	0.7	9.36	4.7
BC-BSEP-2	1	13.37	8.2
BC-BSEP-3	1.5	20.06	16.7
BC-BSEP-4	2	26.74	23

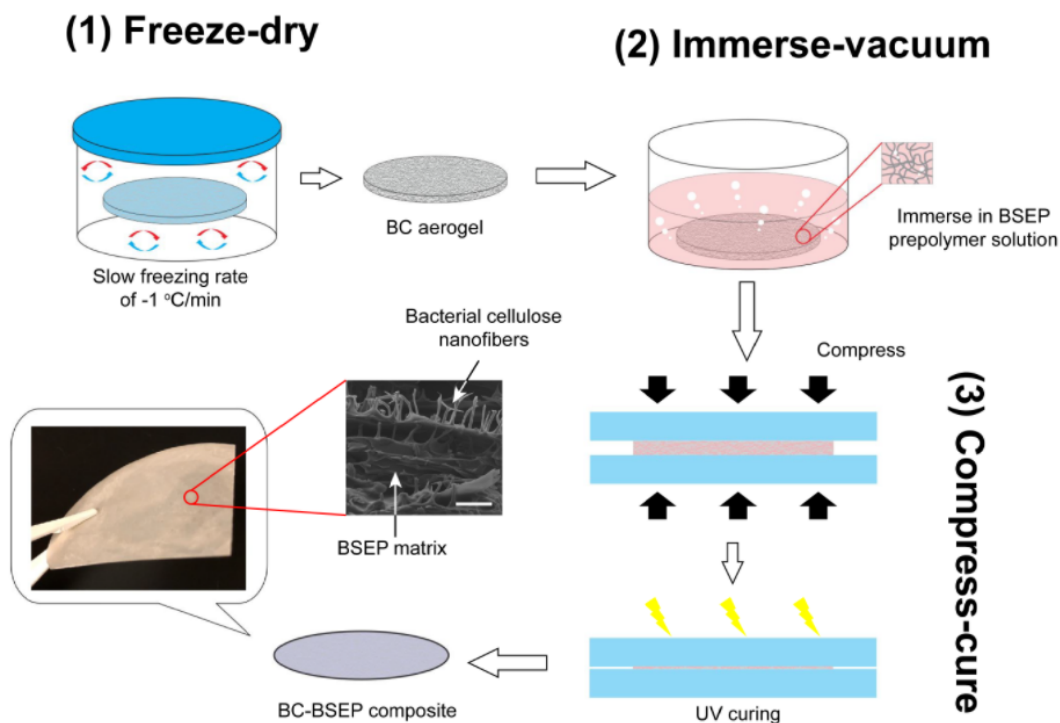


Figure 2-2. Fabrication process of the BC-BSEP composite material.

### 2.3.2 Matrix modification of BSEP

The synthesis of the BC-BSEP composite centers on uniform dispersion or inter-penetration between the BSEP matrix, which is largely hydrophobic, and the BC nanofibers, which are hydrophilic. The BSEP matrix is formulated from a precursor containing urethane diacrylate, stearyl acrylate, hexadecyl acrylate, and carboxyethyl acrylate (See Table 2-2). The long chain urethane diacrylate (UDA, CN9021) used in this formulation has a high elongation at break (1100% for the homopolymer)<sup>54</sup> and crosslinks to afford the BSEP elasticity, improving the toughness of the matrix in the rubbery state. This is important for the incorporation of bacterial cellulose (BC) as the percolation network created by BC provides high stiffness, but also creates a brittle framework within the matrix. Stearyl acrylate (SA) and hexadecyl acrylate (HA) were used as crystalline segments and to adjust transition temperature range. Carboxyethyl acrylate (CEA)

is added to create hydrogen bonding between the matrix and BC as well as increase tear strength. 2,2-dimethoxy-2-phenyl acetophenone (DMPA) and benzophenone (2:1) were employed as co-photoinitiators for complete bulk and surface curing of thin films. The first design consideration of the matrix is to tune the transition temperature to body temperature for a sharp transition from rigid to rubbery at 37 °C. Second, the BSEP matrix inherent hydrophobicity must be considered. Carboxyethyl acrylate, a hydrophilic component, is utilized to facilitate the incorporation of and bonding to BC.

The transition temperature of BSEP was tuned to body temperature by modifying the BSEP formulation to include hexadecyl acrylate (HA). Hexadecyl acrylate has a lower melting temperature than stearyl acrylate. By combining the two components in different ratios, the transition temperature can be precisely tuned to that of body temperature. Higher amounts of stearyl acrylate increase the transition temperature due to the high crystallinity resulting from long sidechains that require higher temperatures to melt. The matrix was comprised of stearyl acrylate and hexadecyl acrylate to provide a reversible and sharp rigid to rubbery transition between 30 °C and 50 °C. A temperature below 30 °C or above 50 °C could result in a loss of shape memory capability at room temperature or use in biomedical devices.

Table 2-2 Formulations of different BSEPs.

BSEP Sample	Weight Part *				
	SA	HA	UDA	CEA	T <sub>m</sub> (°C)
BS1H7	10	70	20	10	30
BS4H4	40	40	20	10	35
BS7H1	70	10	20	10	38
CEA5	70	10	20	5	37
CEA10	70	10	20	10	37
CEA15	70	10	20	15	37
BS80	80	0	20	0	45

Dynamic mechanical analysis (DMA) of the BSEP copolymers during temperature ramp up was conducted to observe the mechanical properties of the material as a function of temperature (Fig. 2-3). The temperature ramp for the three ratios of HA:SA (Table 2-2) showed varying, ratio dependent, transition temperatures between 30 °C and 43 °C. The higher amount of SA, the higher the transition temperature and the higher the modulus at room temperature. The moduli at room temperature ranged from 280 MPa (BS1H7) to 360 MPa (BS7H1) due to the crystallinity of the SA and HA moiety acting as hard segments in the copolymer. The rigid-to-rubbery transition is completed within a range of 5 °C, showing quick phase changing capabilities. Once the transition is complete, the softened modulus remains constant in the rubbery state. The storage modulus during the rigid-to-rubbery transition changes nearly 5,000 fold for each ratio.



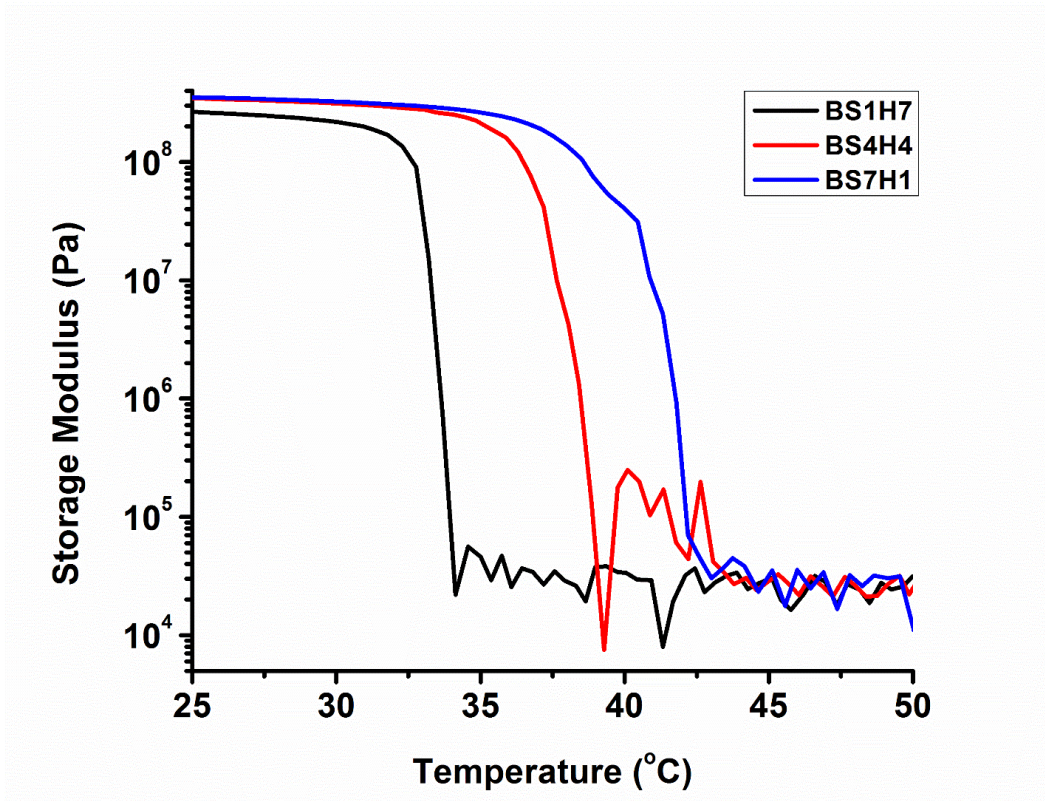


Figure 2-3. Storage modulus versus temperature of the BSEPs with transition temperature below, at, and above body temperature.

For seamless integration of BC into the hydrophobic BSEP matrix, it was necessary to use a hydrophilic component in the formulation. BC is highly hydrophilic, bonding strongly to materials of similar character. Carboxyethyl acrylate was used for hydrophilicity and added hydrogen bonding with BC. Additional hydrogen bonding contributes to the uniformity and stability of the composite. The formulation was tested with different amounts of carboxyethyl acrylate (CEA) (Table 2-2) without BC to review the mechanical properties of the matrix and miscibility with the BSEP prepolymer solution (Fig. 2-4). The prepolymer solutions were obtained by the method described above and shows CEA can effectively strengthen the BSEP matrix. BS80, which contained no CEA, has an elongation at break of 191% and a tensile strength of 0.26 MPa. The addition of CEA results in an increase in tensile strength from 2.5 MPa (CEA5) to 4.5

MPa (CEA15) as more CEA is introduced. All samples had an elongation at break of about 900%, showing the addition of CEA improves the strength of BSEP. CEA10 had a resulting tensile strength of 3.5 MPa and strain of 890%. When compared with the BS80, CEA10 strengthened the BSEP matrix and was miscible in the BSEP prepolymer solution. CEA10 was used as the BC-BSEP matrix

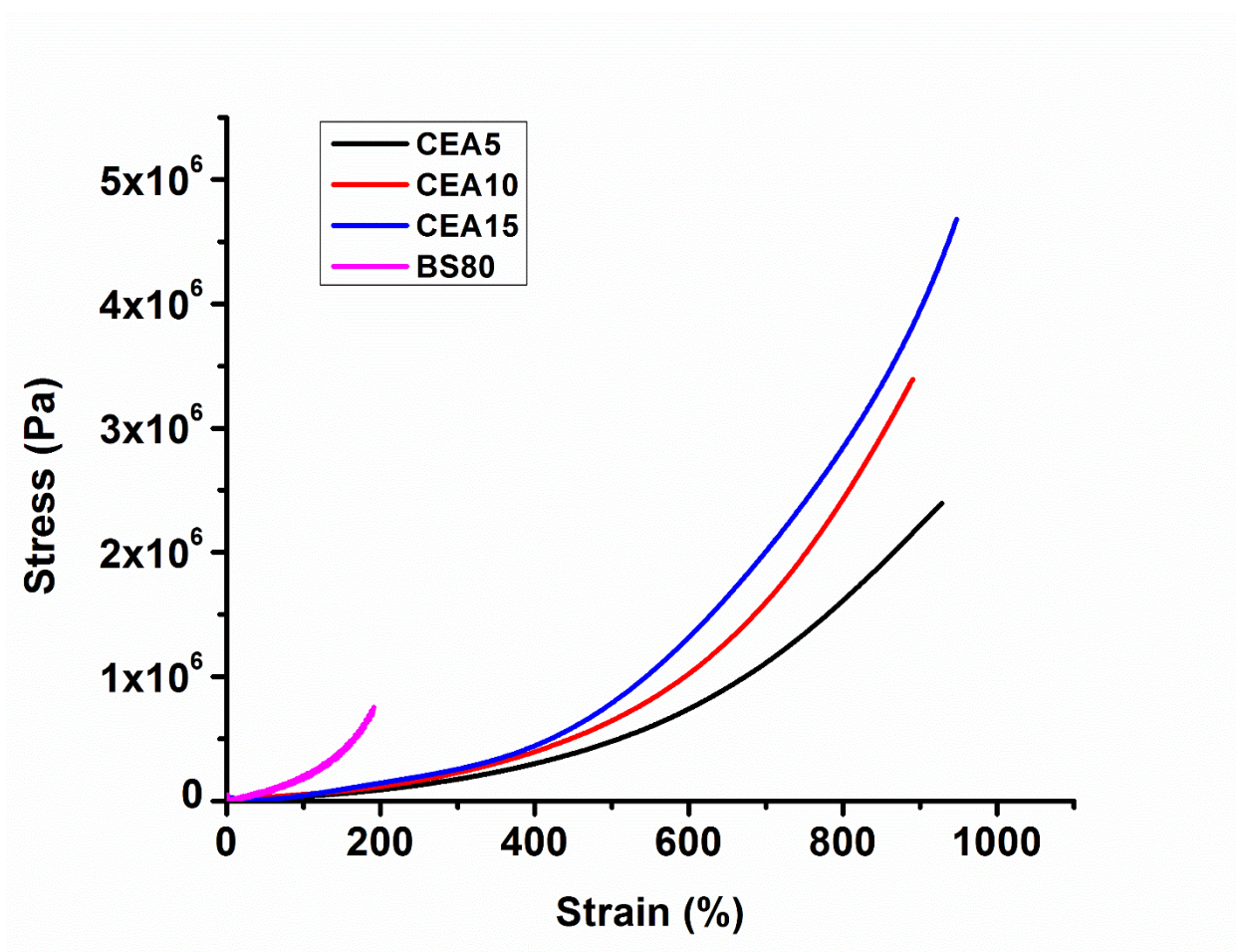


Figure 2-4. Tensile stress-strain behavior of BSEPs in the soft state with different amount of CEA at

40 °C.

### 2.3.4 BC-BSEP composite

The BC-BSEP composite materials were fabricated with different filler content based on the procedure mentioned previously. BC-BSEP composites were tested with four different weight % of BC loaded into the BSEP matrix with filler content of around 4.7 wt% (BC-BSEP-1), 8.2 wt% (BC-BSEP-2), 16.7 wt% (BC-BSEP-3), and 23 wt% (BC-BSEP-4), respectively. The SEM images of the composite reveal that the BC fibers are deeply embedded in the BSEP matrix in a uniform manner (Fig. 2-5a-b).

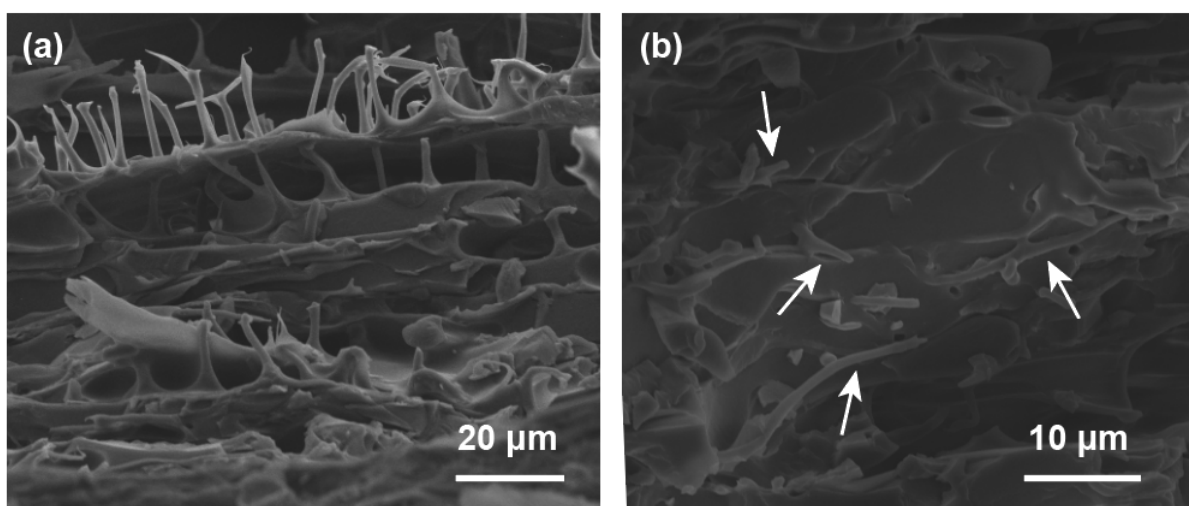


Figure 2-5. a) SEM images of the cross section from a BC-BSEP composite. b) A closer view of the cross section showing BC nanofibers deeply embedded in the BSEP matrix.

The tensile stress-strain behavior and modulus change of the BC-BSEP composite were conducted on fully softened (immersed in water heated to 50 °C) BC-BSEP composite materials (Fig. 2-6). The BC-BSEP-1 showed the tensile strength and strain at break of 0.32 MPa and 974% respectively. As more BC was introduced, 23 wt% for BC-BSEP-4, the tensile stress and strain decreased to 0.24 MPa and 313%, respectively. Overall, as the loading of BC increases, the mechanical toughness decreases. This phenomenon can be attributed to the water absorption of BC fortifying the filler dilution effect.

Notwithstanding, BC-BSEP-1, BC-BSEP-2, and BC-BSEP-3 exhibit high elongation with high tensile strength due to the added CEA, contributing flexible hydrogen bonding within the matrix and with BC hydroxyl groups.

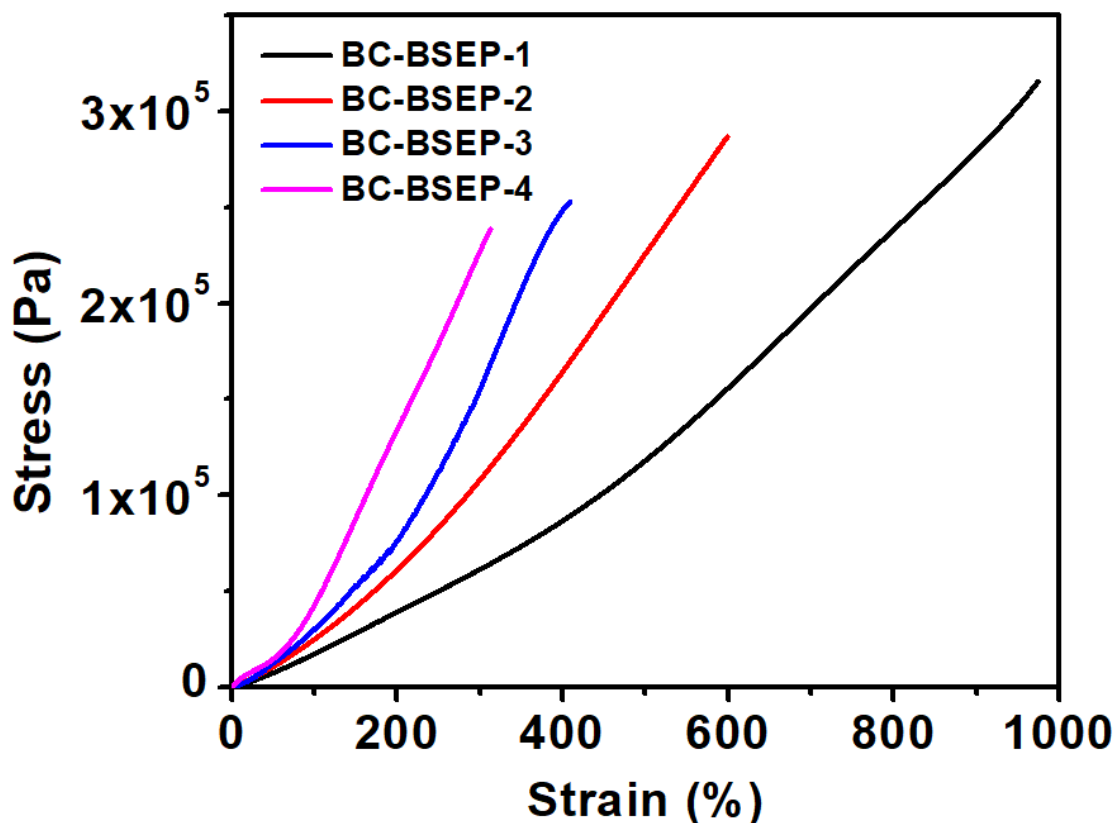


Figure 2-6. Tensile stress-strain behavior of BC-BSEPs in the soft state with different filler content in water at 50 °C.

The storage modulus was measured on a dynamic mechanical analyzer to determine the strengthening effect of the BC network within the BSEP matrix. The resulting storage moduli show significant reinforcement effect of the BC percolating network resulting from strong fiber-fiber interaction. The moduli ranged from 200 MPa for neat BSEP to 1.5 GPa for BC-BSEP-4 (Fig. 2-7). The 5-fold increase in modulus results from the strong reinforcement provided by hydrogen bond interactions among BC

nanofibers. In the soft state, the composite was immersed in hot water (50 °C) for 10 minutes, the storage modulus also exhibited an increase from 14 kPa (neat BSEP) to 69 kPa (BC-BSEP-4). This discrepancy could arise from inherent incompatibility between BC and BSEP, resulting in the incomplete penetration of water through the hydrophobic channel, allowing remaining BC fiber-fiber interactions to increase mechanical stiffness.

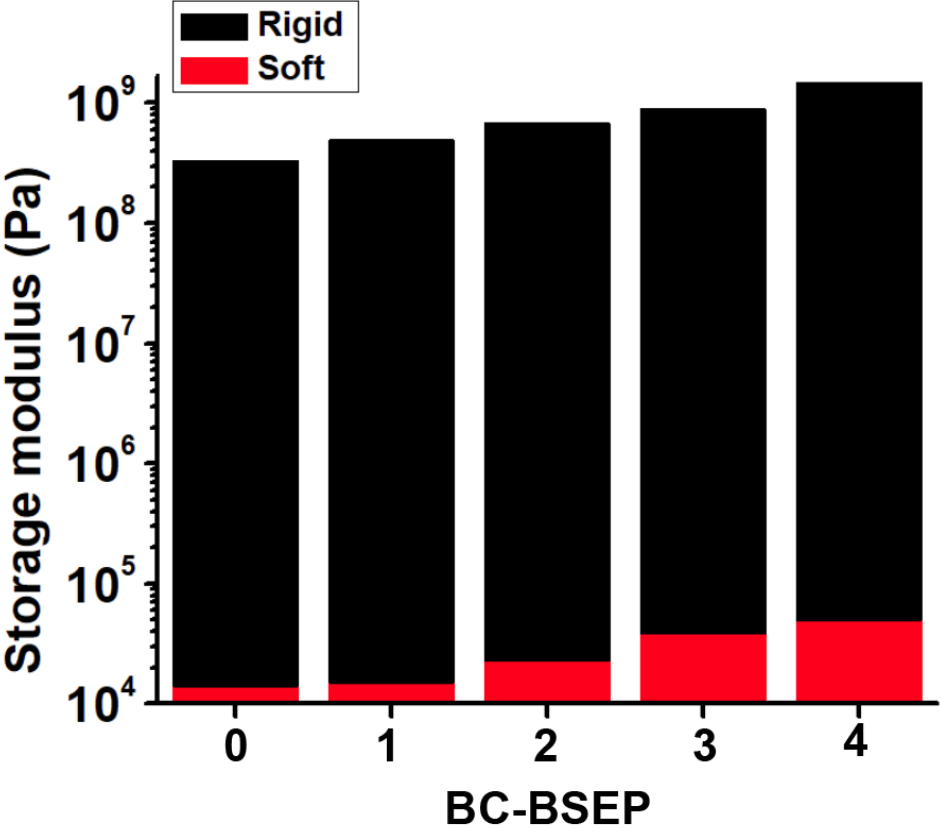


Figure 2-7. Storage modulus comparison of BS-BSEP composites in the rigid (dry and low temperature) and soft (wet and high temperature) state.

The change from rigid-dry to soft-wet state of the composite results in an ultra-wide change in stiffness proving the response to both temperature and water. Both phases in the composite are stable and sustainable under the necessary conditions demonstrated in Figure 2-8. The moduli were tested for BC-BSEP-3 at room temperature and dry (RT-dry), room temperature and wet (RT-wet), elevated temperature

and dry (HT-dry), and elevated temperature and wet (HT-wet) to compare mechanical properties. As demonstrated by Figure 2-8, the composite has a modulus of 900 MPa at room temperature (RT-dry). When wet, the modulus decreases to 114 MPa (RT-wet) indicating the BC percolating network hydration and nullification. At elevated temperature and dry state, the modulus decreased to 77 MPa (HT-dry). The difference in the modulus is due to the melting of the crystalline domains of the SA and HA within the BSEP matrix, but the reinforcement of percolating network from the BC persists even at elevated temperature. With the combination of water and temperature the BC network begins to weaken, and the percolating network absorbs water to drastically reduce the modulus to 38 kPa. The ratio of modulus changes from RT-dry (900 MPa) to HT-wet (38 kPa) is 24,000:1. Compared to VSP materials of similar character, with ratios as high as 5000:1,<sup>56, 57</sup> this ratio far exceeds what has been done with cellulose composites. The composite in the RT-dry state can cut through a piece of printer paper. It can also poke into an agar gel in hot water if the operation was done quickly. Leaving the composite in the hot water for 7 minutes, it will become too soft to penetrate the soft agar gel in hot water. After leaving it to dry in air, the composite returns to the rigid state and can again cut the paper.

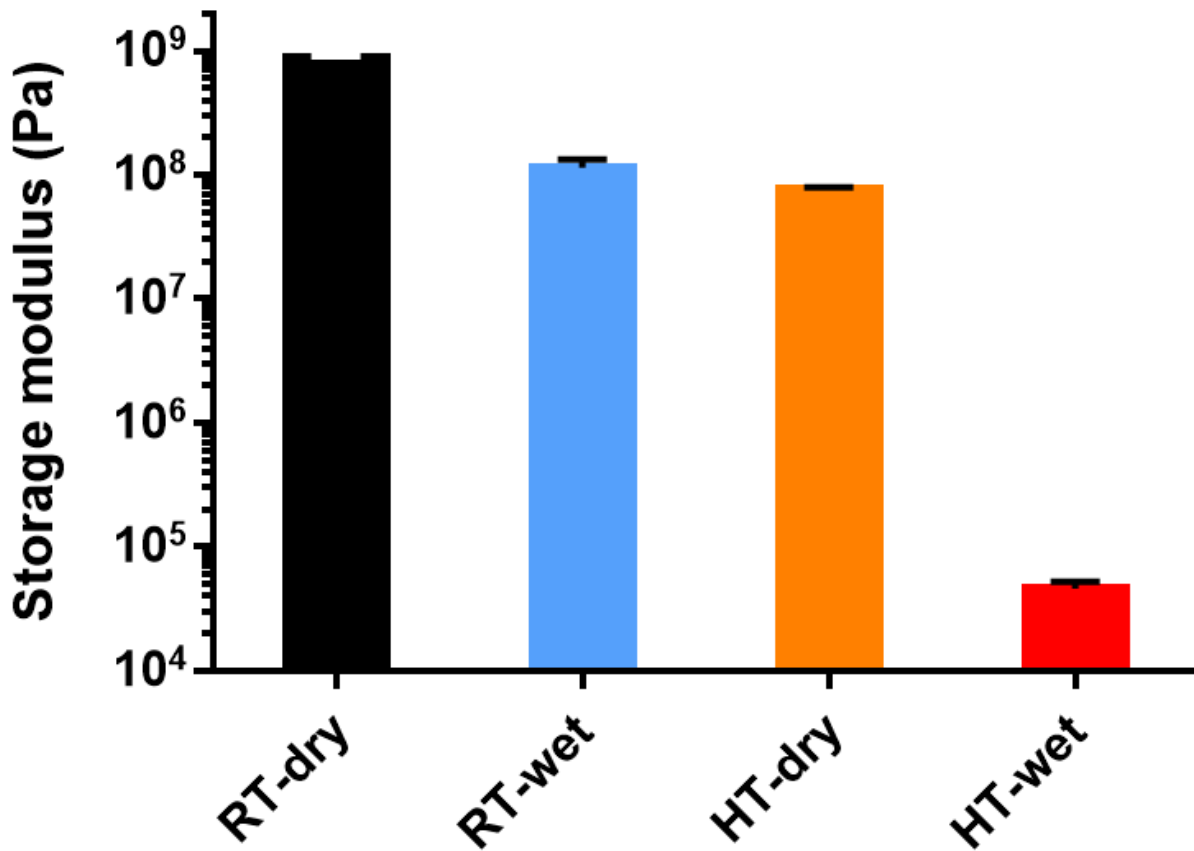


Figure 2-8. The storage modulus measurement of BC-BSEP-3 in room temperature-dry state, room temperature-wet state, high temperature-dry state, and high temperature-wet state.

### 2.3.5 Biocompatibility of BC-BSEP composite

The biocompatibility of the composite was further characterized for potential use in the biomedical field. Bacterial cellulose is a well-known, biocompatible material,<sup>78</sup> tests were conducted on the BSEP matrix and BC-BSEP composite (Fig. 2-9). Figure 2-9 shows BSEP neat (top) and BC-BSEP (bottom) in a Live/Dead cell assay. The assay determines biocompatibility by observing cell growth and death when exposed to the material. Both materials showed distinct cell growth after seeding. This result is indicative

of polymer materials that are biocompatible and will not cause cell death. The existence of dead cells is due to the natural cell growth cycle, which can also be observed in other biocompatible materials. The biocompatibility, in combination with large-range stiffness tunability, grants the BC-BSEP composite the opportunity to be used in biomedical applications. One possible application is to substitute traditional cortical probes which are made from intrinsically rigid materials like silicon or polyimide for easy penetration into brain. The traditional probe has large mechanical mismatch between brain tissue and implant, which can cause inflammation, long term damage, and scar tissue generation. Additionally, this material could be used as a tissue scaffold for small, difficult to reach places. When the transition temperature of BSEP matrix is tuned to body temperature, the dual-stimuli responsive nature is suitable for human body environment. In the rigid state, the BC-BSEP composite can be stiff enough to penetrate through the different body tissues. The physiological environment of human body will then soften the material to match the mechanical property of the tissue, which reduces immune response and scar tissue formation for more stable, long term lifetime.



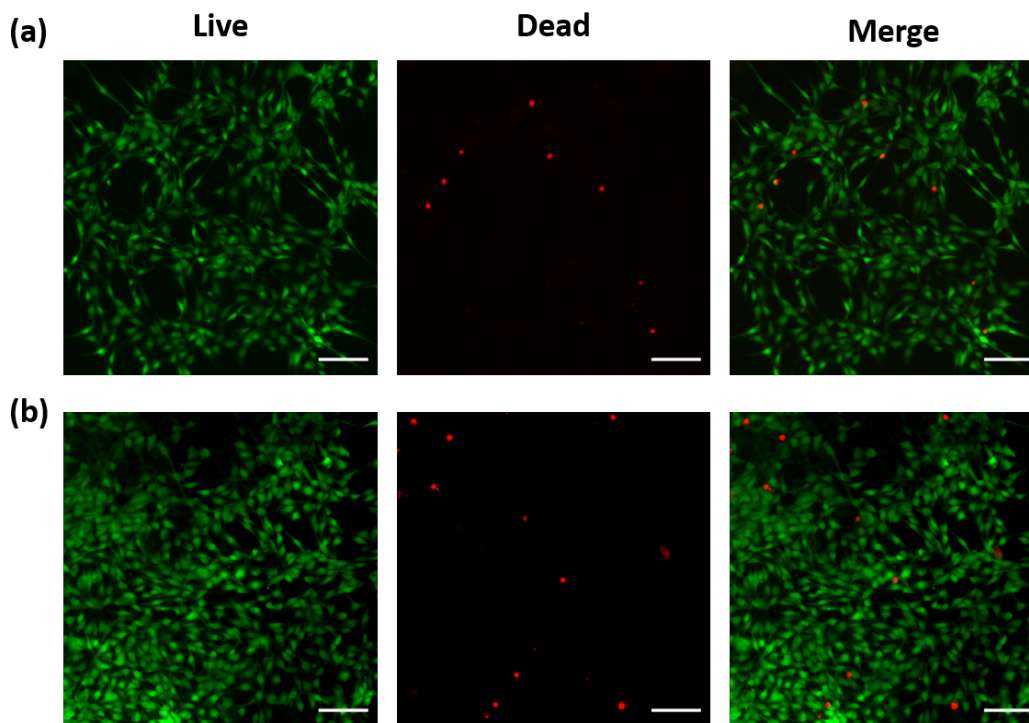


Figure 2-9. Representative fluorescent staining images of live (green) and dead (red) assay of NIH3T3 cells 3 days after cell seeding on BSEP matrix a) and BC-BSEP composite b). Scale bar = 100  $\mu\text{m}$ .

## 2.4. Conclusion

Several composite materials utilizing dual-stimuli response with an ultra-wide tunable stiffness range were fabricated. The hydrophobic BSEP matrix combined with the hydrophilic BC percolating network warranted a modified fabrication process to ensure uniform compositions. The BC percolating network contributed to an increase in the modulus at room temperature, while the BSEP matrix contributed a large modulus differential when heated. With the dual activated stiffness response to water, nullifying the BC contribution, and temperature, to soften the BSEP matrix, the modulus of the BC-BSEP composite can be tuned 24,000 times. A storage modulus of nearly 1 GPa dry at room temperature, decreases to around 40 kPa, wet at 37 °C. The composite exhibits excellent mechanical stretchability with maximum elongation

of over 600% and tensile strength of 0.3 MPa. The composite also passes the biocompatibility test for potential biomedical applications.

## 2.5. References

- (65) Tranoudis, I.; Efron, N. Tensile Properties of Soft Contact Lens Materials. *Contact Lens Anterior Eye* **2004**, *27* (4), 177–191. <https://doi.org/10.1016/j.clae.2004.08.002>.
- (66) Callister, W. D.; Rethwisch, D. G. *Materials Science and Engineering: An Introduction*; Wiley, 2010.
- (67) Wang, L.; Yang, Y.; Chen, Y.; Majidi, C.; Iida, F.; Askounis, E.; Pei, Q. Controllable and Reversible Tuning of Material Rigidity for Robot Applications. *Mater. Today* **2018**, *21* (5), 563–576. <https://doi.org/10.1016/j.mattod.2017.10.010>.
- (68) Shanmuganathan, K.; Capadona, J. R.; Rowan, S. J.; Weder, C. Biomimetic Mechanically Adaptive Nanocomposites. *Prog. Polym. Sci.* **2010**, *35* (1–2), 212–222. <https://doi.org/10.1016/j.progpolymsci.2009.10.005>.
- (69) Pei, Q. Variable Stiffness Materials. *Soft Robot.* **2016**, *3* (1), 1–2. <https://doi.org/10.1089/soro.2016.29006.bat>.
- (70) Sun, J.; Guan, Q.; Liu, Y.; Leng, J. Morphing Aircraft Based on Smart Materials and Structures: A State-of-the-Art Review. *J. Intell. Mater. Syst. Struct.* **2016**, *27* (17), 2289–2312. <https://doi.org/10.1177/1045389X16629569>.
- (71) Hu, X.; Zhou, J.; Vatankhah-Varnosfaderani, M.; Daniel, W. F. M.; Li, Q.; Zhushma, A. P.; Dobrynin, A. V.; Sheiko, S. S. Programming Temporal Shapeshifting. *Nat. Commun.* **2016**, *7* (1), 12919. <https://doi.org/10.1038/ncomms12919>.

- (72) Takigawa, T.; Yamawaki, T.; Takahashi, K.; Masuda, T. Change in Young's Modulus of Poly(N-Isopropylacrylamide) Gels by Volume Phase Transition. *Polym. Gels Netw.* **1998**, *5* (6), 585–589. [https://doi.org/10.1016/S0966-7822\(97\)00028-2](https://doi.org/10.1016/S0966-7822(97)00028-2).
- (73) Trotter, J. A.; Tipper, J.; Lyons-Levy, G.; Chino, K.; Heuer, A. H.; Liu, Z.; Mrksich, M.; Hodneland, C.; Dillmore, W. S.; Koob, T. J.; Koob-Emunds, M. M.; Kadler, K.; Holmes, D. Towards a Fibrous Composite with Dynamically Controlled Stiffness: Lessons from Echinoderms. *Biochem. Soc. Trans.* **2000**, *28*, 6.
- (74) Li, J.; Viveros, J. A.; Wrue, M. H.; Anthamatten, M. Shape-Memory Effects in Polymer Networks Containing Reversibly Associating Side-Groups. *Adv. Mater.* **2007**, *19* (19), 2851–2855. <https://doi.org/10.1002/adma.200602260>.
- (75) Pytel, R. Z.; Thomas, E. L.; Hunter, I. W. In Situ Observation of Dynamic Elastic Modulus in Polypyrrole Actuators. *Polymer* **2008**, *49* (8), 2008–2013. <https://doi.org/10.1016/j.polymer.2008.01.053>.
- (76) Dagnon, K. L.; Shanmuganathan, K.; Weder, C.; Rowan, S. J. Water-Triggered Modulus Changes of Cellulose Nanofiber Nanocomposites with Hydrophobic Polymer Matrices. *Macromolecules* **2012**, *45* (11), 4707–4715. <https://doi.org/10.1021/ma300463y>.
- (77) Yu, Z.; Yuan, W.; Brochu, P.; Chen, B.; Liu, Z.; Pei, Q. Large-Strain, Rigid-to-Rigid Deformation of Bistable Electroactive Polymers. *Appl. Phys. Lett.* **2009**, *95* (19), 192904. <https://doi.org/10.1063/1.3263729>.
- (78) Esa, F.; Tasirin, S. M.; Rahman, N. A. Overview of Bacterial Cellulose Production and Application. *Agric. Agric. Sci. Procedia* **2014**, *2*, 113–119. <https://doi.org/10.1016/j.aaspro.2014.11.017>.

- (79) Hu, W.; Chen, S.; Yang, J.; Li, Z.; Wang, H. Functionalized Bacterial Cellulose Derivatives and Nanocomposites. *Carbohydr. Polym.* **2014**, *101*, 1043–1060.  
<https://doi.org/10.1016/j.carbpol.2013.09.102>.
- (80) Wallin, R. F.; Arscott, E. F. A Practical Guide to ISO 10993-5: Cytotoxicity. *Med. Device Diagn. Ind. Mag.* **1998**, *20*, 96–98.
- (81) Hobzova, R.; Hrib, J.; Sirc, J.; Karpushkin, E.; Michalek, J.; Janouskova, O.; Gatenholm, P. Embedding of Bacterial Cellulose Nanofibers within PHEMA Hydrogel Matrices: Tunable Stiffness Composites with Potential for Biomedical Applications. *J. Nanomater.* **2018**, *2018*, 1–11. <https://doi.org/10.1155/2018/5217095>.
- (82) Hobzova, R.; Duskova-Smrckova, M.; Michalek, J.; Karpushkin, E.; Gatenholm, P. Methacrylate Hydrogels Reinforced with Bacterial Cellulose. *Polym. Int.* **2012**, *61* (7), 1193–1201. <https://doi.org/10.1002/pi.4199>.
- (83) Shimizu, Y.; Sakakibara, K.; Akimoto, S.; Tsujii, Y. Effective Reinforcement of Poly(Methyl Methacrylate) Composites with a Well-Defined Bacterial Cellulose Nanofiber Network. *ACS Sustain. Chem. Eng.* **2019**, *7* (15), 13351–13358.  
<https://doi.org/10.1021/acssuschemeng.9b02602>.

## Chapter 3. A dielectric elastomer with high strain and rapid response

### 3.1. Background of the study

Dielectric elastomers (DEs) are a class of polymer smart materials that transduce electrical energy into mechanical energy to provide large actuation strain and rapid response speed.<sup>26, 52, 53, 84, 85</sup> DEs not only have similar energy density to natural muscle, but they can also exhibit large actuation strain and high response speed which has earned them the moniker “artificial muscles”.<sup>86</sup> As a result, DEs have tremendous potential in not only soft robotics applications,<sup>34, 87, 88</sup> but also soft motors,<sup>89</sup> diffraction gratings,<sup>90, 91</sup> vibration control,<sup>92, 93</sup> and haptic feedback devices.<sup>55, 94, 95</sup> In comparison with other actuation technologies, they are light weight and exhibit large electromechanical strain, high energy density, high coupling efficiency, fast response speed, and silent operation.<sup>96</sup>

#### 3.1.1. Dielectric elastomer principles

Dielectric elastomer actuators (DEAs) act as flexible capacitors that generate mechanical work in response to an applied electric field. For electromechanical actuation, a DE film is sandwiched between two compliant electrodes. When a voltage is applied, an electric field is generated within the film, and the electrostatic interaction between the electrodes compress the film, expanding it in area (Fig. 3-1). The working model describes the Maxwell stress,  $p$ , as the effective compressive stress produced from the compression of the actuated film under an applied electric field<sup>52</sup>

$$\text{Equation 3-1} \quad p = \epsilon_0 \epsilon_r E^2 = \epsilon_0 \epsilon_r (V/z)^2$$

where  $E$  is the electric field,  $\epsilon_r$  is the dielectric constant of the DE material,  $\epsilon_0$  is the permittivity of vacuum,  $V$  is the applied voltage and  $z$  is the film thickness. The electromechanical energy density,  $e$ , is often used for high strain, nonlinear materials, where the compressive stress,  $s_z$ , is known. The electromechanical

energy density,<sup>52</sup> the amount of electrical energy converted to mechanical energy per unit volume of material for one cycle under constant field actuation, is estimated as

Equation 3-2 
$$e = -p \ln(1 + s_z) = -\epsilon_r \epsilon_0 E^2 \ln(1 + s_z)$$

Based on the equations above, the important parameters used to determine DE performance and guide materials selection include stress-strain relationship, elongation at break, dielectric constant of the material, and dielectric breakdown field. When designing DEs it is important to consider elastomeric networks with long segment length between crosslinks, i.e., low crosslink density, tends to have high elongation at break, but exhibit a long plateau during elongation that is vulnerable to electromechanical instability, whereas a network with short segment length would have high stiffness and low actuation strain.<sup>97</sup> High performing DE materials exhibit low modulus, with high elongation at break with rapid stiffening at high strains.

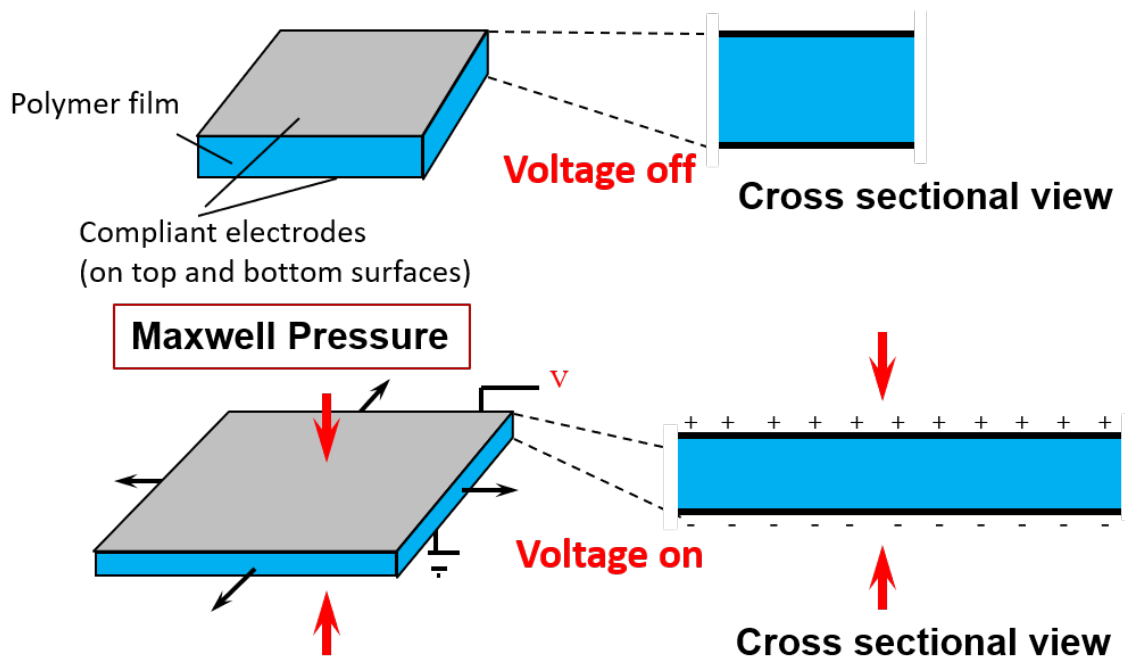


Figure 3-1. Dielectric elastomer actuator working principle. Adopted from Ref 53.

### *3.1.2. Current DE technology and downfalls*

The most widely used DE materials are VHB4905 and VHB4910 which are acrylic elastomers developed by 3M™. These commercially available films can achieve actuation strain over 150% when prestretched. However, for DEA applications, the material must be prestretched to achieve large actuation performance.<sup>52</sup> Prestretching applies uniform strain prior to actuation to suppress the electromechanical instability, improve breakdown strength, and improve energy density. Without prestretching, VHB cannot achieve actuation over 33% strain.<sup>52</sup> Prestretching limits the material applications by reducing the shelf-life of the DE and complicating the fabrication by requiring a rigid frame to maintain the stretch thus limiting its applicability, particularly in soft robotics. Prestretch can also lead to stress concentrations causing non-uniform actuation, rapid fatigue, and premature failure from crack propagation.<sup>98</sup> Furthermore, the response speed of acrylic elastomers is limited to under 5 hertz at large strains due to its high viscoelasticity. Other DE materials, such as silicone elastomers, have low viscoelasticity but exhibit lower maximum strains and energy density due to their low maximum stable operable field. Advances in DE materials such as bottle-brush polymers with ultralow stiffness,<sup>99, 100</sup> silicone elastomers with enhanced dielectric constants<sup>64, 101, 102</sup> have partially improve actuation performance of DEAs. Despite these efforts, the field still lacks a material that does not require prestretching and exhibits both high actuation strain and rapid response.

### *3.1.3. New DE material with high performance*

In this work, we introduce a new bimodal dielectric elastomer that exhibits high actuation strain, fast response, and low viscoelasticity that does not require prestretching. This material utilizes a short chain crosslinker with a long chain crosslinker to create an interpenetrating polymer network with high tensile strength, high elongation at break, and rapid stiffening at high strain. Diluents were added to improve mechanical and electromechanical performance by lowering the viscoelasticity and increasing the

toughness of the material. The new DE exhibits electromechanical properties similar to VHB with maximum actuation near 200% strain with a resulting energy density is  $3.48 \text{ MJ/m}^3$  and Maxwell stress of 3.2 MPa. The material exhibited response speeds as fast as 10 Hz with actuation response over 100% strain at 2 Hz.

## **3.2. Experimental design**

### *3.2.1. Raw materials*

Urethane diacrylate (UDA, catalog name: CN9021), isodecyl acrylate (IDA) and isobornyl acrylate (IBOA) were obtained from Sartomer Company and used as received. Butyl acrylate (BA), acrylic acid (AA), neopentyl glycol propoxylate diacrylate (PNPDA), poly (propylene glycol) acrylate (PPGA), isopropyl alcohol (IPA), poly(acrylic acid) solution ( $M_w \sim 100,000$ , 35 wt % in  $\text{H}_2\text{O}$ ), benzophenone (BP) and 2,2-dimethoxy-2-phenylacetophenone (DMPA) were purchased from Sigma Aldrich and used as received.

### *3.2.2. Preparation of DE prepolymer solution and thin film fabrication*

Each prepolymer solution was weighed out according to wt % predetermined ratios and mixed overnight. The pre-polymer solution was then spincoated onto a poly (acrylic acid) 5% solution in IPA (PAA) coated glass substrate. The PAA coating acts as a sacrificial layer. The prepolymer solution coated on the glass was then UV cured on a UV curing conveyor equipped with  $2.5 \text{ W/cm}^2$  Fusion 300s type “h” UV curing bulb for 2 passes at a speed of 6 ft/min. The glass with the film still coated on it was affixed to an acrylic frame (1/16in thick, 0.8in x 2.5in opening) with double sided tape. The outside of the glass was also taped to the frame and submerged in a water bath. After 1 hour, the film peeled off the glass and left to dry for



at least 1 hour. Once completely dry, the film was coated (cotton swab) on both sides of the film with a thin layer carbon grease (NyoGel 756G, Nye Lubricants) as compliant electrodes.

### 3.2.3. *Dynamic mechanical analysis*

Mechanical properties were measured on a TA Instruments RSAIII dynamic mechanical analyzer (DMA). Dynamic temperature sweep tests were conducted at a temperature ramping rate of 2 °C/min and a frequency of 1 Hz from -50 to 100 °C with samples of 8 mm wide and 50 µm thick loaded onto the DMA with a 10 mm gap between the thin film grips. The maximum elongation strain of the samples were obtained at room temperature with a stretching rate of 0.5 mm/s. The tested samples used were 8 mm wide and 50 µm thick with a 6 mm gap between the thin film grips of the DMA. Samples were measured in triplicate at least.

### 3.2.4. *Permittivity measurement*

Elastomer materials of known thickness were coated in carbon grease to form circular electrodes with diameter 0.3 inches. Capacitance was measured using GwInstek LCR-819 LCR meter at 1 V excitation and 12 Hz-100 kHz frequencies. Relative permittivity  $\epsilon$  was calculated by:

*Equation 3-3* 
$$\epsilon = Cz/\epsilon_0 A$$

Where  $C$  is the measured capacitance,  $z$  is the thickness of the elastomer film,  $\epsilon_0$  is the vacuum permittivity, and  $A$  is the effective area.

### 3.2.5. *DE actuation measurement*

The electrode coated elastomer films were attached to a diaphragm chamber made of aluminum with a

0.333mm circular opening onto with the DE films were attached. A positive air pressure was applied such that when the films were actuated, they would deform out of plane to form a raised dome. The active area of the DE films was flat and circular with a diameter of 0.3 mm, before actuation. A high voltage supply was used to drive the actuation. A digital camera was used to record the actuation of the DE films. The actuation strain was measured from the video frame-by-frame through MATLAB image processing tools and calculated using an equation for the surface area of a dome.

Equation 3-4

$$S_A = \frac{(h^2 + R^2) - (h_0^2 + R_0^2)}{(h_0^2 + R_0^2)}$$

Where  $h$  is the height of the dome and  $R$  is the radius. The strain values at each voltage were calculated after a constant driving voltage at 0.1 Hz. The frequency of the voltage was then increased to 0.5 Hz up to 50 Hz. The applied electric field was calculated by dividing the applied voltage by the instantaneous thickness of the elastomer film at maximum strain. At least three samples were tested for each formulation.

### 3.3. Results and Discussion

#### 3.3.1. Design principles of new DE materials

New dielectric elastomer materials were designed to optimize actuation strains and dielectric breakdown field without prestretching to ensure high actuation performance and rapid response at high frequencies. A short-chain difunctional acrylate crosslinker and a long-chain difunctional acrylate crosslinker were chosen to form a bimodal interpenetrating base matrix network. The bimodal network combines the high elongation at break of low crosslink density (long-chain) with the stiffness exhibited by high crosslink density elastomers (short-chain) to suppress electromechanical instability while retaining elasticity. These base components were formulated with additional mono-functional reactive diluent species (Table 3-1) for quick reactivity and to precisely control the mechanical properties of the DE. The diluents introduce

additional bonding between crosslinks to control the crosslink density and lower the modulus of the material. Urethane diacrylate (UDA, CN9021) was used as a flexible long-chain crosslinker with a high molecular weight for high elasticity and create part of the bimodal base crosslinked polymer matrix. Propoxylated neopentyl glycol diacrylate (PNPDA) was used as a short chain crosslinker to adjust the mechanical and electromechanical properties of the material by adjusting the crosslink density of the bimodal base matrix. Butyl acrylate (BA), isodecyl acrylate (IDA), and poly(propylene glycol) acrylate (PPGA) were used as monofunctional softening diluent materials to lower the viscosity of the prepolymer solution, and lower the modulus of the material. Isobornyl acrylate (IBOA) was used to improve the toughness of the polymer by introducing additional secondary bonding. Acrylic acid (AA) was used to lower the viscoelasticity by introducing hydrogen bonding. 2,2-dimethoxy-2-phenylacetophenone (DMPA) and benzophenone (BP) were used as co-photoinitiators. Each new DE, with monikers P(10)-BA(13), P(10)-IDA(13), P(10)-PPGA(13), and AA(2.5), contained 10 wt% PNPDA, 70 wt% UDA, 13 wt% BA, IDA, or PPGA, 5 wt% IBOA, 1 wt% DMPA and 0.5 wt% BP with an additional AA in 2.5 wt % only for AA(2.5).

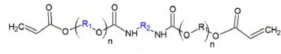
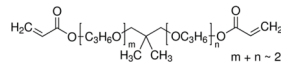
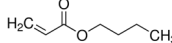
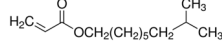
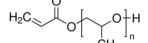
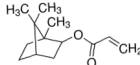
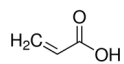
<b>Bimodal Base (Di-functional)</b>	Long Chain Crosslinker	Urethane Diacrylate (CN 9021)		<ul style="list-style-type: none"> <li>• High MW</li> <li>• Adds flexibility</li> <li>• Lowers modulus</li> </ul>
	Short Chain Crosslinker	Propoxylated Neopentyl Glycol Diacrylate (PNPDA)		<ul style="list-style-type: none"> <li>• Controls crosslink density to adjust mechanical and electromechanical properties</li> </ul>
<b>Improving Diluents (Mono-functional)</b>	Softening Component	Butyl Acrylate (BA)		<ul style="list-style-type: none"> <li>• Reduces viscosity</li> <li>• Lowers modulus</li> </ul>
		Isoodecyl Acrylate (IDA)		
		Poly (propylene glycol) Acrylate (PPGA)		
	Toughening Component	Isobornyl Acrylate (IBOA)		<ul style="list-style-type: none"> <li>• Improves elasticity</li> <li>• Increases breakdown field</li> <li>• Reduces viscosity</li> </ul>
	Additional Diluents	Acrylic Acid (AA)		<ul style="list-style-type: none"> <li>• Lowers viscoelasticity to improve response speed</li> </ul>

Table 3-1 Chemical structures of formulation components and materials selection of new DE polymer materials

### 3.3.2. Permittivity determination of new DEs

The dielectric constant of the material was determined to ensure it is sufficient for use within DEAs. The capacitance was measured and permittivity was calculated from Equation 3-3 to be 3.18 and 2.8 for AA(2.5) and 3.58 and 2.9 for P(10)-BA(13) at 12 Hz and 1kHz, respectively. Nominal VHB4905 has been reported with a permittivity of 4.2 at 1kHz. The corresponding permittivity of new DEs are well within the range for DE materials, with values similar to silicone elastomers, specifically Dow Corning HS3 and Nusil CF19-2186 with dielectric constants of 2.8.<sup>52</sup>

### 3.3.3. Mechanical properties of new DEs

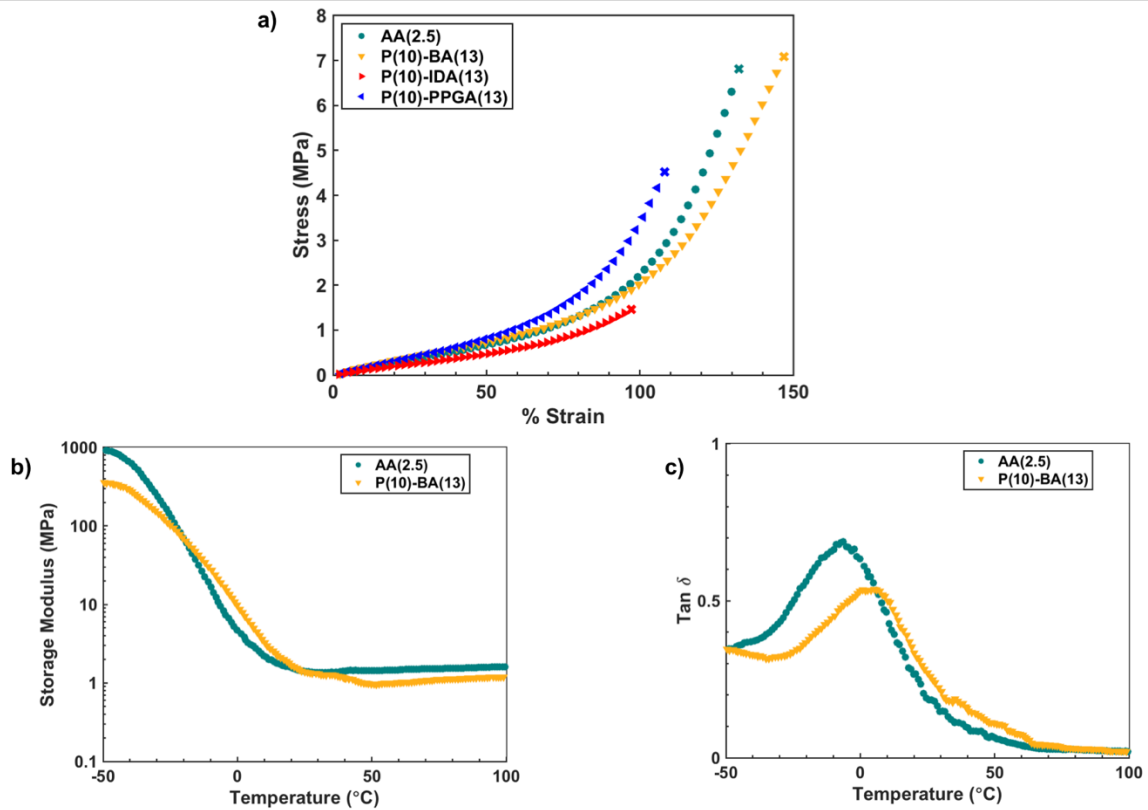


Figure 3-2. Mechanical properties of new DEs a) tensile stress-strain properties of four different formulations with four different diluents b) modulus as a function of temperature for AA(2.5) and P(10)-BA(13) c) tan delta as a function of temperature for AA(2.5) and P(10)-BA(13).

Dynamic mechanical analysis (DMA) was done to determine the mechanical properties of the several new DE materials (Fig. 3-2a). Four formulations were tested, P(10)-BA(13), P(10)-IDA(13), P(10)-PPGA(13), and AA(2.5), for tensile stress-strain properties looking for a rapid rise in the stiffness at high strain. The two materials with the lowest tensile strength and elongation at break were P(10)-IDA(13) and P(10)-PPGA(13) with tensile strength of 1.3 MPa and 4.5 MPa, respectively and strain of 98% and 109%, respectively (Fig. 3-2a). P(10)-IDA(13) had a slight rise in the stiffness at higher strain, but P(10)-

PPGA(13) had a higher slope, thus more pronounced stiffening. The two highest performing materials had similar tensile strengths of 7.3 MPa for P(10)-BA(13) and 7.1 MPa for AA(2.5) (Fig. 3-2a). In addition to the tensile stress-strain test, both materials underwent a temperature ramp test to measure the modulus and tan delta as a function of temperature. At room temperature, the DEs had similar moduli of 1.67 MPa and 1.54 MPa for P(10)-BA(13) and AA(2.5), respectively (Fig. 3-2b). When compared to the modulus and tensile strength of VHB, 0.5 MPa and 0.85 MPa, respectively, the new DE materials have a superior properties. This is likely due to the strong intermolecular bonds formed by the interpenetrating bimodal network of PNPDA and UDA. One significant attribute when determining the potential response speed in the two formulations is the viscoelasticity, as quantified by tan delta. A viscoelasticity below 0.5 indicates a higher contribution of elastic behavior, which is ideal for actuation at higher frequencies. The tan deltas for the new DEs were determined as 0.38 for P(10)-BA(13) and 0.2 for AA(2.5) (Fig. 3-2c). Both materials exhibit a larger contribution of elastic behavior, with AA(2.5) having more elastic behavior as evidence by the lower tan delta.

#### 3.3.4. *Static actuation performance of DEs*

The actuation performance of these materials was characterized by actuation on a diaphragm to limit wrinkling of the film. The films were spincoated onto treated glass and cured in air under UV light to quickly screen optimized formulations. The four DEs were tested were P(10)-BA(13), P(10)-IDA(13), P(10)-PPGA(13), and AA(2.5) using carbon grease electrodes with an applied voltage ranging from 0.5 kV to 5 kV or until failure. Actuation performance was measured in static actuation tests (Fig. 3-3a), where the material had a constant voltage applied for 5 seconds, to test the actuation stability, and characterized by Equation 3-4. Actuation performance for P(10)-IDA(13) was lowest compared with the other diluent materials, with an actuation strain of  $125 \pm 4.5 \%$  and nominal dielectric breakdown field of  $109 \pm 4.9$

V/ $\mu\text{m}$ . P(10)-PPGA(13) had high actuation over  $150 \pm 18.9$  % strain, however the breakdown field was 108 V/ $\mu\text{m}$ , lower than P(10)-IDA(13) with high inconsistency. The materials with the highest, most consistent performance were P(10)-BA(13) and AA(2.5). P(10)-BA(13) had highest actuation of each formulation with strain of 189% and nominal breakdown field of 135 V/ $\mu\text{m}$ . BA proved to be the best diluent material, by far, likely due to the short, flexible side chain compared to the longer side chains of the other two diluent materials. The formulation with the highest nominal field was AA(2.5) at  $151 \pm 4.9$  V/ $\mu\text{m}$ , with a maximum strain of  $188 \pm 4.5$  %. P(10)-BA(13) and AA(2.5) had very similar actuation performance. A visualization of the dome formed by the actuated material can be seen in Figure 3-3b. The AA(2.5) sample was actuated at 4.5 kV with a resulting strain of 188% using a carbon grease electrode. The material has very stable actuation, even at high voltage, with high actuation strain and high breakdown field.

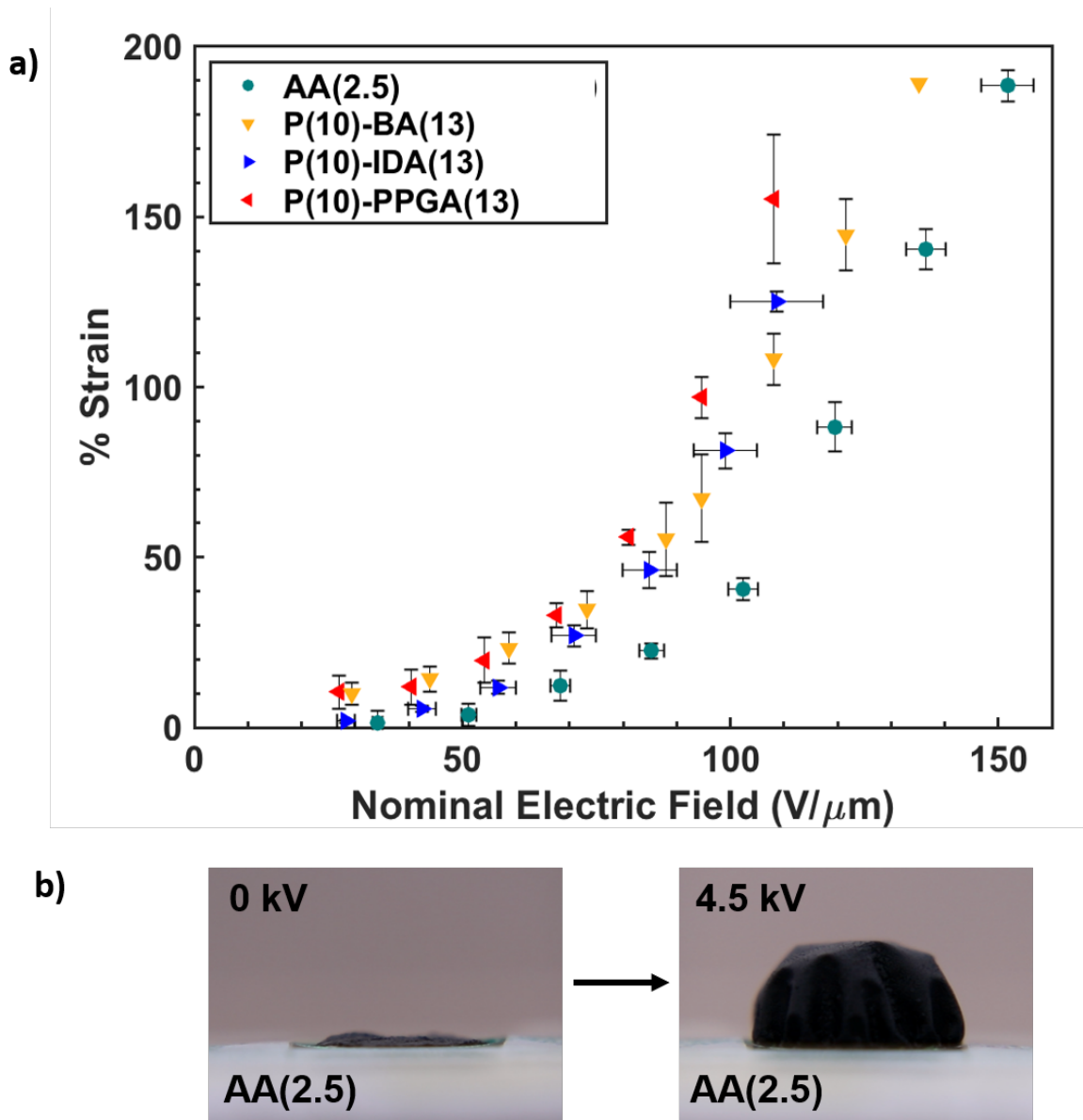


Figure 3-3. a) Static actuation performance of four formulations with different diluent materials b)

Images of dome shape formed when AA(2.5) is actuated at 4.5 kV.

### 3.3.5. Cyclic actuation performance of DEs

The highest performing formulations of AA(2.5) and P(10)-BA(13) were tested for frequency response at 2 Hz. Figure 3-4 shows over 110% average actuation strain of AA(2.5) at 2 Hz and P(10)-BA(13) with an



average of about 75% strain. Although these materials have similar static actuation character, when high frequencies are applied, AA(2.5) shows better performance than P(10)-BA(13). This is due to the difference in the viscoelasticity. AA(2.5) has a tan delta of 0.2 and P(10)-BA(13) has a tan delta of 0.38. The tan delta relates to the viscoelasticity of the material and is indicative of the response speed. The closer to 0.1 the material tan delta, the more elastic and the faster the response speed, thus a higher strain when actuated at high frequencies. AA(2.5) has a lower viscoelasticity, thus a faster response speed, and higher actuation strain at 2 Hz. When comparing the actuation performance of AA(2.5) at 2 Hz (110%) to static actuation at the same voltage (140%) the material actuation recovery at high frequency is 78%, showing high elastic performance and rapid response speed.

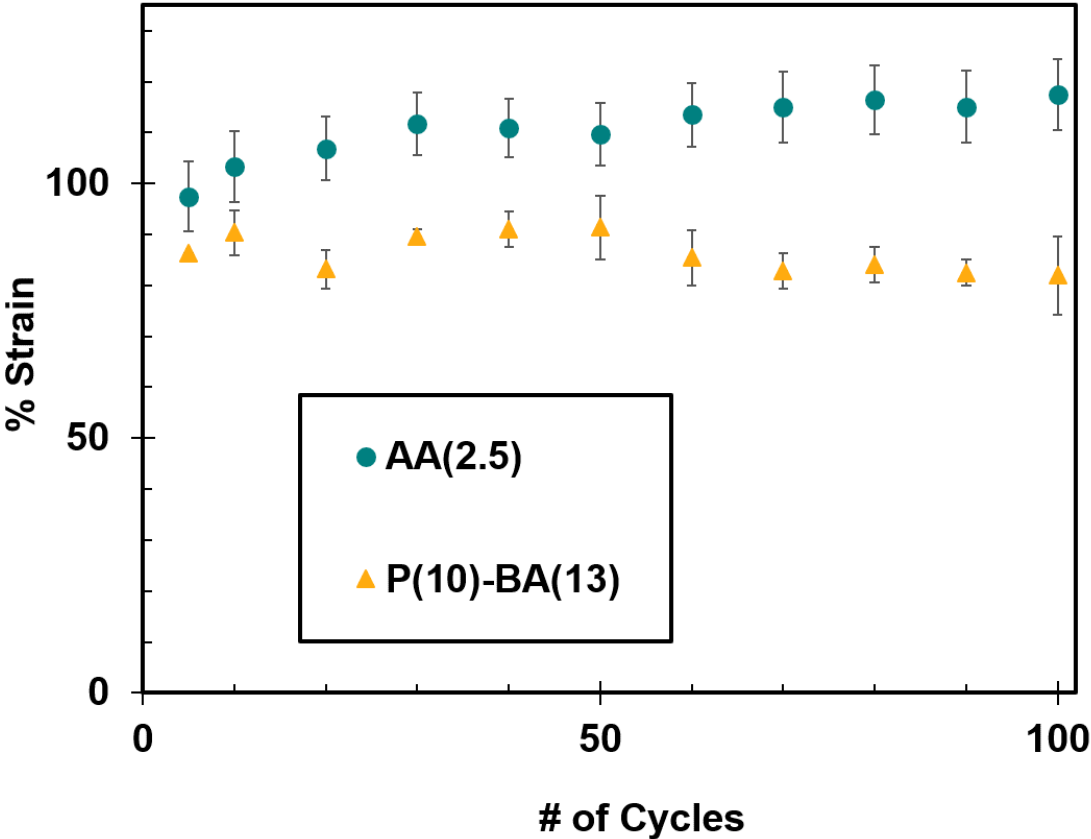


Figure 3-4. Frequency response of AA(2.5) and P(10)-BA(13) at 2 Hz.

### 3.3.6. Comparison of DEs to VHB<sup>TM</sup>

The actuation performances of AA(2.5) and P(10)-BA(13) were compared to 300% biaxially prestretched VHB4905 with carbon grease electrodes. When comparing AA(2.5) to VHB (Fig 3-5a), actuation strain of AA(2.5) at  $188 \pm 4.5\%$  and P(10)-BA(13) at 189%, VHB is much lower, at 163%. The highest preforming AA(2.5) can achieve actuation strain far beyond 300% biaxially prestretched VHB with actuation strains near 200% without prestretch. The nominal electric field of AA(2.5) is higher than VHB at  $151 \pm 4.9 \text{ V}/\mu\text{m}$ , whereas VHB has a field of  $110 \text{ V}/\mu\text{m}$ . Additionally, as seen in Figure 3-4, AA(2.5) can also achieve actuation over 100% strain at 2 Hz, which VHB cannot achieve without modification. This indicates AA(2.5) can withstand higher fields, achieve similar actuation compared, and actuate at high frequencies than VHB without prestretching.

The maximum energy density and Maxwell stress were calculated based on Equation 3-2 and Equation 3-1, respectively. AA(2.5) had a maximum energy density at  $3.48 \text{ MJ}/\text{m}^3$ , slightly higher than VHB, which has a maximum energy density of  $3.4 \text{ MJ}/\text{m}^3$ .<sup>52</sup> The Maxwell pressure generated by the new materials are very similar, with the exception of P(10)-BA(13), which had the lowest compared Maxwell pressure at 1.6 MPa. AA(2.5) was comparable to VHB with maximum of 3.2 MPa for AA(2.5) and 3.5 MPa for VHB4905 300% biaxially prestretched. The difference in Maxwell pressure could be attributed to the lower dielectric constant in the new DE materials. However, AA(2.5) did not require prestretch and achieved a high Maxwell pressure, whereas VHB required 300% biaxial prestretch to achieve nearly the same pressure.

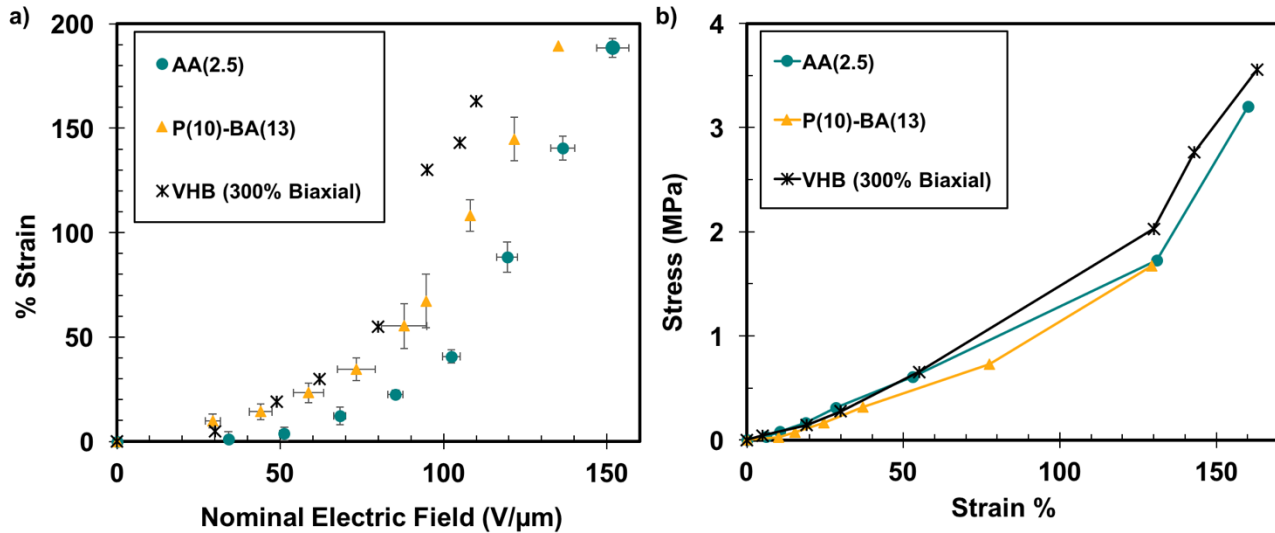


Figure 3-5. a) Static actuation of AA(2.5) and P(10)-BA(13) compared to 300% biaxially prestretched VHB 4905. b) Comparison of the Maxwell pressure of AA(2.5) and P(10)-BA(13) to VHB 4905 300% biaxially prestretched. Information for VHB 4905 adopted from Ref 96.

### 3.4. Conclusion

In conclusion, a new dielectric elastomer was synthesized with properties similar-to and better-than prestretched VHB without prestretching. Several new dielectric elastomers were synthesized for optimized actuation performance and all achieved actuation over 100% strain and breakdown fields over 100 V/ μm. From the materials developed, two showed actuation performances similar to 300% biaxially prestretched VHB, without prestretching. These materials exhibited static actuation performance of nearly 200% strain, exceeding 300% biaxially prestretched VHB. AA(2.5) showed Maxwell pressure and energy density similar to prestretched VHB with a pressure of 3.2 MPa and energy density of 3.48 MJ/m<sup>3</sup>. Lastly, AA(2.5) showed excellent response speed with actuation over 100% at 2 Hz, far exceeding the capability of VHB.

Overall, AA(2.5) exhibited high actuation strain and high pressure similar to VHB, with rapid response without the requirement of prestretch.

### 3.5. References

- (84) Pelrine, R.; Pei, Q.; Koenblug, R. Dielectric Elastomers: Past, Present, and Potential Future. *Electroact. Polym. Actuators Devices EAPAD* **2018**, 10594.
- (85) Meijer, K.; Rosenthal, M. S.; Full, R. J. Muscle-like Actuators? A Comparison between Three Electroactive Polymers; Bar-Cohen, Y., Ed.; Newport Beach, CA, USA, 2001; p 7.  
<https://doi.org/10.1117/12.432649>.
- (86) Artificial Muscles. *Sci. Am.* **2003**, 289 (4), 53–59.
- (87) Kovacs, G.; Ha, S. M.; Michel, S.; Pelrine, R.; Pei, Q. Study on Core Free Rolled Actuator Based on Soft Dielectric EAP; Bar-Cohen, Y., Ed.; San Diego, California, 2008; p 69270X.  
<https://doi.org/10.1117/12.776787>.
- (88) Kofod, G.; Wirges, W.; Paajanen, M.; Bauer, S. Energy Minimization for Self-Organized Structure Formation and Actuation. *Appl. Phys. Lett.* **2007**, 90 (8), 081916.  
<https://doi.org/10.1063/1.2695785>.
- (89) Anderson, I. A.; Tse, T. C. H.; Inamura, T.; O'Brien, B. M.; McKay, T.; Gisby, T. A Soft and Dexterous Motor. *Appl. Phys. Lett.* **2011**, 98 (12), 123704. <https://doi.org/10.1063/1.3565195>.
- (90) Aschwanden, M.; Beck, M.; Stemmer, A. Diffractive Transmission Grating Tuned by Dielectric Elastomer Actuator. *IEEE Photonics Technol. Lett.* **2007**, 19 (14), 1090–1092.  
<https://doi.org/10.1109/LPT.2007.900055>.
- (91) Kollosche, M.; Kofod, G.; Doring, S.; Hildebrandt, N.; Stumpe, J. Optical Transmission Gratings Tuned by Electro Active Polymers. In *2010 10th IEEE International Conference on Solid Dielectrics*; IEEE: Potsdam, Germany, 2010; pp 1–4. <https://doi.org/10.1109/ICSD.2010.5568261>.

- (92) Sarban, R.; Jones, R. W.; Mace, B.; Rustighi, E. Active Vibration Control of Periodic Disturbances Using a DEAP Damper; Bar-Cohen, Y., Ed.; San Diego, California, USA, 2010; p 76422Q. <https://doi.org/10.1117/12.845764>.
- (93) Rustighi, E.; Kaal, W.; Herold, S.; Kubbara, A. Experimental Characterisation of a Flat Dielectric Elastomer Loudspeaker. *Actuators* **2018**, *7* (2), 28. <https://doi.org/10.3390/act7020028>.
- (94) Zhao, H.; Hussain, A. M.; Israr, A.; Vogt, D. M.; Duduta, M.; Clarke, D. R.; Wood, R. J. A Wearable Soft Haptic Communicator Based on Dielectric Elastomer Actuators. *Soft Robot.* **2020**, soro.2019.0113. <https://doi.org/10.1089/soro.2019.0113>.
- (95) Ig Mo Koo; Kwangmok Jung; Ja Choon Koo; Jae-Do Nam; Young Kwan Lee; Hyouk Ryeol Choi. Development of Soft-Actuator-Based Wearable Tactile Display. *IEEE Trans. Robot.* **2008**, *24* (3), 549–558. <https://doi.org/10.1109/TRO.2008.921561>.
- (96) Niu, X.; Stoyanov, H.; Hu, W.; Leo, R.; Brochu, P.; Pei, Q. Synthesizing a New Dielectric Elastomer Exhibiting Large Actuation Strain and Suppressed Electromechanical Instability without Prestretching. *J. Polym. Sci. Part B Polym. Phys.* **2013**, *51* (3), 197–206. <https://doi.org/10.1002/polb.23197>.
- (97) Suo, Z. THEORY OF DIELECTRIC ELASTOMERS. *ACTA Mech. SOLIDA Sin.* **2010**, *23* (6), 30.
- (98) Duduta, M.; Wood, R. J.; Clarke, D. R. Multilayer Dielectric Elastomers for Fast, Programmable Actuation without Prestretch. *Adv. Mater.* **2016**, n/a-n/a. <https://doi.org/10.1002/adma.201601842>.
- (99) Vatankhah-Varnoosfaderani, M.; Daniel, W. F. M.; Zhushma, A. P.; Li, Q.; Morgan, B. J.; Matyjaszewski, K.; Armstrong, D. P.; Spontak, R. J.; Dobrynin, A. V.; Sheiko, S. S. Bottlebrush Elastomers: A New Platform for Freestanding Electroactuation. *Adv. Mater.* **2017**, *29* (2), 1604209. <https://doi.org/10.1002/adma.201604209>.

- (100) Daniel, W. F. M.; Burdyńska, J.; Vatankhah-Varnoosfaderani, M.; Matyjaszewski, K.; Paturej, J.; Rubinstein, M.; Dobrynin, A. V.; Sheiko, S. S. Solvent-Free, Supersoft and Superelastic Bottlebrush Melts and Networks. *Nat. Mater.* **2015**, *15* (2), 183–189. <https://doi.org/10.1038/nmat4508>.
- (101) Ellingford, C.; Bowen, C.; McNally, T.; Wan, C. Intrinsically Tuning the Electromechanical Properties of Elastomeric Dielectrics: A Chemistry Perspective. *Macromol. Rapid Commun.* **2018**, *39* (18), 1800340. <https://doi.org/10.1002/marc.201800340>.
- (102) Opris, D. M.; Molberg, M.; Walder, C.; Ko, Y. S.; Fischer, B.; Nüesch, F. A. New Silicone Composites for Dielectric Elastomer Actuator Applications In Competition with Acrylic Foil. *Adv. Funct. Mater.* **2011**, *21* (18), 3531–3539. <https://doi.org/10.1002/adfm.201101039>.

## **Chapter 4. Synthesis and comparison of three BAB triblock copolymers featuring poly (ethylene glycol) and poly (stearyl acrylate) using RAFT polymerization**

### **4.1. Background of the study**

Block copolymers (BCP) consist of two or more homopolymer materials covalently linked together. In some cases these two blocks are amphiphilic, in which one homopolymer is a water-soluble hydrophilic block and one is a water-insoluble hydrophobic block. These covalently bonded dissimilar materials yield a combination of distinct properties within the macromolecule for unique nanoscale formations that lead to macroscale properties. BCPs have been used as rubber materials,<sup>103–105</sup> biomedical assemblies,<sup>106, 107</sup> surfactants,<sup>108</sup> coatings,<sup>109</sup> nanolithography,<sup>110</sup> and more.<sup>111, 112</sup>

#### *4.1.1. Triblock copolymers*

Several types of triblock copolymer exist, ABA, BAB, and ABC. These different alphanumeric systems represent block formations where A represents the solvophilic block, B represents the solvophobic block, and C represents an additional block of a third homopolymer that can be either solvophilic or solvophobic. These different formations result in very different nanostructure and self assembly. The most common type of triblock is ABA which forms corona-core micelles, where B blocks aggregate within a shell of A-block tails. However, BAB triblock copolymers offer a different self-assembly that can be beneficial in resulting mechanical properties. BAB copolymers in A selecting solvents form a flower-like micelle in which the A middle-block forms a shell around the dangling B-block ends (Fig. 4-1). In some cases, a dangling end of a B-block occurs, branching the micelle aggregated for interconnected micelles, in which two different B-blocks can incorporate into different micelle cores.<sup>113</sup> This bridging results in additional entanglements that lead to interesting thin film properties.

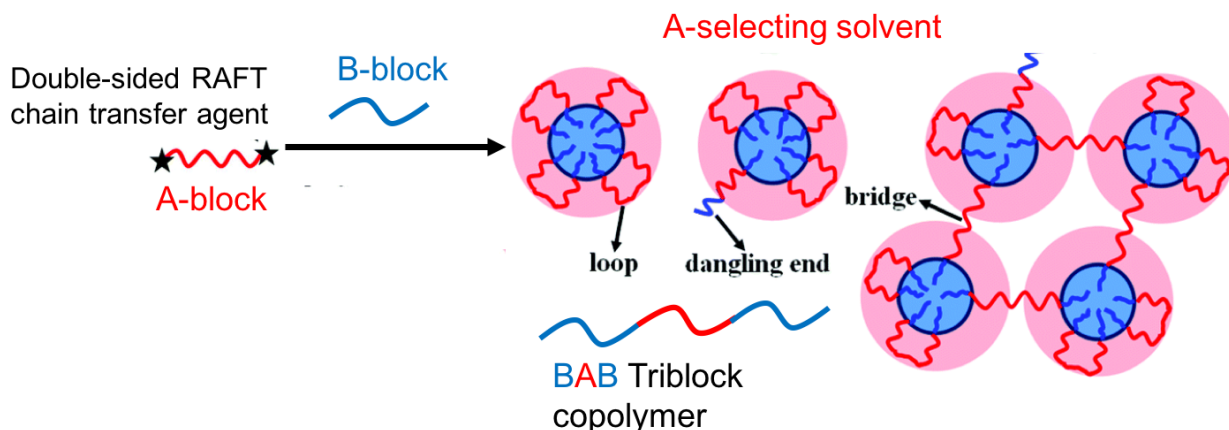


Figure 4-1. Morphology of symmetrical amphiphilic BAB triblock copolymers in A-selecting solvent.

Adopted from Ref 113.

#### 4.1.2. RAFT polymerization

Reversible addition-fragmentation chain-transfer polymerization (RAFT) is a type of “living” polymerization often used to synthesize block copolymers. Typical free radical polymerization techniques yield a wide range of number average molecular weights with a high polydispersity index. RAFT polymerization process begins with a chain transfer agent, typically containing thiocarbonylthio groups, then utilizes a thermal initiator, such as 2,2'-azobisisobutylnitrile (AIBN) to produce radicals. RAFT is considered controlled free radical polymerization because it cannot occur without an external supply of radicals from an initiator and “living” due to the potential for chain reinitiation. The RAFT mechanism is such that individual polymer chain growth begins at the same time equilibrium is achieved, key to obtaining good control of molecular architectures, low polydispersity index (PDI), and high number average molecular weight. Additionally, RAFT chain transfer agents can be designed and modified for multiple initiation sites to form symmetrical block-copolymers or other complex symmetric architectures.



#### 4.1.3. Synthesized BAB triblock copolymers

We introduce three BAB copolymers with poly (ethylene glycol) (PEG) and stearyl (acrylate) (PSA) with different lengths of PSA. The BAB triblock copolymer consists of a poly (ethylene glycol) ( $M_n=100,000$  g/mol) (PEG100K) A- block synthesized as a double sided macro-RAFT chain transfer agent flanked by a poly (stearyl acrylate) (PSA) B-block. Three different lengths of poly (stearyl acrylate) were added to the double-sided macro RAFT chain transfer agent (DDMAT-PEG) synthesized with a degree of polymerization of 100 (50 on each side), 200 (100 on each side), and 400. The polymer combines the flexibility of PEG with the crystallization characteristics of stearyl acrylate for maximum stiffness. The crystallization contributes to high stiffness in the rigid state at room temperature, then melts to viscous liquid at elevated temperature (around 70 °C). The polymer has a modulus at room temperature of 1 GPa and reversibly transitions from a stiff film to a viscous liquid. The polymer also exhibits amphiphilic behavior wherein it is soluble in both water and chloroform.

## 4.2. Experimental design

### 4.2.1. Raw materials

Poly (ethylene oxide)  $M_n=100,000$  g/mol, 2-(dodecylthiocarbonothioylthio)-2-methylpropionic acid (DDMAT), 4-dimethylaminopyridine (DMAP), dicyclohexylcarbodiimide (DCC), 2,2'-Azobis(isobutyronitrile) (AIBN), and octadecyl acrylate were purchased from Sigma Aldrich and used as received. Dichloromethane and toluene were purchased from Fisher Scientific and used as received.

### 4.2.2. Proton nuclear magnetic resonance ( $^1H$ NMR)

Copolymers composition and microstructure were determined by NMR spectroscopy.  $^1H$  NMR spectra

were recorded in chloroform- $d_1$  ( $CDCl_3$ ) using a Bruker AV400 spectrometer operating at 400 MHz. The sample solutions were prepared by dissolving dried polymer in  $CDCl_3$  in 5 mg/mL concentration.

#### 4.2.3. *Gel permeation chromatography (GPC)*

The number- average molecular weights ( $M_n$ ) of copolymers were determined by GPC, using a Shimadzu i-Series Plus that was equipped with a set of one 5 cm styrene column with two 30 cm columns in series. A Wyatt Optilab Rex differential refractometer and a Dawn Eos (Wyatt Technology Corporation) laser photometer (MALS) were used as detectors. The measurements were conducted at 40 °C. The  $dn/dc$  increment of the refractive index of 0.0562, 0.0646, and 0.0685 mL  $g^{-1}$  were used for PSA50-PEG-PSA50, PSA100-PEG-PSA100, and PSA200-PEG-PSA200, respectively. Tetrahydrofuran (THF) was used as eluent at a flow rate of 0.7 mL  $min^{-1}$ .

#### 4.2.4. *Fourier transform infrared (FTIR) spectroscopy*

Fourier transform infrared (FTIR) spectra were measured with a Jasco 420 FTIR spectrometer. The spectra were obtained by adding 32 scans at a resolution of 4  $cm^{-1}$ .

#### 4.2.5. *Differential scanning calorimetry (DSC)*

Differential scanning calorimetry (DSC) analyses were performed under a nitrogen atmosphere at heating and cooling rates of 5 °C  $min^{-1}$ , respectively, on a Perkin Elmer DSC 800. The measurements were performed from 0 °C to 100 °C for the three triblock copolymers.

#### 4.2.6. *Dynamic mechanical analysis (DMA)*

Mechanical properties were measured on a TA Instruments RSAIII dynamic mechanical analyzer

(DMA). Dynamic temperature sweep tests were conducted at a temperature ramping rate of 3 °C/min and a frequency of 1 Hz from 25 to 70 °C with samples of 5 mm wide and ~0.1 mm thick loaded onto the DMA with a 10 mm gap between the thin film grips. The maximum elongation strain of the rubbery copolymers were obtained at 70 °C at a stretching rate of 7.0 mm/s. The tested samples used were 5 mm wide and 100 µm thick with a 6 mm gap between the thin film grips of the DMA.

#### 4.2.7. *Scanning electron microscopy (SEM)*

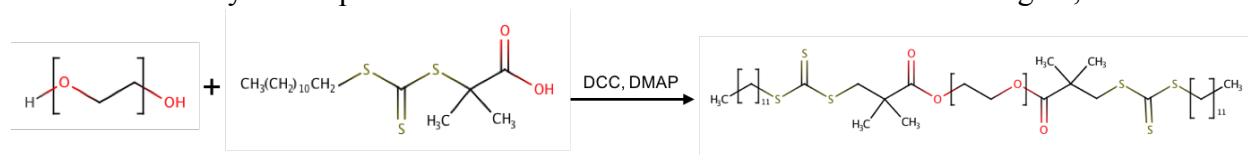
The morphology of obtained microparticles and nanospheres were monitored via scanning electron microscopy (SEM). The images were taken with a JEOL Scanning Electron Microscope (Model JXA-8230) in high-vacuum mode at an acceleration voltage of 5 kV. Samples were coated with a gold conductive layer, ~10 nm thick, using a sputter coater (Anatech Hummer 6.2 Sputter Coater).

#### 4.2.8. *Synthesis of macro-RAFT chain transfer agent*

A PEG based macro-RAFT chain transfer agent (DDMAT-PEG) was synthesized by esterification using the methods described by Liang<sup>114</sup> with slight modification. The reaction was carried out under argon in by dissolving PEG100K (15 g, 1eq) and 2-(dodecylthiocarbonothioylthio)-2-methylpropionic acid (DDMAT) (0.164 g, 3 eq) RAFT chain transfer agent in 50 mL of dichloromethane. The solution was stirred under argon at 0 °C for 20 min. After 20 min, a solution of 4-dimethylaminopyridine (DMAP) (0.007 g, 0.4 eq) and N,N'-dicyclohexylcarbodiimide (DCC) (0.123 g, 4 eq) dissolved in 50 mL of dichloromethane was added dropwise to the flask (Scheme 4-1). The reaction was then stirred at room temperature for 48 hours. The contents of the flask was dried by rotary evaporation and the light yellow product was precipitated by adding an excess of diethyl ether to the filtrate two times. The product was

then washed twice by centrifugation (8000 rpm for 15 min) in excess acetone. The resulting product was dried under vacuum and the structure was proven by  $^1\text{H}$ NMR spectroscopy.

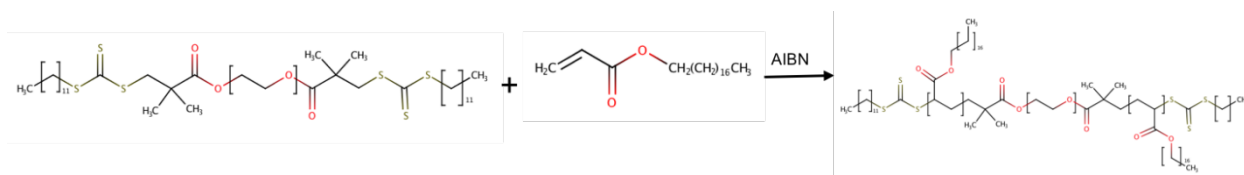
Scheme 4-1: Synthetic process for PEG-based macro-RAFT chain transfer agent, DDMAT-PEG



#### 4.2.9. Synthesis of three PSA-PEG-PSA triblock copolymers

To synthesize three BAB triblock copolymers, the DDMAT-PEG macro-RAFT chain transfer agent (3 eq) was dissolved in a 2:1 mixture of toluene and dichloromethane with 2,2'-Azobis(2-methylpropionitrile) (AIBN) (2 eq) and styryl acrylate (1000 eq, 2000 eq, and 250 eq) (Scheme 4-2). The solution was added into a Schlenk flask and deoxygenated by three consecutive freeze-pump-thaw cycles. The reaction was then heated to 65 °C for 18 hours. The reaction was then immediately cooled, and the solvent was evaporated via rotary evaporation and vacuum drying. The polymer (PSA<sub>x</sub>-PEG-PSA<sub>x</sub>) structure was characterized by  $^1\text{H}$ NMR spectroscopy, gel permeation chromatography (GPC), Fourier transform infrared (FTIR) spectroscopy, and differential scanning calorimetry (DSC). The polymer thin film was characterized by dynamic mechanical analysis (DMA), optical microscopy, and scanning electron microscopy (SEM)

Scheme 4-2: Synthetic process for BAB Triblock PSA<sub>x</sub>-PEG-PSA<sub>x</sub>



### 4.3. Results and Discussion

#### 4.3.1. Proton nuclear magnetic resonance ( $^1\text{H NMR}$ )

$^1\text{H NMR}$  spectroscopy was performed to confirm synthesis of both the DDMAT-PEG macro-RAFT chain transfer agent (Fig. 4-2) and PS $_x$ -PEG-PS $_x$  RAFT BAB triblock copolymer (Fig. 4-3). DDMAT-PEG macro-RAFT agent (Fig. 4-2) contains a peak at  $\delta$  3.67 ppm corresponding to the methylene protons of PEG group [-CH<sub>2</sub>-CH<sub>2</sub>-O-]. The dodecyl segments from the chain ends have a chemical shift at  $\delta$  1.28 ppm. The methyl end group protons from the dodecyl chain have a chemical shift of  $\delta$  0.90 ppm. The methyl peaks from -C(CH<sub>3</sub>)<sub>2</sub>- segment have a chemical shift of  $\delta$  1.72 ppm. The ratios between H<sub>1,2</sub> and H<sub>6</sub> is consistent with the theoretical prediction and the spectra confirms formation of DDMAT-PEG macro-RAFT agent.

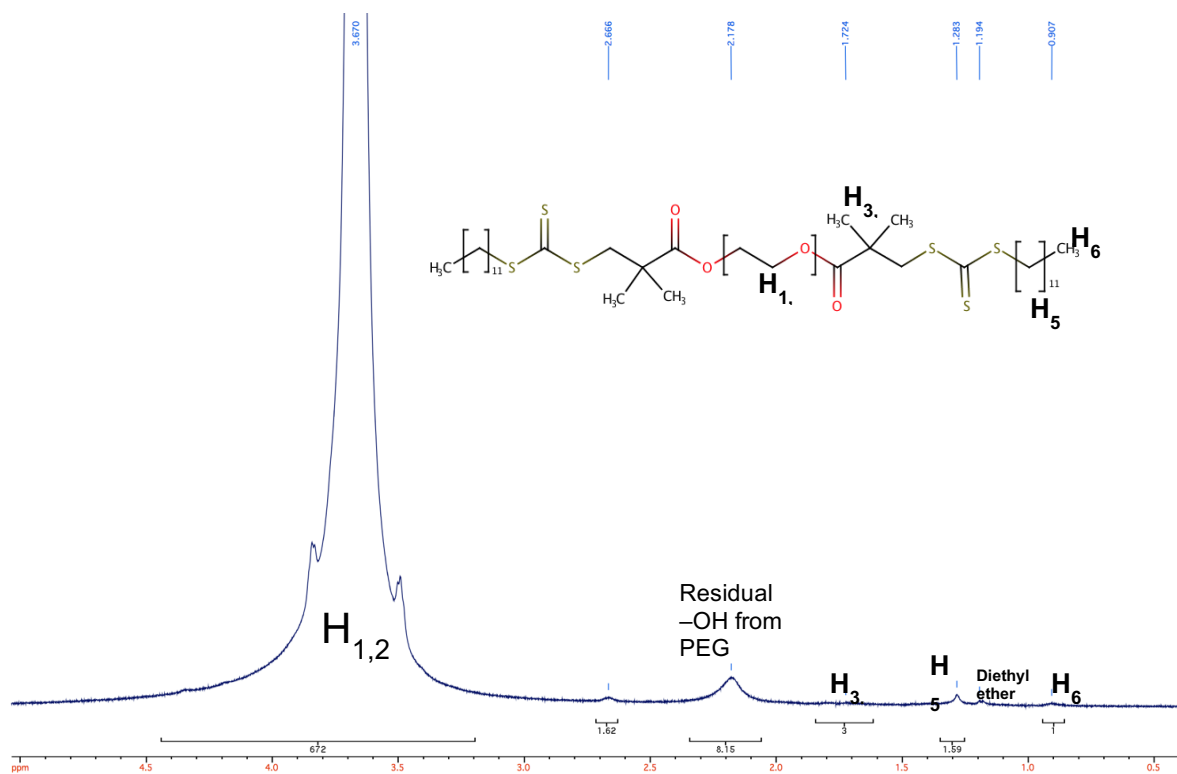


Figure 4-2. DDMAT-PEG100K  $^1\text{H NMR}$  in chloroform- $d_1$

Figure 4-3 overlays each of the three BAB triblock copolymer  $^1\text{H}$ NMR spectra for a direct comparison of chemical shifts. The presence of PEG is indicated by the large peak at  $\delta$  3.67 ppm corresponding to the [-CH<sub>2</sub>-CH<sub>2</sub>-O-] methylene groups. The peak at  $\delta$  4.0 ppm appears and increases corresponding to the methylene protons adjacent to the oxygen atom of PSA. The peaks at  $\delta$  0.9 ppm corresponds to the methyl groups in PSA and dodecyl methyl end groups. The peaks at  $\delta$  1.28 ppm correspond to the alkyl chain methylene groups in the dodecyl segments and PSA segments. As the polymer molecular weight increases with additional poly (stearyl acrylate) (PSA) segments, peaks at 2.25 ppm and 1.6 ppm appear and increase corresponding to the methylene groups along the backbone of the polymer. The overlay plot displays three different, increasing, lengths of triblock copolymer with the same chemical makeup suggesting the formation of three BAB triblock copolymers containing PEG and PSA.

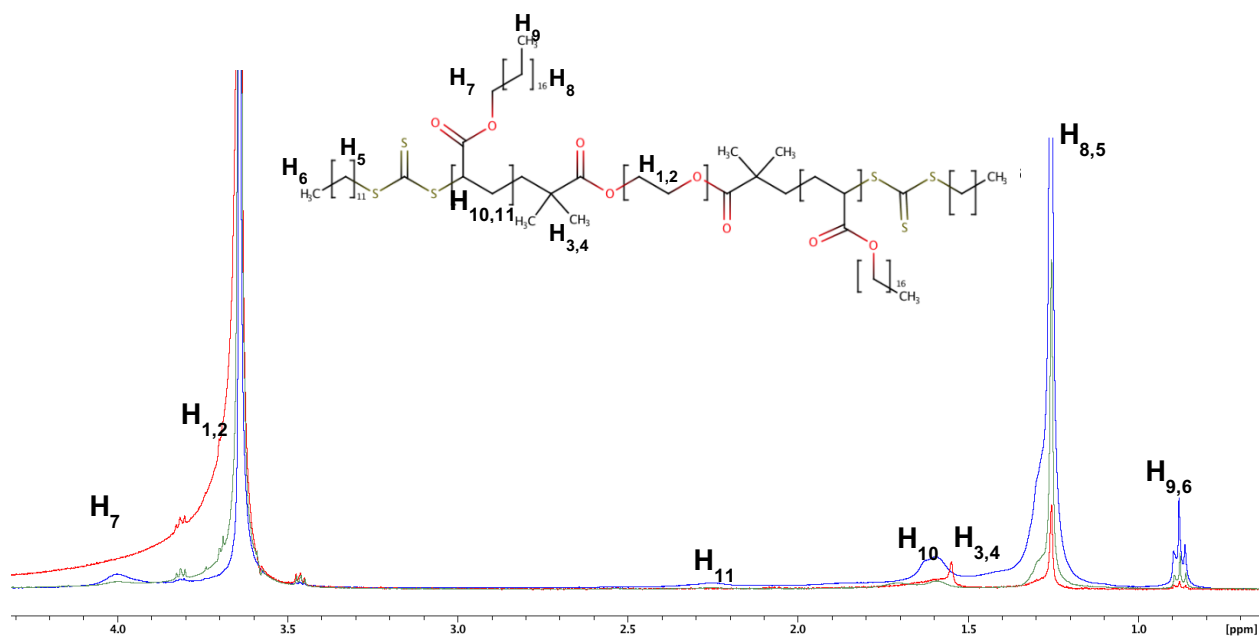


Figure 4-3. PSA50-PEG-PSA50 (red), PSA100-PEG-PSA100 (green), PSA200-PEG-PSA200 (blue)

$^1\text{H}$ NMR in chloroform- $d_1$

#### 4.3.2. Gel permeation chromatography (GPC)

GPC was performed to determine the molecular weight of each synthesized polymer. It was performed in tetrahydrofuran (THF) using MALS light scattering. The change in refractive index with respect to the change in concentration ( $dn/dc$ ) was determined by creating a standard curve with concentrations of 0.25 mg/mL, 0.5 mg/mL, 1 mg/mL, 2 mg/mL, 4 mg/mL and 5 mg/mL. The  $dn/dc$  increment of the refractive index of 0.0562, 0.0646, and 0.0685 mL/g were used for PSA50-PEG-PSA50, PSA100-PEG-PSA100, and PSA200-PEG-PSA200, respectively. The GPC results can be seen in Table 4-1. The GPC results were consistent with the predicted results, except in the case of PSA50-PEG-PDSA50, with a determined molecular weight of 132,220 g/mol and PDI of 1.18. PSA50-PEG-PSA50 was formulated for a degree of polymerization of 50 (25 on each side), but reaction conditions resulted in higher conversion than expected. The polymer had twice the amount of PSA than predicted, likely due to higher reaction temperature. PSA100-PEG-PSA100 and PSA200-PEG-PSA200 had molecular weights of 163,400 g/mol and 238,200 g/mol, respectively, which matched the predicted results. The PDI of each synthesized polymer was very low ranging from 1.13-1.18. Equation 4-1 was used to determine the molar ratio for each reaction. By using the desired final molecular weight minus PEG molecular weight ( $M_n=100,000\text{g/mol}$ ) as the theoretical  $M_n$  and an assumed conversion of 60% as seen in prior iterations, the desired molar ratio was determined. An example calculation for the determination of PSA100-PEG-PSA100 molar ratio is given in Equation 4-2. The GPC results confirm the molecular weights and formation of each synthesized polymer with low polydispersity and high consistency.

Table 4-1. Gel Permeation Chromatography Results for PSA<sub>x</sub>-PEG-PSA<sub>x</sub>

Sample	DP	Equiv RAFT, [RAFT] <sub>0</sub>	Equiv SA, [M] <sub>0</sub>	Equiv AIBN	M <sub>n</sub> (g/mol)	PDI	dn/dc (mL/g)	Conversion
PSA50-PEG-PSA50	98	3	250	2	132,220	1.18	0.0562	86.3%
PSA100-PEG-PSA100	194	3	1000	2	163,400	1.15	0.0646	58.7%
PSA200-PEG-PSA200	426	3	2000	2	238,200	1.13	0.0685	64.0%

Equation 4-1: RAFT polymerization prediction model

$$M_n(\text{theoretical}) = \frac{[M]_0}{[\text{RAFT}]_0} \times \text{conversion} \times M_i$$

where [M]<sub>0</sub> is the initial monomer concentration, M<sub>i</sub> is the monomer molecular weight, [RAFT]<sub>0</sub> is the initial RAFT concentration.

Equation 4-2: Example of theoretical prediction for PSA100-PEG-PSA100

$$M_n(\text{theoretical}) = 164800 \frac{g}{mol} - 100,000 \frac{g}{mol} (\text{PEG}) = 64800 \frac{g}{mol}$$

$$64800 \frac{g}{mol} = \frac{[M]_0}{[\text{RAFT}]_0} \times 0.6 \times 324 \text{ g/mol}$$

$$\frac{[M]_0}{[\text{RAFT}]_0} = 333.33$$

#### 4.3.3. Fourier transform infrared spectroscopy (FTIR)

FTIR was performed for additional characterization of the synthesized polymers and determine distinguishing features from PEG100K. The results of the FTIR (Fig. 4-4) confirm the presence of PSA and PEG in the synthesized polymers. Overall, the peaks grow with the addition of increasing amounts of



PSA to the PEG100K middle block. The CH<sub>2</sub>-CH<sub>2</sub> peak (Fig. 4-5a) from 3000-2600 cm<sup>-1</sup> is present in every sample due to the presence of sp<sup>3</sup> carbons in the PEG block alkyl components but grows with the addition of PSA resulting from the long chain alkyl segments. The formation of a split peak, causing a shrinkage of what would have been a peak similar to PSA100-PEG-PSA100, in PSA200-PEG-PSA200 can be explained by the presence of symmetric and asymmetric bonds. The splitting does not occur in PSA50-PEG-PSA50 or PSA100-PEG-PSA100 because the concentration of PSA is not higher enough. The concentration of PSA is not higher than the PEG methylene concentration and thus a split does not occur. The C=O peak (Fig. 4-5b) at 1770-1650 cm<sup>-1</sup> is another differentiating peak. There is no C=O bonds present in PEG100K, however, each synthesized polymer has this peak present from the carbonyl in the acrylate of PSA. The C=O intensity from the acrylate increases as the PSA amount increases. This confirms the presence of increasing amounts of PSA in the co-polymer.

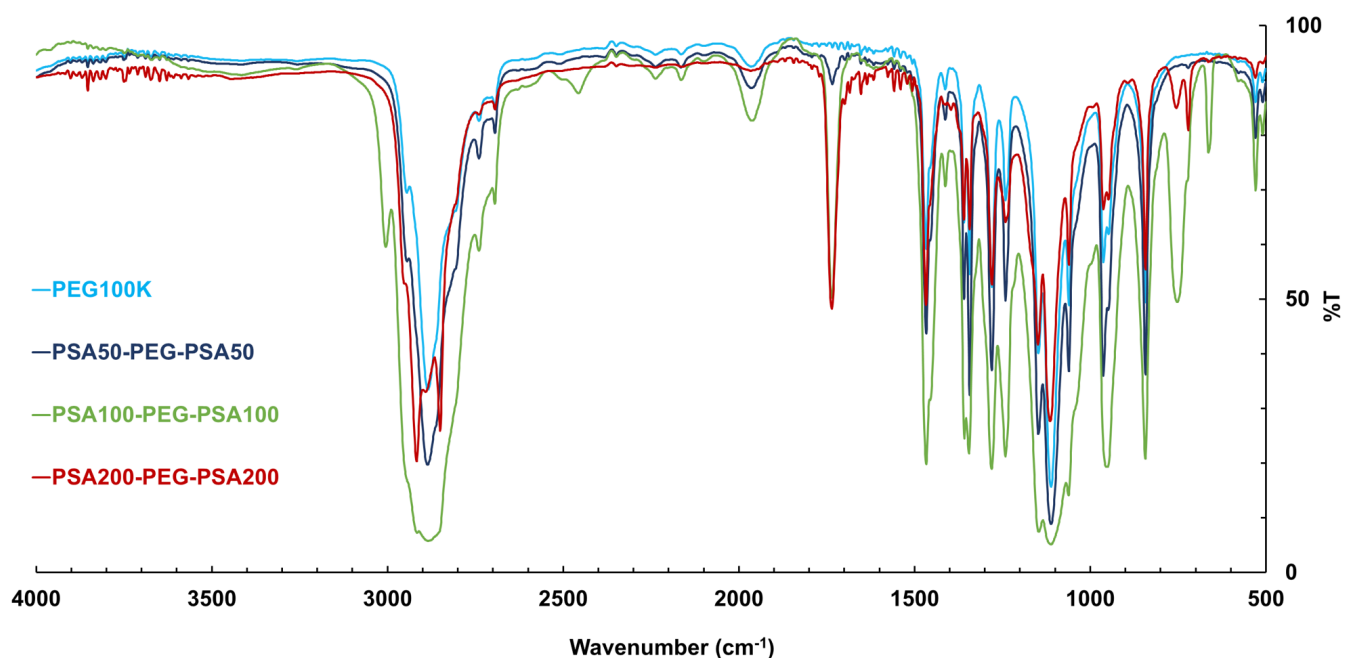


Figure 4-4. FTIR overlay of each synthesized triblock copolymer compared to PEG M<sub>n</sub>=100,000 g/mol

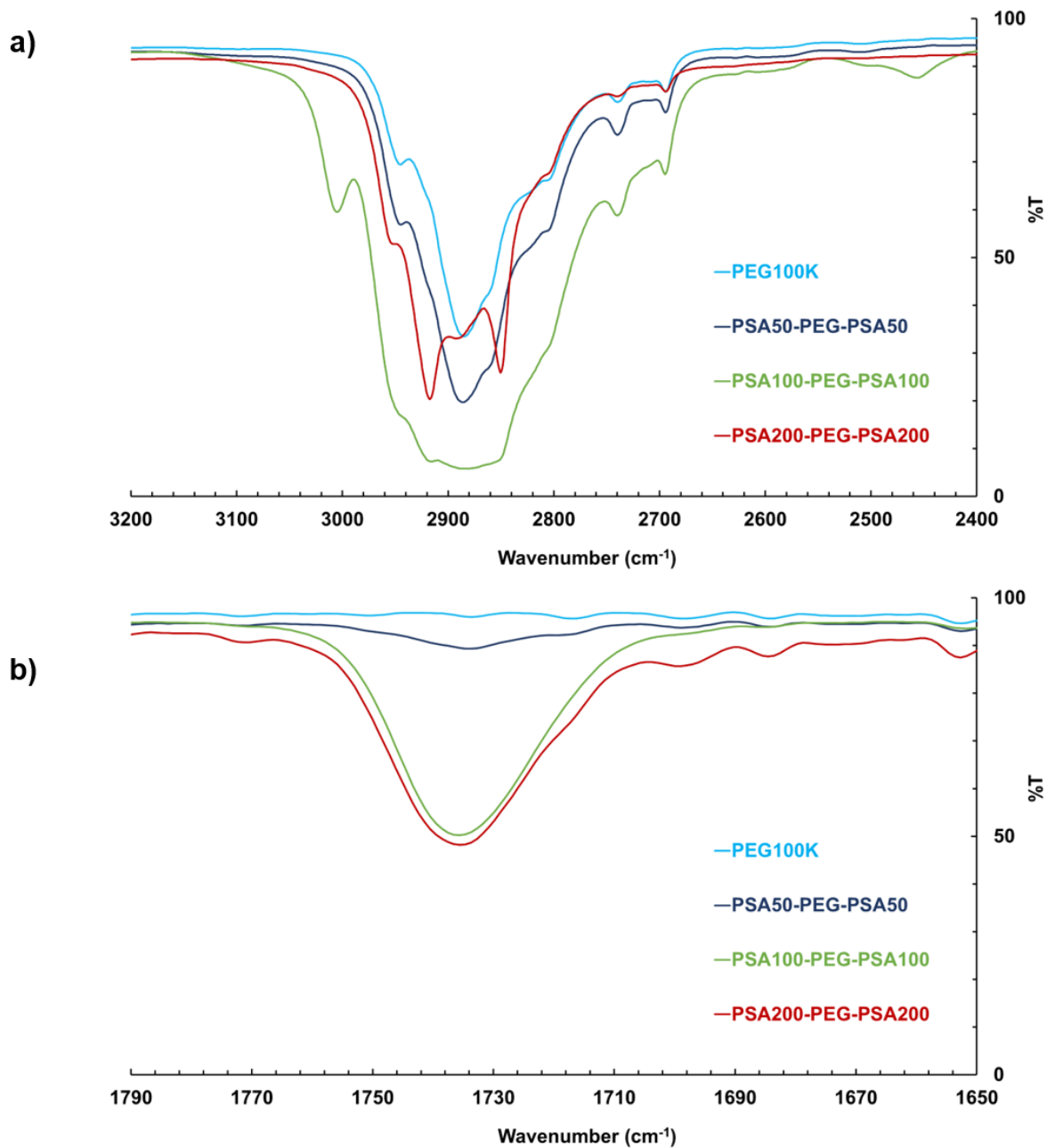


Figure 4-5. a) Zoom in of FTIR for long chain alkyl peak from 3000-2600 cm<sup>-1</sup> b) Zoom in of FTIR carbonyl peak from 1770-1650 cm<sup>-1</sup>

#### 4.3.4. Differential scanning calorimetry (DSC)

DSC was performed to determine the transition temperatures of the synthesized polymers and determine the phase separation of the triblock copolymer. The spectra (Fig. 4-6) show two peaks, thus there is significant phase separation between the PSA domain and PEG domains in each synthesized polymer. In a BAB triblock copolymer, this is expected due to the homopolymers formed within each block. PEG100K has melting peak at 70 °C, which is the melting temperature. PSA50-PEG-PSA50 has a broad glass transition temperature,  $T_g$ , peak from 55-59 °C, then a large  $T_m$  peak at 65°C. This indicates that there is little crystalline PSA present in the sample. This is likely caused by the much higher ratio of PEG:PSA resulting in little phase separation and crystallization within the PSA blocks. The shift from 70 °C in PEG100K to 65 °C for each synthesized polymer is due to the physical bonding and intertwining of the crystalline portions of PEG with PSA in the synthesized polymers. The same explanation can be used for the increase in  $T_m$  of PSA. The reported melting temperature for PSA is 31-34 °C,<sup>54</sup> however, the DSC spectra shows 50 °C, which is slightly higher. As the amount of PSA increases, a large endothermic peak at 50 °C forms, indicating an increasing amount of PSA crystalline segments and the melting of those segments. Overall, the DSC spectra confirm the presence of crystalline PSA and PEG in the three synthesized polymers with transition temperature values as expected for triblock copolymers.

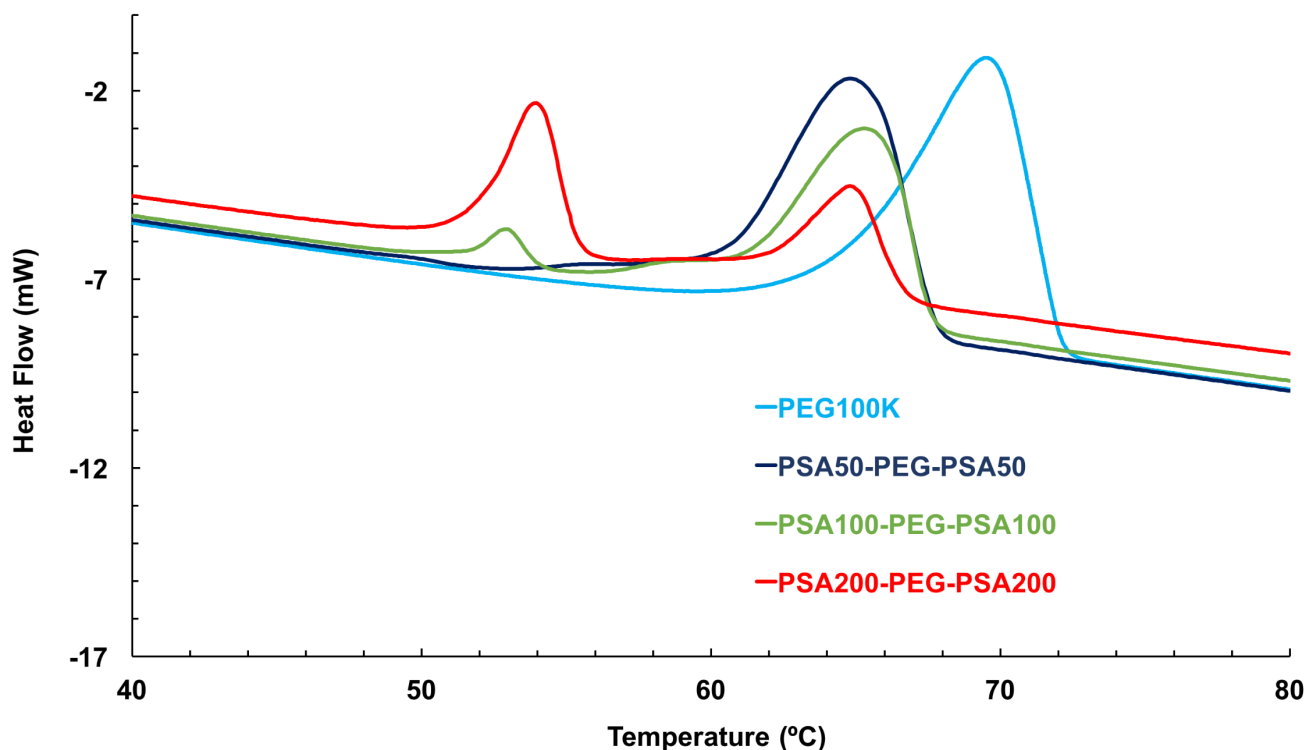


Figure 4-6. Differential scanning calorimetry of synthesized triblock copolymers and PEG100K

#### 4.3.5. Dynamic mechanical analysis (DMA)

Dynamic mechanical analysis was performed to test the mechanical properties of the synthesized triblock copolymer materials. The polymer films were fabricated by dispersing the three synthesized polymers in a water (7 wt%) solution. PSA200-PEG-PSA200 could not be characterized due to aggregation in water. The solution was sonicated for 15 minutes to assist with dispersion. The solution was then dropcast onto untreated glass at 80 °C. The films were left at 80 °C for 40 minutes, with incremental temperature ramp down to 70 °C for 10 minutes, 60 °C for 10 minutes, 50 °C for 20 minutes, 45 °C for 20 minutes, 40 °C for 20 minutes, then 38 °C for 10 minutes, and 30°C for 10 minutes. The films were gently peeled off the glass slides and prepared for DMA testing. The results are outlined in Table 4-2. PEG100K has a modulus at room temperature of 0.745 GPa with elongation at break 356% at 70 °C. As stearyl acrylate is added in

increasing quantities, the modulus increases to 0.838 GPa for PSA50-PEG-PSA and 1.08 GPa for PSA100-PEG-PSA100. This is expected due to the stiff crystalline segments introduced by the addition of stearyl acrylate. The elongation at break only slightly decreases with PSA100-PEG-PSA100 to 320%. This shows high elasticity at elevated temperature with high stiffness at room temperature even with the addition of a large quantity of PSA.

Table 4-2. Average DMA results for PSA<sub>x</sub>-PEG-PSA<sub>x</sub>

<b>Sample</b>	<b>Modulus (GPa)</b>	<b>Elongation at break (%) at 70 °C</b>
PSA50-PEG-PSA50	0. 838	356%
PSA100-PEG-PSA100	1.08	320%
PEG100K	0. 745	356%

Modulus vs temperature (Fig. 4-7) ramp was conducted to determine the transition temperatures of the synthesized polymers. Each polymer has a distinct initial transition temperature determined by the amount of poly (stearyl acrylate) present in the polymer. Both synthesized materials have a room temperature modulus near or over 1 GPa (Table 4-2). The first transitions occur at 46 °C for both PSA100-PEG-PSA100 and PSA50-PEG-PSA50. The modulus drops, then plateaus, with a second transition determined by the PEG segment that occurs at 65 °C. The second decrease in modulus results in a viscous melt, with difficult to determine modulus in the kPa range. The transition is significantly more distinct in PSA100-PEG-PSA100 likely due to the increase in amount of PSA resulting in an increase of crystalline segments of PSA. The phase separation is more distinct in this sample, leading to smaller grains, and as the PSA phase melts, the smaller PEG crystal segments are less mechanically stable than the larger crystalline segments in PSA50-PEG-PSA50, thus a sharper transition. Overall, the materials exhibit a large change

in modulus from about 1 GPa down to kPa range with temperature indicating the synthesis of variable stiffness materials.

Within Figure 4-7 optical images under 10x magnification and polarized light show the spherulite crystalline formations of the triblock copolymer. Spherulite have semicrystalline structure where highly ordered, crystalline lamellae regions are disrupted by amorphous regions, creating a spherical shape. This pattern occurs commonly in linear polymers crystallized from melt. The formation of spherulites within the synthesized polymers confirms the smaller crystalline segments in PSA100-PEG-PSA100, likely due to the higher concentration of PSA.

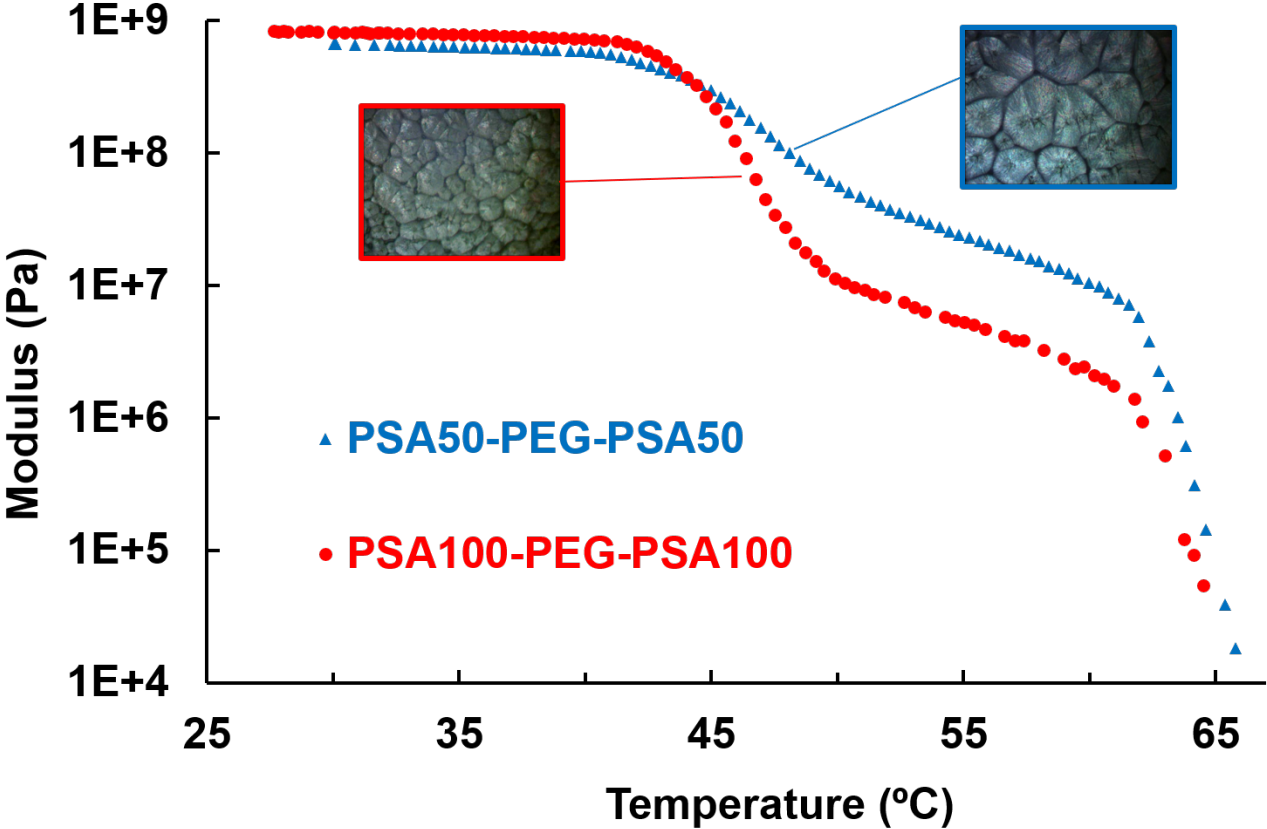


Figure 4-7. Modulus as a function of temperature for PSA50-PEG-PSA50 (blue) and PSA100-PEG-PSA100 (red) with optical microscope images under polarized light at 10x magnification.

#### 4.3.6. Scanning electron microscopy (SEM)

The synthesized polymers were imaged using SEM to determine the morphology and dispersion of the polymer materials in water as compared to PEG100K. PEG100K cast from water (10 mg/mL solution), shows clear spherulite crystallization (Fig. 4-8a) with large spherulites on the order of 100  $\mu\text{m}$ . This is expected and typical crystallization pattern for PEG100K. In PSA50-PEG-PSA50, there is spherulite formation (Fig. 4-8b), with indications of bridging, a phenomenon present in BAB triblock copolymers in A-selecting solvents. The spherulites formed are on the order of 20  $\mu\text{m}$ , smaller than those formed by pure PEG100K. As more PSA is introduced into the triblock copolymer in PSA100-PEG-PSA100, the spherulites formed become even smaller, about 10  $\mu\text{m}$ , and less defined (Fig. 4-8c) tightly packed spherulites create strong molecular interaction within the lamellae. Bridging is also present within PSA100-PEG-PSA100 indicating both synthesized triblock copolymers exhibit phenomena of BAB triblock copolymers in A selecting solvents.

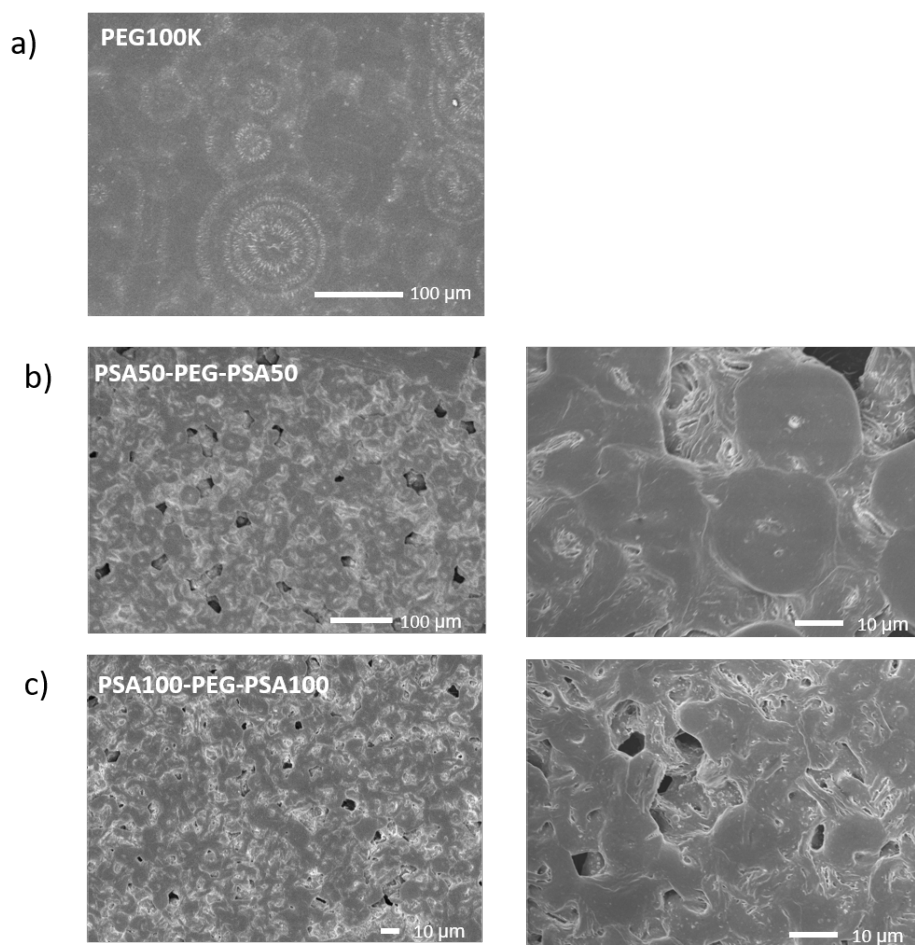


Figure 4-8. SEM images of a) PEG100K b) PSA50-PEG-PSA50 bulk material (left) and individual spherulites (right) c) PSA100-PEG-PSA100 bulk material (left) and individual spherulites (right)

#### 4.4. Conclusion

A series of BAB triblock copolymers of different molecular weights were synthesized by RAFT polymerization, characterized, compared and confirmed via  $^1\text{H}$  NMR, GPC, FTIR, DSC, DMA, and SEM. A highly efficient double-sided macro-RAFT chain transfer agent was successfully synthesized to include a PEG A-block. The macro-RAFT chain transfer agent was then used to synthesize three BAB triblock copolymers with different lengths of poly (stearyl acrylate) B-block.  $^1\text{H}$  NMR confirmed the inclusion of PEG and PSA within the triblock copolymer, GPC confirmed different chain lengths of BAB triblock



were synthesized, and FTIR confirmed the inclusion of PSA into the polymer. DSC and DMA indicated two distinct transition temperatures at 45 °C and 60 °C corresponding to PSA and PEG, respectively. Additionally, DMA showed the mechanical properties indicated the material exhibits variable stiffness triggered by temperature from a stiff polymer at room temperature with modulus of 1 GPa to a viscous polymer melt at elevated temperature with modulus in the kPa range. Lastly, the SEM images showed distinct molecular self-assembly formations of spherulites micelles interconnected through dangling B-block ends, distinctive of BAB triblock copolymer.

#### 4.5. References

- (103) Diamant, J.; Soong, D.; Williams, M. C. The Mechanical Properties of Styrene-Butadiene-Styrene (SBS) Triblock Copolymer Blends with Polystyrene (PS) and Styrene-Butadiene Copolymer (SBR). *Polym. Eng. Sci.* **1982**, *22* (11), 673–683.
- (104) Hermann, A.; Mruk, R.; Roskamp, R. F.; Scherer, M.; Ma, L.; Zentel, R. Poly(*N*-Isopropylacrylamide)-Modified Styrene-Butadiene Rubber as Thermoresponsive Material. *Macromol. Chem. Phys.* **2014**, *215* (1), 32–43. <https://doi.org/10.1002/macp.201300479>.
- (105) Brinkmann-Rengel, S.; Abetz, V.; Stadler, R.; Thomas, E. L.; others. Thermoplastic Elastomers Based on ABA-and ABC-Triblock Copolymers. *Kautsch. GUMMI KUNSTSTOFFE* **1999**, *52* (12), 806–813.
- (106) Fairbanks, B. D.; Gunatillake, P. A.; Meagher, L. Biomedical Applications of Polymers Derived by Reversible Addition – Fragmentation Chain-Transfer (RAFT). *Adv. Drug Deliv. Rev.* **2015**, *91*, 141–152. <https://doi.org/10.1016/j.addr.2015.05.016>.
- (107) Kennedy, J. E.; Higginbotham, C. L. Synthesis and Characterisation of Styrene Butadiene Styrene Based Grafted Copolymers for Use in Potential Biomedical Applications. In *Biomedical engineering, Trends in materials science*; InTech, 2011.

- (108) Huang, J.; Xu, J.; Chen, K.; Wang, T.; Cui, C.; Wei, X.; Zhang, R.; Li, L.; Guo, X. Synthesis of Triblock Copolymers via RAFT Polymerization and Their Application as Surfactants for Crude Oil-in-Water Emulsion. *Ind. Eng. Chem. Res.* **2015**, *54* (5), 1564–1575. <https://doi.org/10.1021/ie504207r>.
- (109) Anastasiadis, S. H. Development of Functional Polymer Surfaces with Controlled Wettability. *Langmuir* **2013**, *29* (30), 9277–9290. <https://doi.org/10.1021/la400533u>.
- (110) Delgadillo, P. A. R. Implementation of a Chemo-Epitaxy Flow for Directed Self-Assembly on 300-Mm Wafer Processing Equipment. *J. MicroNanolithography MEMS MOEMS* **2012**, *11* (3), 031302. <https://doi.org/10.1117/1.JMM.11.3.031302>.
- (111) Zhou, Z.; Calabrese, D. R.; Taylor, W.; Finlay, J. A.; Callow, M. E.; Callow, J. A.; Fischer, D.; Kramer, E. J.; Ober, C. K. Amphiphilic Triblock Copolymers with PEGylated Hydrocarbon Structures as Environmentally Friendly Marine Antifouling and Fouling-Release Coatings. *Biofouling* **2014**, *30* (5), 589–604. <https://doi.org/10.1080/08927014.2014.897335>.
- (112) Ma, Z.; Xie, Y.; Mao, J.; Yang, X.; Li, T.; Luo, Y. Thermoplastic Dielectric Elastomer of Triblock Copolymer with High Electromechanical Performance. *Macromol. Rapid Commun.* **2017**, *38* (16), 1700268. <https://doi.org/10.1002/marc.201700268>.
- (113) Gao, C.; Li, S.; Li, Q.; Shi, P.; Shah, S. A.; Zhang, W. Dispersion RAFT Polymerization: Comparison between the Monofunctional and Bifunctional Macromolecular RAFT Agents. *Polym Chem* **2014**, *5* (24), 6957–6966. <https://doi.org/10.1039/C4PY01069H>.
- (114) Liang, J.; Shan, G.; Pan, P. Double Network Hydrogels with Highly Enhanced Toughness Based on a Modified First Network. *Soft Matter* **2017**, *13* (22), 4148–4158. <https://doi.org/10.1039/C7SM00544J>.

## **Chapter 5. Conclusions and future directions**

### **5.1. Summary of the dissertation**

This dissertation focuses on the research of stimuli responsive polymer materials, specifically thermo- and electro-responsive materials. The study covers important developments of new stimuli responsive materials for variable stiffness with ultra-wide tunable modulus differential, development of high performance electro-responsive materials, and development of a controlled synthetic pathway for thermo-responsive variable stiffness polymers.

The development of a new stimuli responsive variable stiffness material triggered by water and temperature was achieved by combining cellulose fibers with a modified BSEP matrix. The resulting composite had two stimuli, the first was temperature to soften the BSEP by melting the crystalline segments to form a soft crosslinked polymer. The second stimulus was the addition of water, to nullify the reinforcing network formed by percolating cellulose fibers and further soften the material. Combining the BSEP matrix and cellulose fiber network, resulted in a material that softens when exposed to water and heat. The material exhibits a modulus differential of 24,000 times from 1 GPa to 40 kPa. This is a significant improvement on previously studied cellulose composites that exhibited stiffness change up to 5100 times.

New dielectric elastomer materials were designed and fabricated for high performance actuation and rapid response speed. The new materials exhibited electromechanical actuation over 100% with nominal electric field of 100 V/ $\mu\text{m}$ . Two formulations, AA(2.5) and P(10)-BA(13), achieved actuation near 200% with high nominal electric fields. They were further studied for actuation at frequencies of 2 Hz. Although P(10)-BA(13) did not exhibit actuation strain over 100% at 2 Hz, AA(2.5) exceeded this with actuation performance of 110% average strain. AA(2.5) and P(10)-BA(13) were compared to 300% biaxially

prestretched VHB4905 and achieved higher actuation, faster response speed, and higher energy density. The one condition these materials did not exceed VHB performance was Maxwell pressure, where VHB achieved 3.5 MPa, however AA(2.5) was only slightly lower with 3.2 MPa. AA(2.5) showed performance similar to 300% biaxially prestretched VHB4905, but did not require any prestretching.

Lastly, three BAB triblock copolymers were developed for use as a thermo-responsive variable stiffness bistable electroactive polymer (BSEP). BSEP materials are difficult to process due to the crosslinked nature. A controlled synthetic pathway for microstructure control and finely tuning mechanical properties is desirable. Three BAB triblock copolymers of different lengths were synthesized via RAFT polymerization using poly (ethylene glycol) (PEG) A-block and poly (stearyl acrylate) (PSA) B-block. The synthesized materials were characterized and confirmed by <sup>1</sup>H NMR, GPC, FTIR, DSC, DMA, and SEM. The materials exhibited two distinct transition temperatures at 45 °C and 60 °C corresponding to PSA and PEG, respectively. The mechanical properties indicated the material exhibits variable stiffness triggered by temperature from a stiff polymer at room temperature with modulus of 1 GPa to a viscous polymer melt at elevated temperature with modulus in the kPa range.

## **5.2. Future directions**

Development of the BSEP synthetic process can be perfected to design a thermoplastic elastomer BSEP material. A linear polymer with the attributes of an elastomer material, could open more applications of BSEP and finely tune the properties for each application. The modified BSEP composite material shows great promise for future biomedical applications. The material shows biocompatibility and a large modulus differential, which could widen the application range. This material could be used as part of an intercortical implant. Such materials are desired in cortical probe applications due to the mechanical mismatch of current probe materials. The mechanical mismatch can cause an inflammatory response resulting in scar tissue formation and a loss of signal. With a material that can change stiffness at body

temperature, it would be stiff upon insertion, then soften over time to match the modulus of brain tissue and slow the inflammatory response. However, the lowest modulus the material can currently reach is 40 kPa, but the modulus of brain tissue is 6 kPa. Another future direction of this material would be lowering the low-end modulus for exact match to brain tissue or other body tissues.

Dielectric elastomer materials that are commercially available are not made for DE applications. By developing a new DE material from design to fabrication, modifications can be made to further optimize the material. AA(2.5) shows great promise with characteristics similar to VHB without the need for prestretching. Additional modifications could be made such as increasing the dielectric constant for lower driving voltage or improving the elongation at break. As the material is optimized, it could be used in a multilayer dielectric elastomer to improve robustness, lower driving voltage and increase work output to further widen the application range of DE materials.

Filename: Erin Askounis Thesis Final Draft.docx  
Folder: /Users/Erin/Library/Containers/com.microsoft.Word/Data/Documents  
Template: /Users/Erin/Library/Group Containers/UBF8T346G9.Office/User  
Content.localized/Templates.localized/Normal.dotm  
Title:  
Subject:  
Author: 肖 炜琨  
Keywords:  
Comments:  
Creation Date: 6/1/20 12:36:00 PM  
Change Number: 2  
Last Saved On: 6/1/20 12:36:00 PM  
Last Saved By: Erin Askounis  
Total Editing Time: 1 Minute  
Last Printed On: 6/1/20 12:36:00 PM  
As of Last Complete Printing  
Number of Pages: 100  
Number of Words: 20,068  
Number of Characters: 117,551 (approx.)